

DEVELOPMENT OF DUAL-LAYER MEMBRANE AND
METAL ORGANIC FRAMEWORK FOR GAS
SEPARATION TO IMPROVE INDOOR AIR QUALITY

CHONG KOK CHUNG

DOCTOR OF PHILOSOPHY (ENGINEERING)

LEE KONG CHIAN FACULTY OF ENGINEERING AND
SCIENCE
UNIVERSITI TUNKU ABDUL RAHMAN
SEPTEMBER 2023

**DEVELOPMENT OF DUAL-LAYER MEMBRANE AND METAL
ORGANIC FRAMEWORK FOR GAS SEPARATION TO IMPROVE
INDOOR AIR QUALITY**

By

CHONG KOK CHUNG

A thesis submitted to the Department of Chemical Engineering,
Lee Kong Chian Faculty of Engineering and Science,
Universiti Tunku Abdul Rahman,
in partial fulfillment of the requirements for the degree of
Doctor of Philosophy (Engineering)
September 2023

*To my wonderful family and my wife, Gee Chin
the finest people who I've ever met.*

ABSTRACT

DEVELOPMENT OF DUAL-LAYER MEMBRANE AND METAL ORGANIC FRAMEWORK FOR GAS SEPARATION TO IMPROVE INDOOR AIR QUALITY

Chong Kok Chung

Humans spend up to 80% of their lifetime either at their workplaces or homes. The World Health Organization (WHO) report indicated that higher proportions of individuals associated with indoor environmental sickness (such as asthma and sick building syndrome) are children, the elderly, and people with chronic diseases. Enhancing indoor oxygen (O₂) levels and decreasing indoor carbon dioxide (CO₂) levels are ways to effectively decrease indoor air pollution and maintain optimal indoor air quality (IAQ).

Traditional approaches for oxygen gas production, including pressure swing adsorption (PSA) and cryogenic distillation, are known for their high energy consumption. In contrast, membrane technology offers a more cost-effective alternative with reduced energy demands. However, the gas separation efficiency in terms of permeance and selectivity is still constrained by Robeson's upper limits. The conventional methods of CO₂ removal from ambient air involve solvent adsorption, physical adsorption, and cryogenic fractionation. A promising recent development in this regard is the use of MOF due to their exceptional material properties and extensive surface area.

By exploring the synergy between membrane technology and MOF, there is a potential to improve indoor air quality.

This study aimed to enhance indoor air quality by separating O₂ and CO₂ from the ambient air using membrane technology with the following objectives. In this study, PSU or PEI membranes were fabricated by phase inversion methods. The membranes were dip coated by either PDMS or PEBAX to evaluate its performance in O₂/N₂ gas separation. The study results revealed that the pristine polysulfone (PSU-3) and polyetherimide (PEI-3) hollow fiber membranes exhibited superior permeance performance than the same materials at varying bore fluid flow rates. The polydimethylsiloxane (PDMS) coating layer in the dual-layer membrane indicated the coating could improve surface defects on the membrane. Moreover, it had a superior affinity with O₂ and N₂ gases, enabling better diffusion of these gases across the membrane. In this study, the most superior O₂/N₂ gas separation membrane was PSU membrane with 3wt% coating of PDMS (PSU-3PDMS).

Two types of MOF were investigated, namely chromium (Cr) and copper (Cu) based MOF with either terephthalic acid (BDC) or trimesic acid (BTC) as organic ligand. The BET surface analysis revealed Cu-BTC MOFs generally showed a greater surface area (516 to 1,039 m²/g) than other MOFs in this study. The physiochemical findings were coherent with the CO₂ gas adsorption results. The Cu-BTC MOFs typically yielded a better CO₂ adsorption performance relative to other MOFs, whereby Cu-BTC-1:1 recorded the most significant impact at 1.31 mmol/g.

In summation, the PSU-3PDMS dual-layer hollow fiber membrane was found to be able to increase the O₂ concentration up to 0.2% at 12 hours sampling time where the performance of the gas separation decreased attributed to the accumulation of particles and dust on the membrane surface. In the meantime, the Cu-BTC-1:1 MOF successfully reduced the CO₂ concentration to 16 ppm. The results from this study suggested the possibility of integrating the dual-layer membrane with MOF to improve indoor air quality for the betterment of human life.

ACKNOWLEDGEMENTS

I am indebted and grateful to my dearest supervisor, the director of Division of Community and International Networking, Associate Professor Dr Lai Soon Onn, for his relentless patience and support despite his hectic schedule until the completion of this research. Dr Lai has been my supervisor since my undergraduate studies, master's degree study and today, my PhD studies. One Chinese proverb - *A teacher for a day, a father for life* means a lot to me.

Thousand thanks to assistant professor Dr Thiam Hui San, my co-supervisor, and Associate Professor Dr Lau Woei Jye, my external co-supervisor, for their guidance throughout. I want to express my deep appreciation to the laboratory staff from UTAR and UTM for their unknowing yet remarkable contribution to this work.

Also, I would like to thank MayAir Postgraduate Sponsorship Research Project and UTAR research grant for financially supporting my research activities.

I owe much gratitude to my parents and wife for their constant encouragement throughout and beyond this work; without them, this work would have ended somewhere before this page.

LEE KONG CHIAN FACULTY OF ENGINEERING AND SCIENCE
UNIVERSITI TUNKU ABDUL RAHMAN

Date: 25.09.2023

SUBMISSION OF FINAL YEAR PROJECT /DISSERTATION/THESIS

It is hereby certified that *Chong Kok Chung* (ID No: 15UED06669) has completed this thesis entitled “*Development of Dual-layer Membrane and Metal Organic Framework for Gas Separation to Improve Indoor Air Quality*” under the supervision of *Associate Professor Dr Lai Soon Onn* (Supervisor) from the Department of Chemical Engineering, Lee Kong Chian Faculty of Engineering and Science, *Assistant Professor Dr Thiam Hui San* (Co-Supervisor) from the Department of Chemical Engineering, Lee Kong Chian Faculty of Engineering and Science, and *Associate Professor Dr Lau Woei Jye* (External Co-Supervisor) from the Department of Energy Engineering, School of Chemical and Energy Engineering, Universiti Teknologi Malaysia.

I understand that University will upload softcopy of my thesis in pdf format into UTAR Institutional Repository, which may be made accessible to UTAR community and public.

Yours truly,

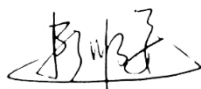


(*Chong Kok Chung*)

APPROVAL SHEET

This thesis entitled “**DEVELOPMENT OF DUAL-LAYER MEMBRANE AND METAL ORGANIC FRAMEWORK FOR GAS SEPARATION TO INDOOR AIR QUALITY IMPROVEMENT**” was prepared by CHONG KOK CHUNG and submitted as partial fulfillment of the requirements for the degree of Doctor of Philosophy (Engineering) at Universiti Tunku Abdul Rahman.

Approved by:



(Associate Professor Dr. Lai Soon Onn)

Date: 25.09.2023

Associate Professor/Supervisor

Department of Chemical Engineering

Lee Kong Chian Faculty of Engineering and Science

Universiti Tunku Abdul Rahman

Thiam

(Assistant Professor Dr. Thiam Hui San)

Date: 25.09.2023

Assistant Professor/Co-supervisor

Department of Chemical Engineering

Lee Kong Chian Faculty of Engineering and Science

Universiti Tunku Abdul Rahman



(Associate Professor Dr. Lau Woei Jye)

Date: 25.09.2023

Associate Professor/External co-supervisor

Department of Energy Engineering

Faculty of Chemical and Energy Engineering

Universiti Teknologi Malaysia

DECLARATION

I hereby declare that the dissertation is based on my original work except for quotations and citations which have been duly acknowledged. I also declare that it has not been previously or concurrently submitted for any other degree at UTAR or other institutions.



Name: Chong Kok Chung

Date: 25.09.2023

TABLE OF CONTENTS

	Page
ABSTRACT	ii
ACKNOWLEDGEMENTS	v
PERMISSION SHEET	vi
APPROVAL SHEET	vii
LIST OF TABLES	xii
LIST OF FIGURES	xiii
LIST OF ABBREVIATIONS/SYMBOLS	xvi
CHAPTER	
1.0 INTRODUCTION	1
1.1 General introduction	1
1.2 Importance of study	4
1.3 Problem statement	6
1.4 Aim and objectives	8
1.5 Scope and limitations of the study	9
2.0 LITERATURE REVIEW	11
2.1 Overview of indoor air quality and its effect on human health	11
2.2 Oxygen/nitrogen (O ₂ /N ₂) separation techniques	13
2.3 Membrane technology	18
2.3.1 Membrane fabrication methods	18
2.3.2 Polymeric materials	21
2.3.2.1 Polyimide	21
2.3.2.2 Polysulfone	23
2.3.2.3 Polyetherimide	24
2.3.4 Membrane performance and Robeson upper bound	25
2.3.5 Dual-layer composite membrane	27
2.3.5.1 Polydimethylsiloxane (PDMS)	28
2.3.5.2 Poly(ether block amide) (PEBAX)	29
2.4 Metal organic framework (MOF)	31
2.4.1 Synthesis methods of MOF	34
2.4.1.1 Solvothermal method	35
2.4.1.2 Microwave-assisted method	36
2.4.1.3 Sonochemical method	37
2.4.1.4 Electrochemical method	38
2.4.1.5 Mechanochemical method	39
2.4.2 Factors affecting MOF physical properties	40
2.4.2.1 Effect of molar ratio	40

	2.4.2.2 Effect of temperature	43
	2.4.2.3 Effect of material composition	45
	2.4.3 Copper and chromium based metal organic framework	49
Chapter 3	Methodology	52
3.1	Process flow chart	52
3.2	Preparation of hollow fiber membrane and O ₂ /N ₂ gas separation	53
3.2.1	Materials	53
3.2.2	Fabrication method	53
3.2.3	Hollow fiber membrane coating technique	55
3.2.4	Characterisation method	57
3.2.5	O ₂ /N ₂ gas separation setup	57
3.3	Preparation of metal organic framework and CO ₂ gas adsorption	59
3.3.1	Materials	59
3.3.2	Fabrication method	59
3.3.3	Characterisation methods	61
	3.3.3.1 Scanning electron microscopy with energy dispersive X-ray (SEM-EDX)	62
	3.3.3.2 Powder X-Ray diffraction (XRD)	62
	3.3.3.3 Brunauer-Emmett-Teller (BET)	62
3.3.4	CO ₂ gas adsorption setup	63
3.4	Indoor O ₂ enrichment and CO ₂ reduction setup	64
Chapter 4	Results and discussion	66
4.1	Effect of polymeric materials and fabrication parameters on O ₂ /N ₂ gas separation	66
4.1.1	Characterisation of physical properties	66
4.1.2	Performance of O ₂ /N ₂ gas separation	69
4.1.3	Summary	71
4.2	Performance of dual-layer membrane on O ₂ /N ₂ gas separation	72
4.2.1	Characterisation of physical and chemical properties	72
4.2.2	Effect of coating material on O ₂ /N ₂ gas separation	77
	4.2.2.1 Gas permeance and selectivity of PEI dual-layer membrane	77
	4.2.2.2 Gas permeance and selectivity of PEI dual-layer membrane	78
4.2.3	Summary	81
4.3	Effect of MOF materials and composition in CO ₂ adsorption	81
4.3.1	Characterisation of physical and chemical properties	81
	4.3.1.1 Surface morphology studies by scanning electron microscopy (SEM)	81
	4.3.1.2 Elemental analysis by energy dispersion X-ray (EDX)	88
	4.3.1.3 Crystallographic structure studies by X-ray diffraction analysis (XRD)	90
	4.3.1.4 Surface area analysis by Brunauer, Emmett and Teller (BET)	91
4.3.2	Performance of CO ₂ adsorption	93

4.3.3	Summary	94
4.4	O ₂ enrichment and CO ₂ reduction in actual environment	96
4.4.1	Indoor O ₂ enrichment	96
4.4.2	Indoor CO ₂ reduction	97
4.4.3	Summary	98
Chapter 5 Conclusions and recommendations		100
5.1	Conclusions	100
5.2	Recommendations	101
References		103
Appendix A – List of Publication		124
Appendix B – Annual cost calculation of membrane technology in indoor oxygen air enrichment		126

LIST OF TABLES

Table		Page
2.1	Comparison of PSA, cryogenic distillation and membrane technology in gas separation	13
2.2	The effect of fabrication parameter on hollow fiber membrane characteristics	19
2.3	Comparison of O ₂ /N ₂ gas separation from hollow fiber membrane	27
2.4	CO ₂ gas adsorption by copper and chromium based MOF	50
3.1	Membrane fabrication parameters	54
3.2	Coating condition for the PSU and PEI hollow fiber membranes	55
3.3	Composition of MOFs sample	59
4.1	Physical properties of the PSU and PEI hollow fiber membranes	67
4.2	Coating thickness of PSU and PEI dual-layer hollow fiber membranes	72
4.3	Elemental analysis of PSU dual-layer hollow fiber membranes	74
4.4	Elemental analysis of PEI dual-layer hollow fiber membranes	75
4.5	Elemental analysis of chromium-based MOFs	87
4.6	Elemental analysis of copper-based MOFs	88
4.7	BET surface area analysis of MOFs	91
4.8	CO ₂ gas adsorption of MOFs	92

LIST OF FIGURES

Figures		Page
2.1	Schematic diagram of cryogenic distillation process	15
2.2	Schematic diagram of pressure swing adsorption process	16
2.3	Schematic diagram of phase inversion setup for the fabrication of hollow fiber membrane	18
2.4	Chemical structure of imide	21
2.5	Chemical structure of Matrimid [®]	22
2.6	Repeating units of polysulfone	23
2.7	Structure of polyetherimide	24
2.8	Typical structure of MOF	31
2.9	Schematic diagram on the modification of (a) metal sites, and (b) ligand	33
2.10	MOF synthesis methods and conditions	34
2.11	Solvothermal MOF fabrication method	35
2.12	Microwave-assisted MOF fabrication method	36
2.13	Sonochemical MOF fabrication method	37
2.14	Electrochemical MOF fabrication method	38
2.15	Mechanochemical MOF fabrication method	39
2.16	(a) XRD analysis, and (b) Pore size distribution of copper-based metal organic framework	41
2.17	SEM morphology of (a) Cu-BTC, (b) Cu-BTC (80%), (c) Cu-BTC (60%) and (d) Cu-BTC (40%)	42
2.18	CO ₂ gas adsorption by copper-based metal organic framework at 25°C	42
2.19	Morphology image of Co-MOF fabricated at temperature (a) 120°C, and (b) 160°C	43

2.20	SEM morphology of thulium-based MOF fabrication at 100 and 180°C	44
2.21	CO ₂ adsorption of MOFs fabricated from different metal	45
2.22	CO ₂ uptake at different temperature for Uio-66, Uio-66-Br, Uio-66-NH ₂ and Uio-66-NO ₂ at (a) 0.1 MPa and (b) 3.0 MPa	48
3.1	Overall process flow chart	51
3.2	Schematic diagram on the setup used for the fabrication of hollow fiber membranes	53
3.3	Dip coating technical of hollow membrane	55
3.4	Schematic setup for pure gas permeation study	57
3.5	Schematic setup for CO ₂ gas adsorption study	62
3.6	Schematic setup for indoor O ₂ gas enrichment study	63
3.7	Schematic setup for indoor CO ₂ gas adsorption study	64
4.1	Cross sectional morphology of (a) PSU-1, (b) PSU-2, (c) PSU-3, (d) PEI-1, (e) PEI-2, and (f) PEI-3	66
4.2	(a) Oxygen and nitrogen gas permeance, and (b) Oxygen and nitrogen gas selectivity of PSU and PEI hollow fiber membranes with different bore fluid flow rates	69
4.3	Cross sectional morphology of (a) pristine membrane, (b) PDMS dual-layer hollow fiber membrane, and (c) PEBAX dual-layer hollow fiber membrane	72
4.4	(a) Oxygen and nitrogen gas permeance, and (b) Oxygen and nitrogen gas selectivity of PSU dual-layer hollow fiber membrane with PDMS or PEBAX coating	77
4.5	(a) Oxygen and nitrogen gas permeance, and (b) Oxygen and nitrogen gas selectivity of PEI dual-	78

	layer hollow fiber membrane with PDMS or PEBA _X coating	
4.6	SEM morphologies at 2,000x and 10,000x magnification, respectively for (a) Cr-BDC-1:1, (b) Cr-BDC-1:2, (c) Cr-BDC-1:3, (d) Cr-BDC-1:4, and (e) Cr- BDC -1:5	82
4.7	SEM surface morphology at 2,000x and 10,000x magnification, respectively for (a) Cr-BTC-1:1, (b) Cr-BTC-1:2, (c) Cr-BTC-1:3, (d) Cr-BTC-1:4, and (e) Cr-BTC-1:5	83
4.8	SEM surface morphology at 2,000x and 10,000x magnification, respectively for (a) Cu-BDC-1:1, (b) Cu-BDC-1:2, (c) Cu-BDC-1:3, (d) Cu-BDC-1:4, and (e) Cu-BDC-1:5	85
4.9	SEM morphologies at 2,000x and 10,000x magnification, respective for (a) Cu-BTC-1:1, (b) Cu- BTC-1:2, (c) Cu- BTC-1:3, (d) Cu- BTC-1:4, and (e) Cu- BTC -1:5	86
4.10	XRD analysis for (a) Cr-BDC, (b) Cr-BTC, (c) Cu-BDC, and (d) Cu-BTC	90
4.11	Temporal changes of the oxygen gas concentration with respect to the sampling time	96
4.12	Temporal changes of the carbon dioxide gas concentration with respect to the sampling time	97

LIST OF ABBREVIATIONS/SYMBOLS

6FDA	2,2-bis(3,4-dicarboxyphenyl) hexafluoropropanedianhydride
ASHRAE	American Society of Heating, Refrigerating and Air Conditioning Engineer
BDC	Terephthalic acid
BET	Brunauer-Emmett-Teller
Br	Bromine
BTC	Trimesic acid
BTDA	3-3'-4-4'-benzophenone tetracarboxylic dianhydride, BTDA
C	Carbon
CMS	Carbon molecular sieve
Co	Cobalt
CO ₂	Carbon dioxide
Cr	Chromium
CTF-1	Covalent triazine framework
Cu	Copper
CUS	Coordinatively unsaturated sites
DAPI	Diaminophenylindane
DMAc	N,N-Dimethylacetamide
DMF	Dimethyl formamide
DOBDC	2,5-dioxido-1,4-benzene-dicarboxylate
EDX	Energy Dispersive X-ray Spectroscopy
EBTC	1,1'-ethynebenzene-3,3',5,5'-tetracarboxylate
EtOH	Ethanol
Fe	Iron
H ₄ OATA	N,N'-bis(3,5-dicarboxyphenyl)oxalamide
HKUST	Hong Kong University of Science and Technology
IAQ	Indoor air quality
ID	Inner diameter
IRMOF	Isorecticular metal-organic frameworks
LAG	Liquid-assisted grinding
M/DOBDC	Dobdc ₄₋ = 2,5-dioxido-1,4-benzenedicarboxylate
Mg	Magnesium
MgO	Magnesium oxide
MIL-101	Materials Institute Lavoisier-101
Mn	Manganese
MOF	Metal organics framework
N ₂	Nitrogen
ND	Not detected
NDCA	2,6-naphthalenedicarboxylic acid
NH ₂	Amine
Ni	Nickel
NO ₂	Nitrite
O ₂	Oxygen
OD	Outer diameter
PDMS	Polydimethylsiloxane
PEBAX	Poly(ether block amide)
PEI	Polyetherimide

PI	Polyimide
PSA	Pressure swing adsorption
PSM	Post-synthetic modification
PSU	Polysulfone
S	Sulphur
SEM	Scanning electron microscopy
Si	Silicon
STP	Standard temperature and pressure
T_g	Glass transition temperature
TEPA	Tetraethylenepentamine
THF	Tetrahydrofuran
VSA	Vacuum swing adsorption
WHO	World Health Organization
XRD	X-Ray Diffraction
Zn	Zinc
\AA	Armstrong (10^{-10} m)
Δp_i	Pressure difference transport across membrane
$\alpha_{A/B}$	Gas selectivity
$^{\circ}\text{C}$	Degree Celcius
λ	Wavelength
μm	Micronmeter
A	Surface area
at%	Atomic weight percentage
cm	Centimeters
GPU	Gas permeance unit (10^{-6} cm ³ (STP)/cm ² cm Hg)
kHz	Kilohertz
kV	Kilovolt
mA	Miliampere
MHz	Megahertz
MPa	Mega Pascal
K	Kelvin
L	Thickness of the membrane
m ²	Square meter
m ³	Cubic meter
min(s)	Minutes(s)
mL	Milliliters
P_i	Permeability of gas species i
ppm	Part per million
Q_i	Volumetric flow rate of the gas particles
t	Time
T	Temperature
wt%	Weight percentage

CHAPTER 1

INTRODUCTION

1.1 General introduction

Air pollution is a subject of extensive discourse in both academic and industrial spheres worldwide, posing a significant threat to human well-being. A risk assessment study conducted by the Global Burden of Disease Study in 2019 revealed that air pollution caused 6.85 million deaths globally, with 4.3 million of those resulting from household air pollution (Lancet, 2020). This type of pollution significantly impacts human health, leading to respiratory tract infections, pneumonia, and lung cancer. Most of the human life is spent indoors, with up to 80% of our time being spent either at home or in the workplace. Because of this, indoor air quality (IAQ) is an essential factor in determining the overall health and productivity of individuals. The quality of the air inside buildings can have a significant impact on human health and well-being, which is why it is important to maintain good IAQ. Poor IAQ can result in a range of health problems, including headaches, fatigue, allergies, and respiratory problems, while good IAQ can lead to improved concentration, better cognitive function, and increased productivity. Therefore, it is crucial for building managers and occupants to take steps to ensure that the air quality inside buildings is maintained at a high level. The World Health Organization (WHO) report found that higher proportions of individuals associated with

indoor environmental sickness (such as asthma and sick building syndrome) were children, the elderly, and people with chronic disease (Khamal et al., 2019).

To maintain good indoor air quality (IAQ) and reduce indoor air pollution, one effective method is to introduce air enriched with oxygen. By introducing oxygen-enriched air into an indoor space, it is possible to increase or restore the oxygen levels, thereby enhancing the overall indoor air quality and creating a more revitalizing atmosphere for those occupying the space (Sivarethinamohan et al., 2021). In addition to the oxygen enrichment in the indoor air quality, the reduction of carbon dioxide (CO₂) content in the dwelling space also plays a vital role because CO₂ is an odourless indoor contaminant that poses a significant health risk for the indoor occupants (Chen and Chen, 2020). In most countries, government regulatory bodies impose strict regulations on the CO₂ limit in indoor air conditions. For instance, the Department of Occupational Safety and Health (DOSH), Malaysia and The American Society of Heating, Refrigerating and Air-Conditioning Engineers (ASHRAE) Standard 62-2007 (The American Society of Heating, Refrigerating and Air-Conditioning Engineers, 2007; Department of Occupational Safety and Health, Malaysia, 2010) cap 1,000 ppm CO₂ as ceiling limit to ensure that the occupants' health and productivity are not affected when exposed to the indoor environment. Salleh et al. (2015) reported that only 2 out of 16 studied samples for school met the ASHRAE Standard 62-2007 indoor CO₂ level guidelines, and five samples recorded more than 1,500 ppm of CO₂ content during the sampling period. The trends are

worrying as most schools are exposed to the inferior IAQ, which will lead to sick building syndrome and eventually affect children's academic performance as they are more prone to unfavourable environment surrounding them.

The process of producing O₂ is typically accomplished using either pressure swing adsorption (PSA) or cryogenic distillation technique. Both techniques can produce high purity O₂ levels of more than 95% at high production volumes ranging from 20 to 300 tons per day (Lulianelli and Drioli, 2020). However, these methods are known to consume high amounts of energy, which can result in elevated operational costs. As a result, membrane separation is increasingly viewed as an attractive alternative, as it requires relatively low energy input and has the potential to reduce costs associated with O₂ production. Liang, Chung and Lai (2019) reported membrane separation is a viable option for achieving high purity O₂ production while maintaining low energy requirements.

Many studies on O₂/N₂ separation by polymeric membranes were conducted, but the results were not promising due to the performance limitation by the permeability and selectivity trade off (Han et al., 2019, Adhikari et al., 2021). The O₂/N₂ trade-off curve indicated that most of the polymeric membrane performances were well below the upper bound line proposed by Robeson in 1991, and was revisited later in 2008. Lately, the studies of dual-layer polymeric membrane, carbon molecular sieve membranes (CMS) and facilitated transport membrane have demonstrated the potential to record the performance above the Robeson upper bound line.

Conventionally, several methods to remove CO₂ from the ambient air include solvent adsorption, physical adsorption, cryogenic fractionation, and membrane system (Zhao, Yang and Gu, 2023). MOF is one of the recent exciting methods in CO₂ removal due to its good materials properties and high surface area. A previous study suggested that CO₂ could be well adsorbed into the MOF, and it was able to undergo desorption easily under the long-term operation (Al-Rowaili et al., 2021).

1.2 Importance of study

One of the methods to reduce indoor air pollution and maintain a good IAQ is to enhance the O₂ content and reduce the CO₂ content. The enrichment of the O₂ content can improve freshness of the air, whereas the reduction of CO₂ content in the dwelling space plays a vital role because CO₂ is an odourless indoor contaminant that poses a health risk for the indoor occupants (Suzuki et al., 2021).

Over the past decade, membrane separation technology has gained significant interest from both academics and industry as a promising alternative for producing oxygen-enriched air. A study conducted by the United States Department of Energy ranked a polymer with high selectivity for separating oxygen and nitrogen gases as the fifth highest priority research area for membrane technology (Baker, 2002). Despite significant efforts by commercial and research institutions to develop polymeric membranes that are both economically feasible and capable of achieving high levels of

permeability and selectivity on a large scale, to date, there is still no commercially feasible membrane that has been successfully produced. The polymeric membrane always has the limitation between permeability and selectivity as these two parameters are always inversely proportional (Edens et al., 2023). In view of this, the focus of this study was to conduct a comprehensive investigation on the impact of fabrication parameters, specifically the influence of polymeric materials and bore fluid flow rates, on the properties of the membrane. This research aimed to elucidate the relationship between these parameters and their subsequent effects on the membrane performance in the gas separation.

MOF is made from the linkage of inorganic and organic units by tough bonding through reticular synthesis. It consists of a metal ligand complexes framework connected with organic linkers to form a porous structure (Shi et al., 2021). MOF possesses the characteristics of high porosity, permanent pore with size ranging from micro to meso scale, high surface area and good thermal and mechanical stabilities. Previous literature reported that thousands of MOFs have been developed and widely applied in catalyst, drug delivery, sensor technology and microelectronics (Wang and Astruc, 2020). The versatility of the MOF materials has caught the attention of the researchers to examine further the possibility of integrating MOF in the membrane for gas separation. The commonly used metal precursors in MOFs for CO₂ adsorption are copper and chromium, which were investigated in this study alongside with trimesic and terephthalic acid as organic ligand to evaluate their performance in CO₂ gas adsorption.

1.3 Problem statement

Nowadays, the gas separation process involves various industrial applications such as hydrogen separation, CO₂ separation, O₂/N₂ separation, and dehydration of air. Several techniques involving gas separation from the air have been widely used in the industry, such as PSA and cryogenic distillation for O₂ production. However, these techniques require high energy consumption in O₂ production. Undoubtedly, membrane separation has started to gain attention from the academics and industry in gas separation due to its relatively low energy requirement and ability to provide optimum performance under long term operation. Although there are advantages of the membrane separation in the gas separation, a breakthrough performance from the membrane from the Roberson upper bound (selectivity versus permeability plot) is highly required for superior performance in the gas separation. Presently, prior research efforts have assessed the fabrication parameters governing the production of high-performance hollow fiber membranes, particularly in terms of gas permeance and selectivity. However, bore fluid flow rate, which is one crucial parameter that can significantly influence the properties of the resulting membranes, remains relatively underexplored according to the literature. Concurrently, it is well-established that both PDMS and PEBAX exhibit commendable attributes as polymeric materials for membrane fabrication in gas separation applications, notably excelling in permeance and selectivity. Conversely, alternative membrane materials like PSU and PEI possess notable mechanical strength which is a paramount characteristic, especially in gas separation scenarios where the inherent

properties of dense, low-diameter hollow fibers favor superior gas permeance performance. In light of these considerations, the academic community has expressed growing interest in investigating the performance of dual-layer membranes featuring PDMS or PEBAX coatings for gas separation applications. This endeavor seeks to comprehensively evaluate the performance of membrane in gas separation.

As humanity strives to minimize outdoor air pollution in order to prevent irreversible damage to the environment, the issue of indoor air pollution is receiving increasing attention due to its significant impact on human health. With people engaged in various indoor activities daily, indoor air pollution has become a dominant source of exposure. The harmful effects of indoor air pollution are largely attributable to changes in construction materials, consumer products, and building operations. Shockingly, indoor air pollution exposure leads to the deaths of an estimated 4.3 million people worldwide every year (Lancet, 2020). In indoor air quality improvement, the multi-disciplinary phenomenon is involved and determines several pathways such as chemical, biological and physical contaminants. One of the strategies to improve the indoor air quality is to increase the O_2 content in the indoor space to enhance the freshness of the occupants and reduce the CO_2 concentration . MOFs have emerged as highly promising materials for physical gas adsorption, for example they have notable CO_2 adsorption capacity. MOFs fabricated with various metal precursors, including iron, aluminum, magnesium, copper, and chromium, have demonstrated commendable performance in gas adsorption applications. Of particular note,

copper and chromium metal precursors have garnered substantial attention due to their ability to yield MOFs with exceptional CO₂ adsorption performance. Extensive research in the literature have demonstrated the fabrication of MOFs utilizing either copper or chromium in conjunction with organic ligands such as BDC or BTC for gas separation purpose. Up to date, limited research has been carried out to assess the CO₂ adsorption by copper and chromium metal precursors using either BDC or BTC as organic ligands, specifically in terms of their molar ratio, which remains as an interesting topic to be explored to further understand its behavior.

1.4 Aim and objectives

The aim of this research project was to improve indoor air quality by utilizing membrane technology to separate oxygen and carbon dioxide from ambient air. The following are the specific objectives:

1. Examine the effects of polymer materials (i.e., polysulfone and polyetherimide), bore fluid flow rate (during spinning process) and coating concentration (post-treatment) on the properties of hollow fiber membrane for O₂/N₂ gas separation.
2. Determine the effects of metal precursor and organic ligand on the MOF synthesis and the properties of MOF for CO₂ gas adsorption.
3. Evaluate the integrated performance of dual-layer hollow fiber membrane and MOF for indoor O₂ enrichment and CO₂ reduction, respectively in actual indoor environment.

1.5 Scope and limitations of the study

In this project, two techniques were suggested for the improvement in indoor air quality in terms of the O₂ and CO₂ contents in the air. Firstly, the O₂ and N₂ gas separation performance of the self-fabricated hollow fiber membrane with different polymeric and coating materials was studied. The selected polymeric materials were PSU and PEI, with N,N-dimethylacetamide (DMAc) and ethanol (EtOH) as the solvents, and tetrahydrofuran (THF) as an additive. The bore fluid flow rate was precisely configured at 0.3, 0.7, and 1.0 mL/min in order to mitigate potential adverse effects on the membranes, including the occurrence of surface defects, which could arise from excessively high bore fluid flow rates (i.e., more than 1.0 mL/min). Subsequently, the membrane with the best performance from each polymeric material was further used to investigate the performance of dual-layer membrane, where the membrane was coated with either PDMS or PEBAX to evaluate its performance in terms of its gas permeance and selectivity. The weight percentage of PDMS and PEBAX was controlled no more than 5%, as higher weight percentages could result in a negative effect in thickness, leading to reduction in gas permeation as reported in the literature (Zulhairun et al., 2015). The experimental study on gas separation was carried out with single gas (i.e. oxygen or nitrogen gas). Secondly, metal organic frameworks fabricated with different molar ratios of metal precursor (copper or chromium) to organic ligand (terephthalic acid, BDC or trimesic acid, BTC) were studied based on their physiochemical properties. The molar ratios of metal precursor to organic ligand were set at 1:1, 1:2, 1:3, 1:4 and 1:5, respectively to evaluate

its effect on the fabricated MOFs. The next step involved investigating the efficacy of the metal-organic frameworks for CO₂ adsorption by analyzing its performance under varying molar ratios. Lastly, the dual-layer membrane and metal organic framework were used to evaluate their performance on the indoor air quality enrichment in the actual indoor environment with no dehumidification.

CHAPTER 2

LITERATURE REVIEW

2.1 Overview of indoor air quality and its effect on human health

The atmosphere forms a layer of gases that protects the Earth by absorbing ultraviolet light generated from the Sun and acts as a conductor to reduce the temporal temperature between. By nature, the air in the atmosphere consists of 78% of N₂, 21% O₂ and 1% of other gases. O₂-enriched air can replenish and/or increase the indoor O₂ level, which will lead to good indoor air quality for the betterment of the dweller. Air pollution is a severe risk to human health, and this topic has been broadly discussed in developing countries like Malaysia and China. The Global Burden of Diseases Study conducted in 2019 suggested that 4.3 million out of 6.85 million deaths related to air pollution worldwide were caused by indoor air pollution (Wang, 2020). The pollution will affect human health, leading to lung cancer, pneumonia, and other respiratory tract infections. One of the major indoor air pollutants is CO₂. The reduction of CO₂ and introduction of O₂-enriched air can decrease indoor air pollution and enhance IAQ. In most countries, strict imposed strict law and regulations are imposed to limit the CO₂ concentration in indoor air conditions. For instance, the Department of Occupational Safety and Health, Malaysia and ASHRAE Standard 62-2007 cap 1,000 ppm as ceiling limits to ensure that the occupants are not exposed to the hazardous indoor environment (The

American Society of Heating, Refrigerating and Air-Conditioning Engineers, 2007; Department of Occupational Safety and Health, Malaysia, 2010).

Maintaining high oxygen levels within indoor spaces is paramount for human well-being. Elevated oxygen concentrations not only enhances cognitive function by improving attention and problem-solving skills, but also bolsters physical performance. Moreover, a well-oxygenated environment aids in bolstering the immune system, helping the body fend off infections more effectively. In summary, maintaining high indoor oxygen levels is instrumental to optimize human health and overall well-being. Oxygen gas enrichment techniques like pressure swing adsorption (PSA), membrane separation, and cryogenic distillation play a vital role in various industries. PSA utilizes adsorbent materials to selectively remove nitrogen from air, providing a continuous supply of oxygen-enriched gas. Membrane separation relies on semipermeable membranes to separate oxygen from other gases, offering a compact and energy-efficient solution for moderate enrichment needs. On the other hand, cryogenic distillation cools air to cryogenic temperatures and distills it to produce high-purity oxygen.

CO₂ can be encapsulated by different techniques, for example, solvent adsorption, physical adsorption, and membrane technology. Conventionally, the solvent adsorption method has been widely utilised in commercials for over 50 years, and this method is primarily based on the chemical solvent, namely monoethanolamine (Chuhadiya et al., 2021). This method used the aqueous amine solution with a 20 to 30% concentration to collect CO₂ gas in the gas adsorption tower. This method, however, is not commercially viable to be applied in the CO₂ removal for IAQ improvement as it involves high

capital cost and intensive energy requirement (Abdul et al., 2020). MOF has been a recent interest arising material for CO₂ adsorption attributed to its high tunability flexibility in gas adsorption. The properties of the MOF can be manipulated by adjusting the fabrication materials such as the choice of fabrication technique and type of metal oxide and organic ligand (Ahmad et al., 2020). For this reason, it has spurred much attention from the academic and industry on the exploration for the chance of commercialisation feasibility.

2.2 Oxygen/Nitrogen (O₂/N₂) separation techniques

Conventional methods for generating oxygen gas, such as pressure swing adsorption (PSA) and cryogenic distillation, are recognized for their substantial energy requirements. Conversely, membrane technology presents a more economically viable option characterized by lower energy consumption. Nevertheless, the effectiveness of gas separation, as measured by permeance and selectivity, remains constrained by the upper boundaries which is commonly referred to as Robeson's upper bound. The comparison of the pros and cons of each technique were tabulated in Table 2.1.

Table 2.1 Comparison of PSA, cryogenic distillation and membrane technology in gas separation

Method	Advantages	Disadvantages
Pressure swing adsorption	<ul style="list-style-type: none"> • Ease of installation and start up • Rapid plant start up and shut down • High purity gas production 	<ul style="list-style-type: none"> • High operation cost attributed periodical adsorbent replacement • Complex process control • Limited scale up ability due to limitation of adsorbent capacity
Cryogenic distillation	<ul style="list-style-type: none"> • High purity gas production • Ability to produce liquid gas on site • Scalable in term of size to meet large or small production 	<ul style="list-style-type: none"> • Energy intensive • High complexity as its required specialized equipment • High initial cost • Slow in plant start up and shut down
Membrane technology	<ul style="list-style-type: none"> • Low capital cost • Small footprint • Ease of installation and start up • High degree of customization depending on production needs 	<ul style="list-style-type: none"> • Low gas purity • Moderate gas separation efficiency • Pre-treatment of feed gas is required to remove contaminates

Cryogenic distillation is a separation technique identical to the concept of a distillation system where the fluid is separated according to the difference in boiling point. This method is widely used to produce O₂-rich air where it can produce O₂ gas with a high purity level up to 99.9% and a good production capacity at more than 100 tonnes per day (Chen and Yu, 2021). In addition to the application of O₂/N₂ gas separation, cryogenic distillation is also commonly used to recover H₂ gas in the oil and gas industry (Wang, 2020). In the gas separation by cryogenic distillation, the ambient air is drawn into the column using a compressor. The air passes through the air filtration system to remove contaminants such as particles and water vapor (Figure 2.1). The compressed air is cooled down below 0°C at the cryogenic temperature, liquefying the air. The O₂ gas with a higher boiling temperature exists the column at the bottom, whereas N₂ gas leaves at the top. The product (N₂ or O₂ gas) will be collected in a storage tank before the purification process to obtain a high purity gas (Lulianelli and Driolli, 2020). Despite the advantage of large daily gas volume production, this method also possesses some drawbacks, including high space requirement for the setup and extensive energy consumption in regeneration (Luyben, 2018).

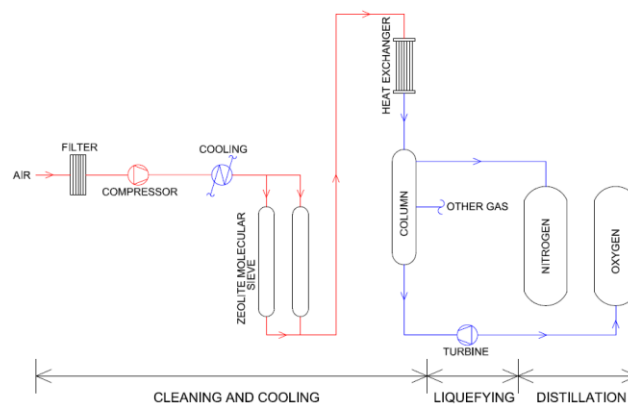


Figure 2.1 Schematic diagram of cryogenic distillation process (Chong et al., 2020)

Skarstrom patented the PSA method in O₂ enrichment to obtain O₂ gas in 1960 (Kamin, Bahrun and Bono, 2022). Since then, the PSA experienced rapid development in O₂ gas production, attributed to its high O₂ purity at 99%. Nevertheless, the production volume of PSA is relatively lower than cryogenic distillation with a daily O₂ gas production between 30 and 100 tonnes which is suitable for medium-scale production (Chin et al., 2023). The typical construction of the PSA gas separation method comprises two absorption columns containing gas absorbents in the column, such as zeolite (Figure 2.2) (Chin et al., 2023). As the PSA process is an energy extensive gas absorption method and substantial gas is lost to the atmosphere during the desorption, the vacuum swing adsorption (VSA) was introduced (Shen et al., 2018). The process is carried out in the vacuum condition instead of the pressurised column to reduce the energy used, while preserving equivalent production output (Rumbo et al., 2022).

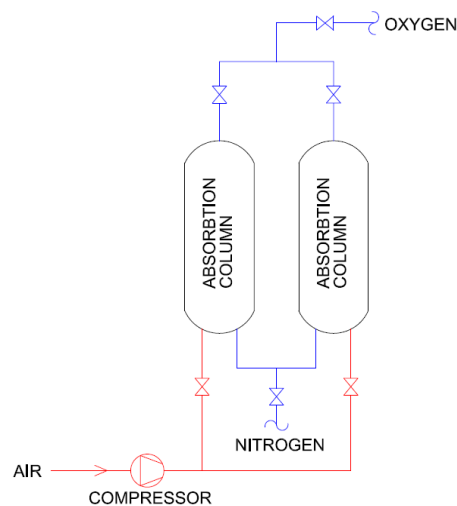


Figure 2.2 Schematic diagram of pressure swing adsorption process (Chong et al., 2016)

Membrane gas separation is a process that works on the principle of pressure difference, where the gas moves from an area of higher pressure to an area of lower pressure through a semi-permeable membrane. The gas molecules are absorbed into the membrane layer, diffuse through it, and finally desorbed at the other end of the membrane. The desired gas is collected at the gas-enriched portion and collected downstream of the process. To maintain the pressure difference across the membrane, a vacuum pump is used, which enables the products to flow under the desired pressure (Liu et al., 2022)

Currently, the use of membrane technology in large-scale industrial gas separation is still uncommon, whereby this technique is only limited to the low volume gas production from 10 to 25 tonnes of daily production (Sasikumar, 2018). Theoretically, the polymeric membrane shall possess high selectivity of the desired gas produced, good thermal and mechanical stability, and competitiveness (Valappil, Ghasem, and Al-Marzouqi, 2021). These membrane characteristics are generally affected by the type of polymer used as dope solution as different polymers may have discrete porosity, morphology, and cross-linkage. Apart from its current drawbacks, membrane technology is gaining interest from academia and industry due to its several advantages over traditional methods like PSA and cryogenic distillation, including energy efficiency, compact design, continuous operation, adjustable selectivity, lower maintenance, and ease of operation. These advantages make membrane technology an attractive choice for various gas separation applications (Deng et al., 2021)

2.3 Membrane technology

2.3.1 Membrane fabrication methods

Membrane fabrication parameters will affect the performance of the membrane because the porosity, morphology and structure are greatly dependent on the condition controlled during the fabrication process, such as winding speed and bore fluid velocity. A wide range of fabrication methods can be found in membrane fabrication, such as phase inversion, interfacial polymerisation, electrospinning and melt pressing (Deng et al., 2021). Among the various fabrication methods, phase inversion and electrospinning are commonly employed techniques for membrane fabrication in gas separation.

During the phase inversion stage, a flat blade is used to synthesize spiral wound or flat sheets membranes onto a backing material with pores. In contrast, the casting of hollow fiber membranes is carried out by extrusion using a hollow fiber spinneret (Figure 2.3) (Chong et al., 2017). The fabricated membrane is then put into a non-solvent coagulation bath, which is typically a water bath. This immersion process allows the exchange of solvent-nonsolvent to transform the dope solution into solid state. This is also known as the demixing process in which the evaporation of solvent happens, resulting in the solidification of the polymeric membrane (Tang et al., 2021).

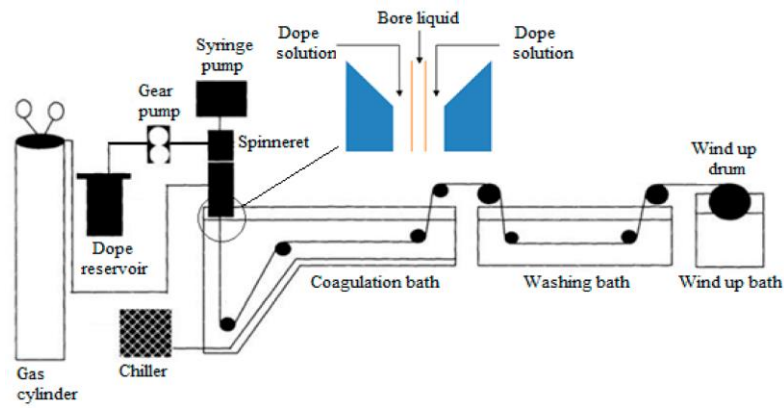


Figure 2.3 Schematic diagram of phase inversion setup for the fabrication of hollow fiber membrane (Chong et al., 2017)

The gas separation performance is greatly dependent on both the spinning parameters and type of materials used. Table 2.2 summarizes the impact of spinning parameters on various aspects of hollow fiber structure, morphology, diameter, selective layer thickness, and gas separation performance. As shown in Table 2.2 composition of the dope solution plays a pivotal role in the phase inversion process, which in turn affects the structure and morphology of hollow fibers. Additionally, increasing the solvent concentration in the bore fluid is associated with the creation of a loose skin layer on the inner surface and the suppression of finger-like macro-voids.

Moreover, spinning parameters significantly influence hollow fiber structure. Parameters like the air gap and extrusion rate impact the orientation of polymer molecules within the selective layer and the thickness of the skin layer. Meanwhile, the flow rates of the dope solution and bore fluid have notable effects on both the outer and inner diameters of the hollow fibers, as well as the thickness of the fiber wall and skin layer. Therefore, it is evident that the careful design of the composition of the dope and bore fluid, along

with the optimization of spinning parameters, are critical factors in the production of hollow fiber membrane that exhibit superior gas separation performance.

Table 2.2 The effect of fabrication parameter on hollow fiber membrane characteristics (Li et al., 2021)

Fabrication parameter	Effect on hollow fiber membrane characteristics
Dope flow rate	Increase in the flow rate of the dope solution results in larger outer and inner diameters and a thicker fiber wall.
Bore flow rate	Raising the bore flow rate results in an increase in both the outer and inner diameters of the hollow fiber, while reducing the thickness of the fiber wall and the dense layer within it.
Extrusion shear	Increasing extrusion shear leads to a reduction in the thickness of the active layer, an elevation in gas permeance, and higher selectivity compared to the intrinsic characteristics of amorphous membrane polymers.
Air gap distance	Raising the air gap during the spinning process leads to several outcomes, including reduced gas permeance, increased selectivity, decreased thickness of the hollow fiber wall, heightened thickness of the skin layer, and improved mechanical properties.
Curing time	Extended curing time results in detrimental effects by causing the intrusion of undesirable non-solvent substances from the inner lumen of the hollow fiber.

2.3.2 Polymeric materials

The common polymeric materials applied in membrane fabrication for gas separation purposes include polyimide, polysulfone and polyetherimide. All these polymers are made up of different repeating units. Hence, the structures of membranes are highly dependent on the chosen polymeric material. Consequently, the decision made during the selection of polymeric material for the membrane fabrication is crucial as it will affect the performance of the membrane in gas separation.

2.3.2.1 Polyimide

Polyimide (PI) is an attractive membrane material for gas separation owing to its excellent chemical stability and heat resistance (Sanaeepur et al., 2019). The building block or monomer of polyimide is imide which is made up of diacid and diamine through amic acid intermediate. Figure 2.4 shows the chemical structure in which the hydrocarbon group (R) can be represented by a linear chain or cyclic hydrocarbon (Babu et al., 2018). Polyimide membrane is typically used in both OEA production and carbon capture process. It can provide good permeability and selectivity of gases which can be further improved through fluorination. Alqaheem and Alomair (2019) reported that the addition of 2,2-bis(3,4-dicarboxyphenyl) hexafluoropropanedianhydride (6FDA) during the fluorination process in PI fabrication led to an increase of permeability in binary gas separation (Alqaheem and Alomair, 2019).

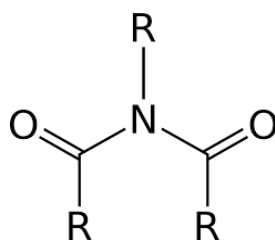


Figure 2.4 Chemical structure of imide (Chong et al., 2016)

Aromatic polyimides commonly show relatively better selectivity and permeability than linear polyimide due to stronger intermolecular bonds between chains. An example of industrial aromatic polyimides used in the membrane separation process is Matrimid[®] with the structure shown in Figure 2.5. It is composed of DAPI known as diaminophenylindane and 3-3'-4-4'-benzophenone tetracarboxylic dianhydride, (BTDA). The structure of Matrimid[®] gives rise to better mechanical strength. Besides the high glass transition temperature (T_g) property makes it suitable to be used under high temperature. Matrimid[®] is also a favourite material used to manufacture membrane for separation due to its good solubility in the organic solvent (Xu et al., 2021). Sari et al. (2019) reported the O_2 permeance, N_2 permeance, and O_2/N_2 selectivity of pristine PI membrane were recorded at 8.57, 2.09 and 4.11 GPU, respectively. It is interesting to note that similar membrane with PDMS coating can improve the O_2/N_2 selectivity from 4.11 to 7.46 arisen from the improvement of the surface by PDMS coating. On the other hand, Himma et al. (2016) found that the O_2 and N_2 permeance of the pristine PI membrane for gas separation ranged from 0.94 to 71 GPU and 0.12 to 14.1 GPU, respectively, with a selectivity range of 5.0 to 8.4.

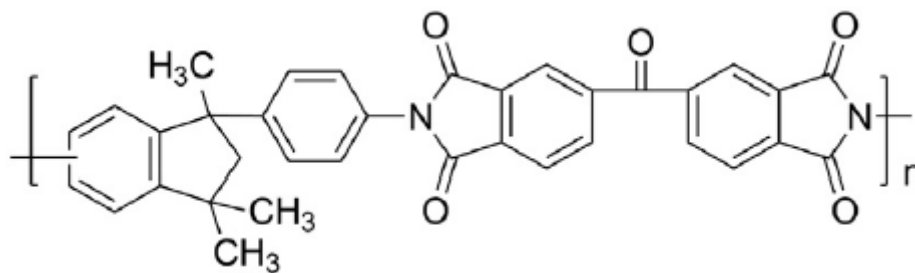


Figure 2.5 Chemical structure of Matrimid[®] (Chong et al., 2016)

2.3.2.2 Polysulfone

Polysulfone (PSU) is one of the polymers that is extensively applied in commercial membrane technology. The PSU monomer is made up of diphenylenesulfone with the structure of aryl-SO₂-aryl (Figure 2.6) (Serbanescu, Voicu and Thakur, 2020). PSU is produced from a dihalogenateddiphenylsulfone and a bisphenol condensation reaction. Vitrex[®] PES and Radel[®] R are the typical commercial polysulfone polymer that are commonly used in the industry. In the late 1970s, the first application of polysulfone in the membrane separation industry was implemented by Monsanto Corporation in a large-scale pilot plant. Nowadays, PSU is widely utilised in the gas separation industry, such as carbon capture, hydrogen recovery, and air separation (Zulhairun, 2015). The properties of PSU, such as high mechanical strength, high rigidity, and good chemical stability, are enhanced by the repeating phenylene ring structure. However, the gas permeability can be varied by modifying the bonding between phenyl rings. Also, the presence of functional groups on the phenyl rings has a notable impact on the gas transport properties of the PSU membrane. For instance, the chain mobility declines due to the incorporation of a trimethylsilyl group

through an ether linkage. Consequently, the rigidity of polysulfones is further enhanced, which influences the membrane performance in the gas separation process (Yuan et al., 2023). Dey and co-workers studied the effect of covalent triazine framework (CTF-1) loading on the PSU membrane on the performance of the PSU membrane in O₂/N₂, CO₂/N₂ and CO₂/CH₄ binary gas pair separation (Dey et al., 2019). The results obtained by Dey et al. (2019) recorded the range of 32 to 54 GPU and 3.57 to 7.44 GPU for O₂ and N₂ gas permeance, respectively with the selectivity ranging from 5.0 to 5.4. Their study also found that 24 wt% loading of CTF-1 yielded the best result due to the enrichment of the membrane surface and affinity of gas separation.

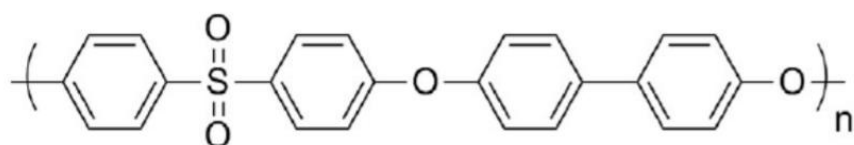


Figure 2.6 Repeating units of polysulfone (Chong et al., 2016)

2.3.2.3 Polyetherimide

Polyetherimide (PEI) is a thermoplastic developed from polyimide to overcome its drawback of the low shaping and processing ability attributed to low flexibility (Jamil et al., 2018). Ether group (R-O-R') is added to the polyimide structure to improve the higher flexibility in melting, improving the shaping capabilities and enhancing the mechanical and thermal stability. The chemical structure of polyetherimide (C₃₇H₂₄O₆N₂)_n is commonly produced with condensation reaction (Figure 2.7). Polyetherimide was first developed by General Electric in 1980 and marketed under the tradename of Ultem®.

Polyetherimide is widely used in the automotive and medical industry to make car lamps and medical tools in commercial applications (Ma et al., 2020). Alqaheem and Alomair (2019) reported that polyetherimide possessed superior permeability in various binary gas pair separations, including O₂/N₂ gas separation. Nevertheless, the improvement in the membrane was recommended due to the trade-off in selectivity.

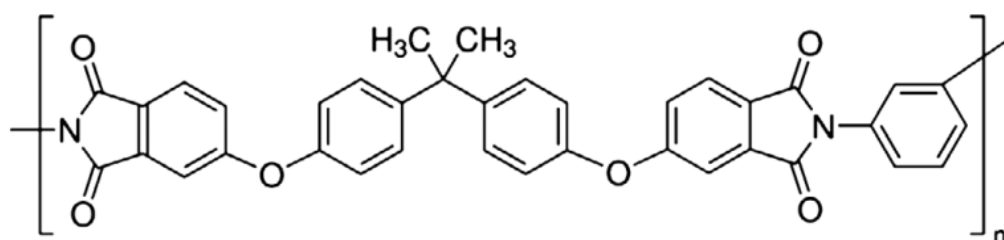


Figure 2.7 Structure of polyetherimide (Chong et al., 2016)

2.3.4 Membrane performance and Robeson upper bound

The principle of membrane technology in gas separation is widely discussed in literature studies. The separation mechanism can be generally categorised into the flow model governed by either porous or non-porous membrane (Yong and Zhang, 2021). The pore flow and solution diffusion models are the mass transport models proposed in the membrane separation. The pore flow model describes the flow of the particles over the membrane layer with the assumption of the layer as micropore. In contrast, the solution diffusion model evaluates the particle flow across the membrane, which is dense without pores. Unlike the water separation using membrane technology, the non-porous membrane possesses its advantage compared to the porous membrane in binary gas separation due to lower gas leakage and higher mechanical strength (Ding et al., 2019). Thus, the solution diffusion model is

more preferable in gas separation. There are three phases involved in this model, and firstly, the gas particles move from the ambient to the boundary layer of the membrane. Secondly, the particles diffuse over the membrane layer, and lastly they are desorbed to a lower pressure regime.

The permeability and selectivity are significant indications for evaluating the gas separation performance. Good permeability allows more gas to be collected as products and good selectivity denotes superior separation between binary gases (Kamble, Patel and Murthy, 2021). The academic and industrial researchers are focusing on improving selectivity for more superior gas separation to obtain higher purity of products and improve the permeability, pushing higher gas production capability in the route of commercialization (Kamble, Patel and Murthy, 2021). Nonetheless, the gas separation performance using membrane technology is constrained by compromising permeability and selectivity where these two parameters are always inversely proportional relationships. Robeson is the first membrane technologist who proposed this idea in 1980. He plotted the Robeson upper bound, showing the trade-off between permeability and selectivity from various membrane materials with different gas separation pairs such as O₂/N₂ gas. The upper bound is plotted in the logarithm line graph, comprising data collected from literature studies under constant operating parameters. The upper bound was later revised in 1991 and 2008 by Robeson with the improvement of membrane technology in terms of materials and setup of the separation techniques (Robeson, 1991; Robeson, 2008).

2.3.5 Dual-layer composite membrane

Nanocomposite membrane attracts the attention from the academia and industry owing to its customisation ability in superior separation performance and improved anti-bacteria capability (Sarkar and Chakraborty, 2021). To date, there are various polymeric materials evaluated in scientific research. Amongst all notable nanocomposite layers are metal organic frameworks (MOF), rubber (PDMS) and poly(ether block amide) (PEBAX) (Chong et al., 2016). The thin composite layer generally consists of porous and non-porous materials. The porous coating can enhance the separation performance, and usually record permeability performance near or surpasses the upper bound limit line. But the major setback of the porous membrane is that gases are allowed to transport across the membrane layer, resulting in low selectivity of the binary gas pair. Thus, careful porosity control is essential to obtain an optimum level to balance the trade-off between permeability and selectivity.

On the contrary, the non-porous nanocomposite layer can improve the surface defect, enhancing tortuosity by improving the diffusion path to reduce the flow of sizable particles through the membrane. However, the literature suggested that the non-porous composite layer recorded increased in the selectivity due to the selective layer (Alobaidy et al., 2017). Still, the reduction in the non-porous layer increased mass transfer resistance, resulting in fewer molecules to diffuse across the membrane (Lai, Chong and Lau, 2020). The performance of the dual-layer membrane in O₂/N₂ gas separation in the recent literature is summarized in Table 2.3.

Table 2.3 Comparison of O₂/N₂ gas separation from hollow fiber membrane

Membrane	Permeance (GPU)		α_{O_2/N_2}	Reference
	O ₂	N ₂		
PEI/PDMS-CoTPP	53	19	2.8	Park et al., 2019
PEI/MIL-53	5.0	0.8	6.2	Chi et al., 2020
PIM/HMDA/HKUST-1	74.2	18.5	4.2	Fuoco et al., 2017
PIM/PDMS/PAN	69	21	3.2	Choi et al., 2019
PIM/BTC/HMDA/HKUST-1	46.9	10	4.7	Fuoco et al., 2017
PSU/PDMS	21	11	1.9	Prajapati et al., 2016
PSU/fumed silica	16	2.5	6.4	Li et al., 2021
PSU/ZIF-8	6.1	1.7	3.6	Chi et al., 2020
PSU/MCM-41	2.9	0.7	4.0	Chi et al., 2020
PSU/ETS-10	2.4	0.6	4.1	Chi et al., 2020

2.3.5.1 Polydimethylsiloxane (PDMS)

Polydimethylsiloxane (PDMS) is a rubbery material commonly used as a membrane coating. This particular coating material can improve the membrane's mechanical strength and chemical stability, but it can also provide excellent permeability in gas separation (Yong and Zhang, 2021). The characteristics of PDMS of high permeability are mainly related to the high degree of flexibility from the siloxane linkages (Dong et al., 2020). Despite the high permeability, this coating material can firmly adhere to the support and provide excellent sensitivity by plugging the pinholes and defects (Kamble, Patel and Murthy, 2021). Besides, PDMS coating can repair the defects of the membrane surface, reduce the membrane pores and improve the selectivity in gas separation (Suleman, Lau and Yong, 2017).

Literature studies revealed that PDMS positively affected the O₂/N₂ permeability and selectivity in the PDMS nanocomposite membrane (Dong et al., 2020). At the low PDMS coating concentration, the PSU hollow fiber membrane recorded an increment of 17% on the permeability, while the membrane's selectivity remained. Further increment of the coating concentration to 5% PDMS led to the decrease in permeability (Dong et al., 2020). This study revealed that at an optimum level concentration of the PDMS coating, the superior affinity of this coating on the oxygen gas molecule was likely to improve the permeability of oxygen, while maintaining the permeability of nitrogen. Another attribution on the PDMS coating on the surface of the membrane was believed to enhance the surface morphology by covering the surface defects. However, increasing the concentration of PDMS coating on the polymeric membrane led to a deterioration in the O₂/N₂ separation performance due to the thicker PDMS layer forming, which increased the resistance of diffusivity (Chong et al., 2018).

2.3.5.2 Poly(ether block amide) (PEBAX)

PEBAX, or poly(ether block amide), is a type of polymer that contains both hard and soft segments. The hard segments are made up of polyamide polymer chains, while the soft segments are composed of a polyether section. These hard polyamide blocks contribute to the mechanical strength required for the membrane. Meanwhile, the soft polyether segments allow the components to permeate easily and drive the separation process due to the high chain mobility of the ether linkage (Chong et al., 2018). In short, the

hardness and flexibility of the copolymer are strongly dependent on the total amount of polyamide and polyether within (Yuan et al., 2023). Moreover, these coating materials possess specific resistances to corrosive chemicals and good mechanical stability.

Several studies showed excellent results of separation by membrane coated with PEBAX. For instance, Karim et al. (2021) reported high selectivity for O₂/N₂ gas separation when a series of PEBAX copolymers were applied. Besides selectivity, the membrane's permeability remained acceptable despite the increment of selectivity of the membranes. Wahab and Rahman (2018) experimented to determine the permeation of several gases through PEBAX membranes. Their results showed that the membranes remained high permeability for light hydrocarbons. Kim and co-worker reported their works on the gas separation using PEBAX coated poly(ether imide) (PEI) nanocomposite flat sheet membrane which showed a two-fold increase of the permeability on nitrogen gas relative to the pristine membrane (Afshoun et al., 2019). On the other hand, PEBAX/PEI nanocomposite flat sheet membrane synthesised by dip-coating method recorded an improvement in the permselectivity of binary gas separation. Generally, the incorporation of PEBAX into nanocomposite membrane can improve the amorphous nature of the membrane, increasing the permeance substantially. However, the work done by Chong and co-workers revealed that the PEBAX nanocomposite membrane hollow fiber membrane brought a negative effect on the separation performance on O₂/N₂ gas separation from the rapid gelation of PEBAX on the membrane surface resulted in an increased mass transfer resistance (Chong

et al., 2018). In a nutshell, PEBAX can improve O₂/N₂ gas separation using flat sheet nanocomposite membrane, but further optimisation is essential for nanocomposite hollow fiber membrane on the coating condition due to the circular shape of the membrane. Sections 2.2 and 2.3 provided an in depth and critical review of the O₂/N₂ gas separation and membrane technology. Subsequently in Section 2.4, the metal organic frameworks and their application in CO₂ adsorption were reviewed.

2.4 Metal organic framework (MOF)

MOF is advanced inorganic-organic materials consisting of inorganic nodes and organic linkers that are bonded by covalent bonding. The inorganic nodes are mostly metal ions, comprised of mono-, di-, tris- or tetravalent ligands of O₂. Several studies were carried out to study various MOF due to the many types of metal and ligand (Alqaheem and Alomair, 2019). By incorporating different components, MOF displays unique properties depending on how the components are bonded. The MOF possesses three distinctive features, namely high porosity and surface area, a regulated and adaptable pore structure, and a malleable surface chemistry (Rowaili et al., 2021). The structure of MOF consists of a metal node connected by the organic ligand to form a uniform lattice structure in three dimensions (Figure 2.8) (Lai, Chong and Lau, 2020). Recently, MOF has garnered interest from academics and industry due to its distinct properties, such as porous structure, high degree of crystallinity, and superior surface area. Additionally, tunable property is the most significant advantage of MOF relative to other adsorbents

as one can easily alter the pore size and structure of MOF by modifying the connection between the metal node and organic linker. These tunable properties allows MOF to be applied in various gas adsorption applications, such as methane and CO₂ gas capture.

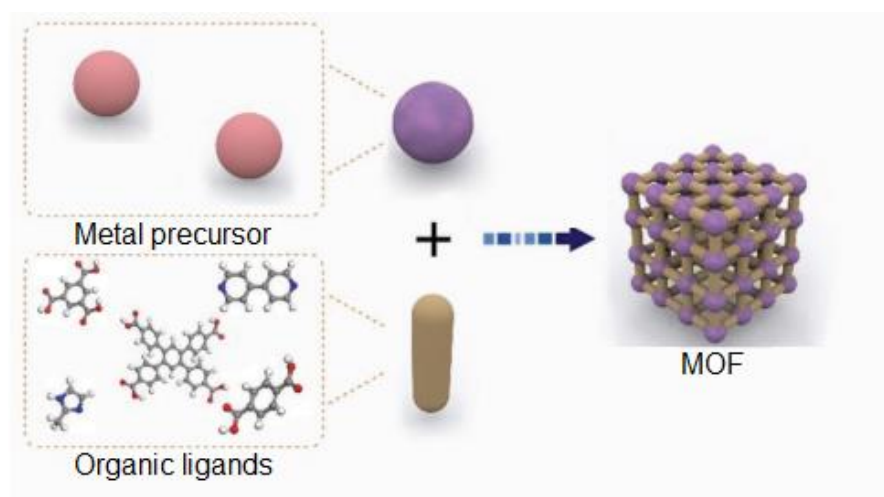
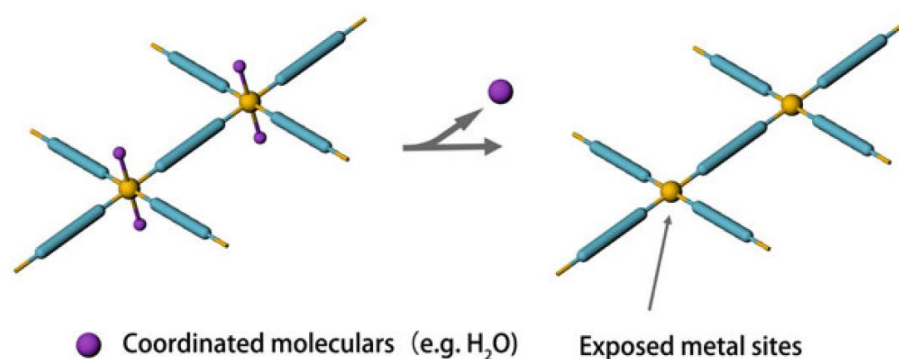


Figure 2.8 Typical structure of MOF (Li et al., 2021)

One important criterion in assessing porous materials is the specific surface area. Adsorbents with a high surface area favour the interaction between active sites and the feed, hence providing property in the gas adsorption performance. MOF exhibits a higher BET surface area between 1,000 and 8,000 m²/g relative to other gas adsorption materials, such as zeolites and activated carbons with a surface area of 500–1,500 m²/g. Over the past decades, the MOF record with the highest BET surface had been constantly broken. At present, NU-100E, synthesised in 2018, has the highest recorded BET surface area of 7,140 m²/g (Xia, 2018). It is expected that the MOF's surface area will continue to increase shortly as more MOFs are synthesised. Another advantage of MOF is the ability to adjust the pore size and shape to meet specific requirements. The interaction between the host and

guest atoms can be optimized by controlling the size and shape of the pores. Most MOF are categorised as microporous materials with an effective diameter of less than 2 nm (Chen et al., 2020). These microporous topologies could enhance the selectivity and performance of gas adsorption.

Porous materials, such as activated carbon and zeolites, have simple and homogenous surfaces. As a result, these materials have limited applications. On the other hand, MOF offers a diverse surface environment to enhance surface functionalisation. This can be achieved by modification of either weakly bonded metal sites or ligands which schematically shown in Figure 2.9(a) and (b) (Xia, 2018). The removal of bonded metal records coordinatively unsaturated sites (CUS) which are capable of interacting with guest molecules to enhance catalytic activity. Furthermore, the modification of functional groups attached to the ligands is responsible for different surface natures, such as charged, acidic, or primary surfaces. Besides, post-synthetic modification (PSM) can be implemented after the complete synthesis of MOF. This strategy involves fine-tuning of original MOF through chemical transformation without changing the initial framework (Wang and Astruc, 2020). The advantage of PSM is the formation of surface structures that cannot be synthesised through conventional methods.



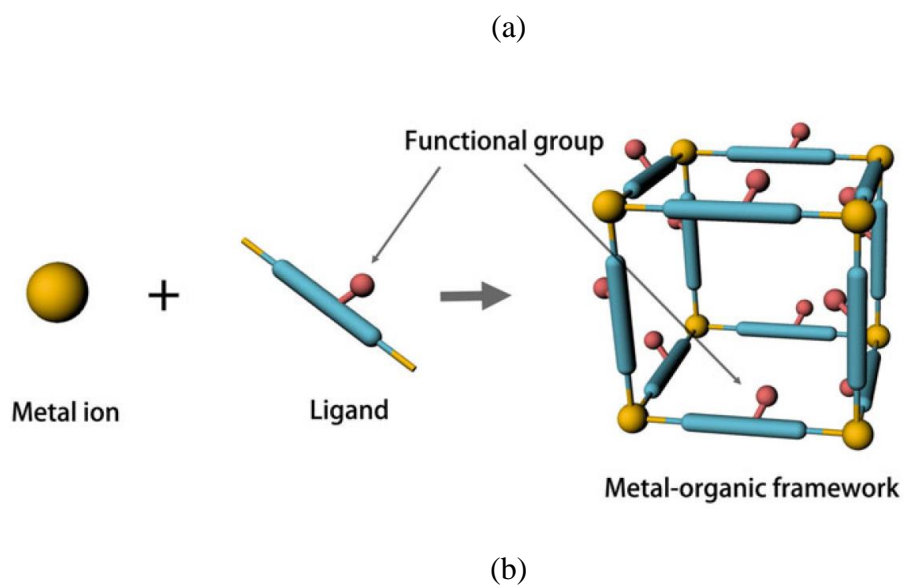


Figure 2.9 Schematic diagram on the modification of (a) metal sites, and (b) ligand (Xia, 2018)

2.4.1 Synthesis methods of MOF

MOF syntheses are categorised into five categories, as illustrated in Figure 2.10, depending on the mode of energy input to form a linkage between metal precursor and organic linker. It is noteworthy to mention that various synthesis methods will eventually influence the size, pore structure, and morphology. In this section, the synthesis methods, as well as their pros and cons, are discussed.

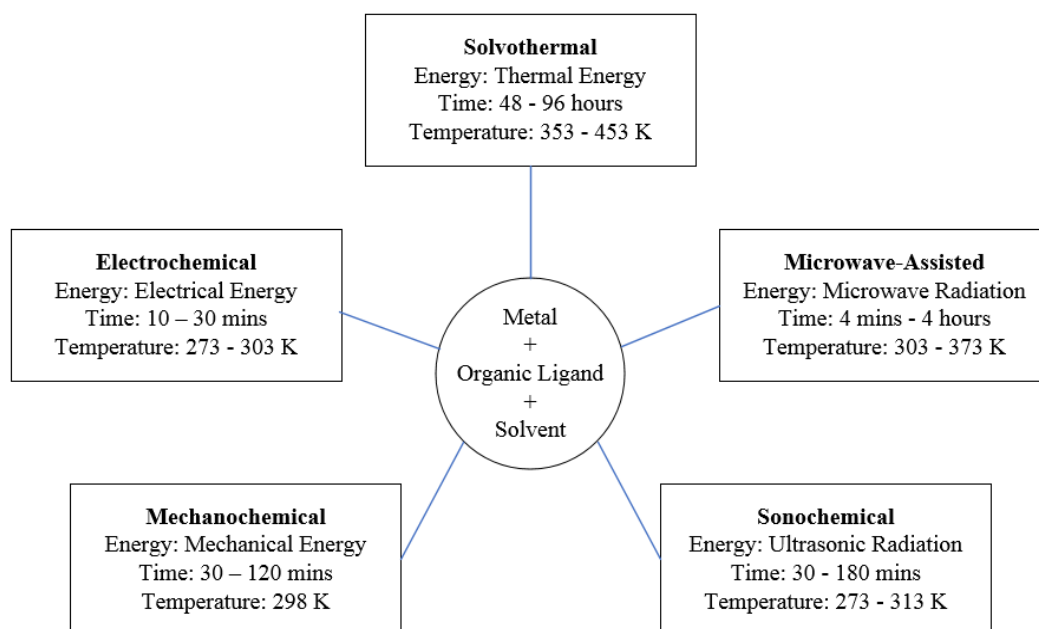


Figure 2.10 MOF synthesis methods and conditions

2.4.1.1 Solvothermal method

The term solvothermal means that solvent is used in the method with heat energy. The types of commonly used solvents are dimethyl formamide (DMF), diethyl formamide, glycol, acetone, ethanol and methanol in the fabrication process (Sud and Kaur, 2021). The main selection criteria of the solvent are the high boiling point and the type of linkage formed with metal precursor. The role of solvents used is to generate uniform pressure during the formation of MOF crystals. Also, mixed solvents are considered to alter the solubility of precursors and the polarity of the solution (Figure 2.11). Metal precursor and organic ligands precursors are homogeneously mixed in solvents with a specific ratio. The mixture is later placed in a Teflon tube and sealed. Subsequently, it is either heated or positioned in closed vessels whereby the formation of MOF crystals takes place under elevated temperature and

pressure. The benefit of this method is the use of low viscosity solvent leads to better movement of precursors, subsequently increasing the rate of crystal formation. Another advantage of this method is relatively more uncomplicated in the preparation compared to other MOF fabrication methods. The solvothermal method, although frequently used in laboratory experiments, is not suitable for industrial scale production attributed to its low efficiency, high energy consumption, and long synthesis time (Al Obeidli et al., 2022).

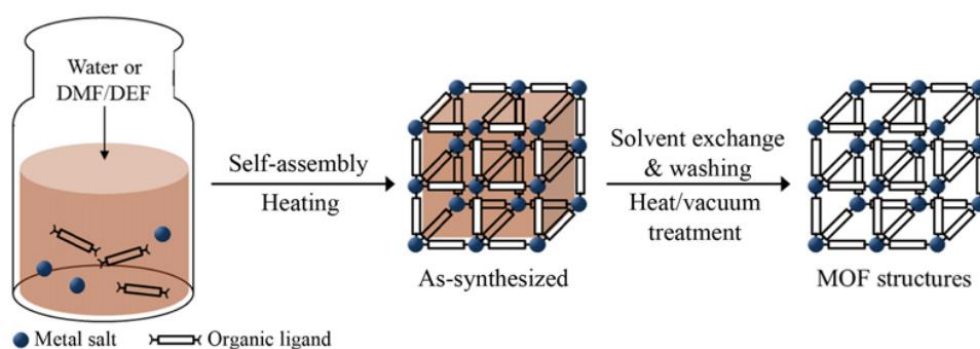


Figure 2.11 Solvothermal MOF fabrication method (Lee, Kim and Ahn, 2013)

2.4.1.2 Microwave-assisted method

The microwave-assisted method utilizes induced microwaves from a magnetron, comprising an oscillator that transforms direct current into frequency radiation. The approach has been extensively utilized in the production of nanoscale materials. The microwave-assisted method has proven to offer a rapid MOF synthesis route, as reported in literature studies (Kumar et al., 2020). The reduction in synthesis time is associated with the solvent-superheating effect. In the microwave, dipole molecules move rapidly due to the oscillation of the electric field. The movement of molecules increases the heating rate of the MOF solvent, increasing the nucleation rate.

Additionally, this method ensures homogeneous heating conditions compared to conventional heating methods. This is because energy from the radiation is directly supplied to the bulk sample, whereas conventional heating methods utilise the external surface. MOFs with consistent size and morphology can be obtained in a shorter preparation time. In the microwave-assisted method, metal salt and organic linkers are mixed and immersed in a solvent (Figure 2.12). The mixture is transferred into a Teflon tube and tightly sealed. The sealed tube is then inserted into a microwave unit and heated for a specific duration. As the microwaves are radiated to the sample, the dipole moments of the solvent molecules tend to rotate and align with the propagated wave. The movement led to friction and dielectric losses in the form of heat. The heating process is further improved through ionic conduction. This is due to collision between ions which generated heat to speed up the synthesis process (Feng et al., 2023).

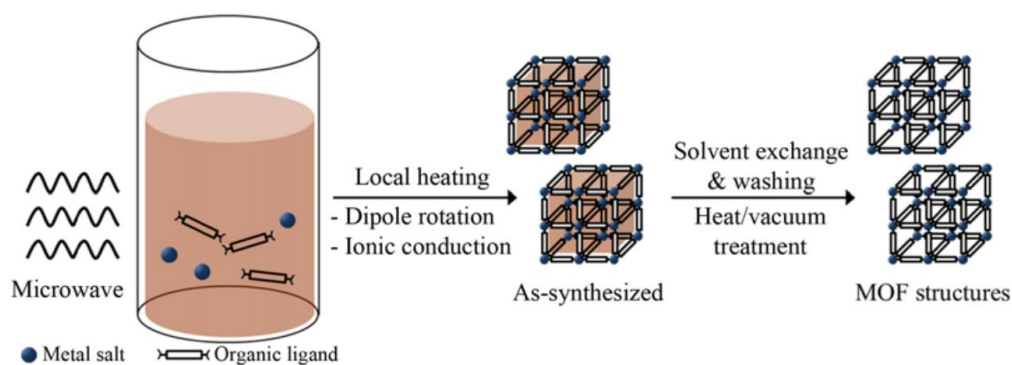


Figure 2.12 Microwave-assisted MOF fabrication method (Lee, Kim and Ahn, 2013)

2.4.1.3 Sonochemical method

The ultrasonic method, also known as the sonochemical method,

involves the use of high-frequency ultrasonic radiation ranging from 20 kHz to 10 MHz to cause physical or chemical modifications in molecules (Figure 2.13) (Lee, Kim and Ahn, 2013). The metal ions and organic ligands mixture undergoes ultrasonic radiation without external heat transfer. The radiation causes acoustic cavitation in the mix, where bubbles (cavities) grow and collapse (Vaitsis et al., 2022). This phenomenon produces high local temperatures and rapid heating and cooling rates, leading to homogeneous nucleation in these cavitation sites, leading to the speedy formation of consistent and more exemplary crystals compared to solvothermal synthesis (Xia, 2018).

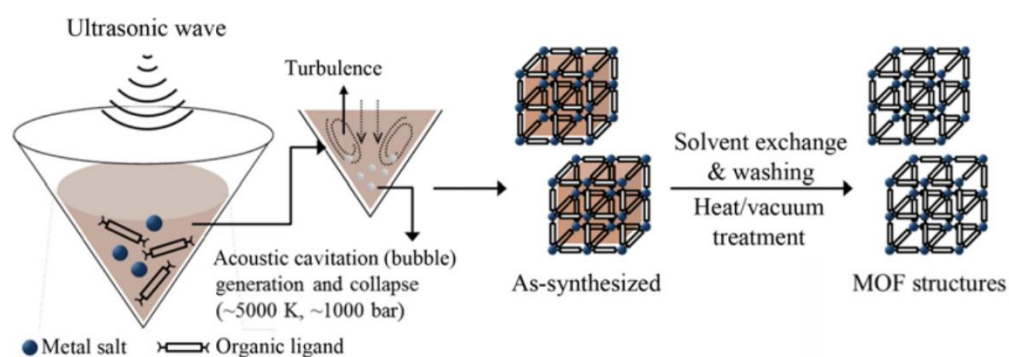


Figure 2.13 Sonochemical MOF fabrication method (Lee, Kim and Ahn, 2013)

2.4.1.4 Electrochemical method

The electrochemical method is a method for MOFs synthesis that utilises two electrodes and an electrolyte (Zhang et al., 2020). In this method, metal ions are continuously formed through anodic dissolution instead of metal salts when voltage is supplied to the electrodes (Figure 2.14). The formed metal ions react with organic linkers dissolved in the electrolyte to form MOF. Deposition of metal on the cathode is avoided through the use of

protic solvents. Synthesis of MOFs is the main advantage of using this method as the synthesis process will be ended when all the precursors are used up. Hence, by replacing metal electrodes and replenishing organic ligands regularly, the process could attain continuous production (Al Obeidli et al., 2022). Moreover, conducting this reaction at low temperature and pressure can result in decreased energy usage. This continuous and low-cost method is highly favourable in the mass production of MOF materials.

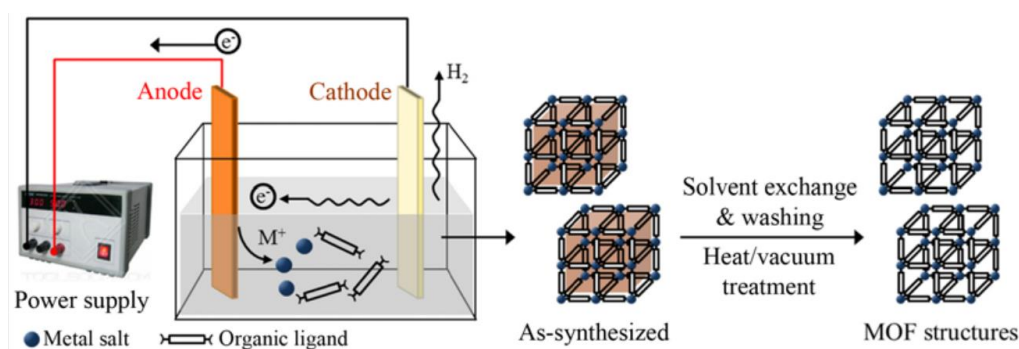


Figure 2.14 Electrochemical MOF fabrication method (Lee, Kim and Ahn, 2013)

2.4.1.5 Mechanochemical method

A mechanochemical method is a form of solid-phase MOF synthesis to avoid the use of solvents and to shorten the reaction time, typically around 10 to 60 minutes. The mechanochemical process entails the chemical conversion followed by the mechanical disruption of intramolecular bonds (Figure 2.15) (Lee, Kim and Ahn, 2013). In the mechanochemical method, metal precursor and organic linkers are contained in a ball mill for grinding. In the ball mill, mechanical energy breaks the intermolecular bonds of the precursors. The

unstable precursors then form new bonds to produce MOFs (Sud and Kaur, 2021). In some cases, liquid-assisted grinding (LAG) may be employed to expedite mechanochemical reactions by increasing precursor mobility through the use of solvents. The advantage of this method is that the reaction can be conducted at room temperature without solvents. Additionally, this method allows a shorter fabrication time to obtain a higher yield of MOF crystals.

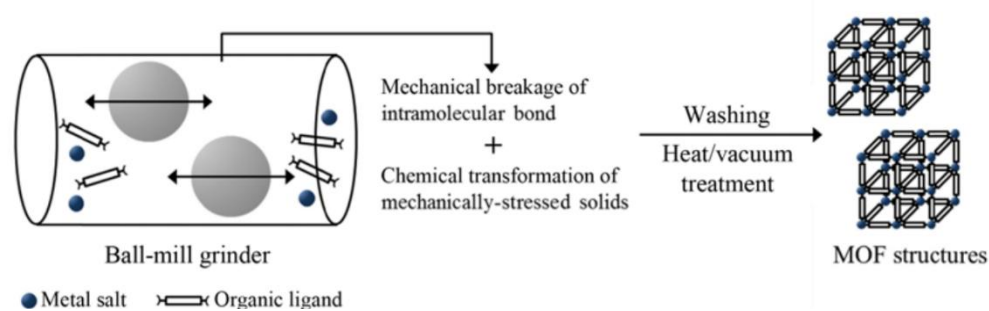


Figure 2.15 Mechanochemical MOF fabrication method (Lee, Kim and Ahn, 2013)

2.4.2 Factors affecting MOF physical properties

MOFs are well known for their tuneable structures. Over the years, new MOFs of various sizes, shapes, and structures are being discovered. The following section will discuss the few factors that affect the MOF structures.

2.4.2.1 Effect of molar ratio

The molar ratio of precursors is one decisive aspect in producing MOFs. The topology and structural features are affected by the availability of precursors. To put this theory to test, Yin et al. (2011) synthesised MOFs from

the different molar ratios of metal and organic ligand. They used Cd(II) salts and 1,2,4 triazole ligand (TAZ). A molar ratio of metal to ligand of 1:1.2 and 1:1.7, $\{[\text{Cd}_3\text{Cl}_3(\text{TAZ})_3(\text{DMF})_2]_n\}$ (1) and $\{[\text{CdCl}_2(\text{TAZ})]_n \cdot n(\text{H}_2\text{O})\}$ (2) were formed, respectively. These MOFs differ in dimensionality, whereby (1) exhibited three-dimensional frameworks while (2) displayed one-dimensional coordination polymer (Yin et al., 2011). Besides, the number of TAZ coordination also dropped from 3 in (1) to 2 in (2). Apart from that, another study conducted on the molar ratio variation was synthesised from Co(II) ions and 1,2-bis(tetrazol-1-yl)ethane (btze). $\{[\text{Co}(\text{btze})_2(\text{SCN})_2]_n\}$ (3) is formed at a molar ratio of metal to ligand of 1:1, while $\{[\text{Co}(\text{btze})_2(\text{SCN})_2]_n\}$ (4) at molar ratio of 1:2. Similarly, (3) from molar ratio 1:1 produces a two-dimensional framework. This is due to the short base ligands which bridge the two-dimensional square grid. Conversely, (4), formed at a molar ratio of 1:2, is made up of three-dimensional structures (Yin et al., 2011).

In addition to the structural differences reported by Yin et al. (2011), Liu et al. (2018) investigated the impact of the molar ratio between the copper metal precursor and benzene-1,3,5-tricarboxylate (BTC) ligand on the physiochemical and carbon dioxide gas adsorption performance. The copper based MOFs in present study were fabricated by copper nitrate ($\text{Cu}(\text{NO}_3)_2$) with BTC at the molar ratio of 1.81:1.0 (Cu-BTC), 1.45:1.0 (Cu-BTC (80%)), 1.09:1.0 (Cu-BTC (60%)), and 0.72:1.0 (Cu-BTC (40%)). It is noteworthy to mention that all the Cu-BTC MOFs in regardless of the molar ratio possessed similar chemical properties in the elemental composition, but different physical properties in terms of degree of crystallinity formed for the MOF

made from copper precursor and different ratio of the BTC ligand (Figure 2.16a) and the consistent pore size distribution in the range from 0.45 to 0.65 nm (Figure 2.16b) (Liu et al., 2018). The Cu-BTC MOF in regardless of the ratio of BTC ligand illustrated a regular square crystal shape, attributed to the fact that the copper metal ion is coordinated by four ligands in a square plane, giving the MOF unit a square-shaped geometry (Figure 2.17) (Liu et al., 2018). It was found that Cu-BTC (60%) recorded the highest CO₂ gas adsorption performance (Figure 2.18), attributed to its h BET surface area and lowest pore size relative to other copper-based MOF with different molar ratio in this study (Liu et al., 2018).

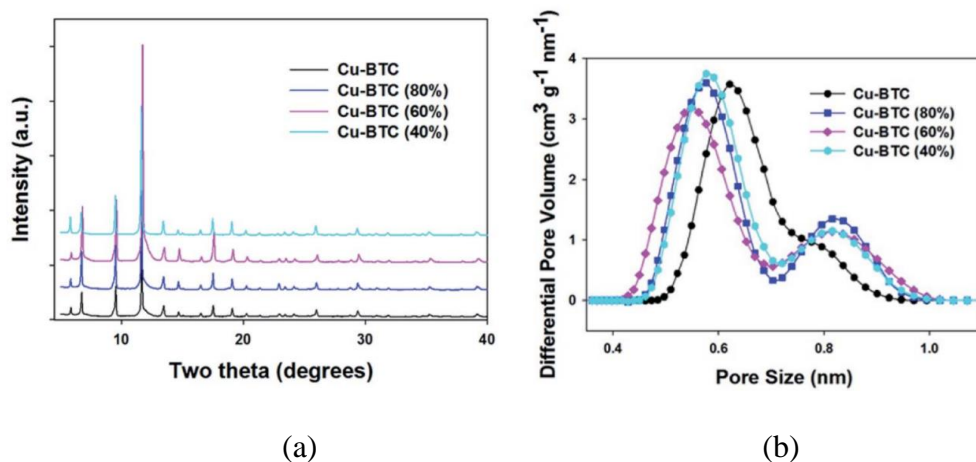


Figure 2.16 (a) XRD analysis and (b) Pore size distribution of copper-based metal organic framework (Liu et al., 2018)

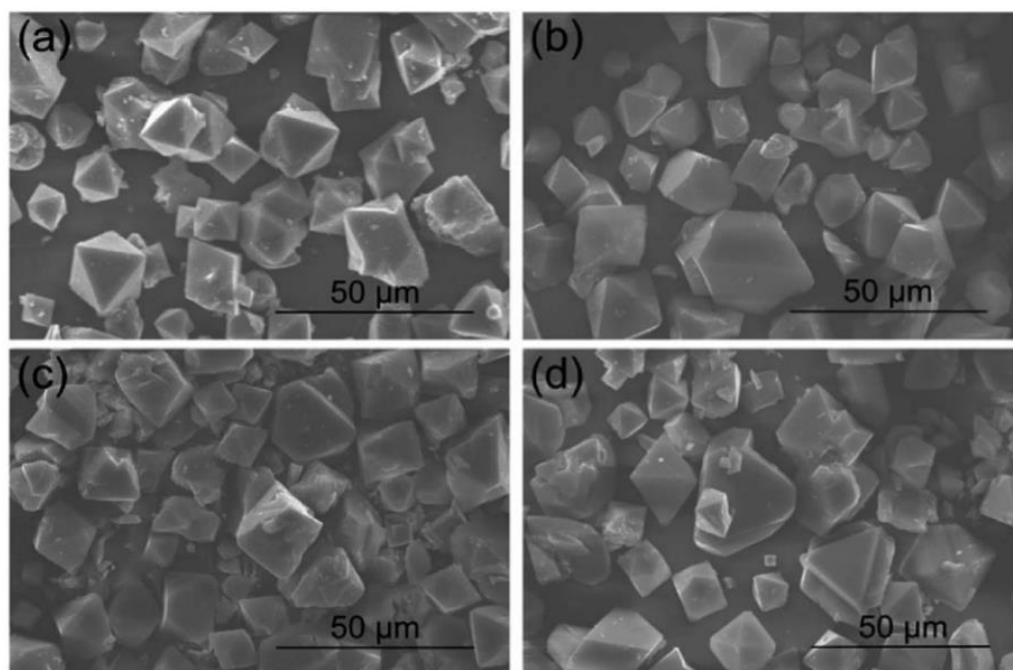


Figure 2.17 SEM morphology of (a) Cu-BTC, (b) Cu-BTC (80%), (c) Cu-BTC (60%) and (d) Cu-BTC (40%) (Liu et al., 2018)

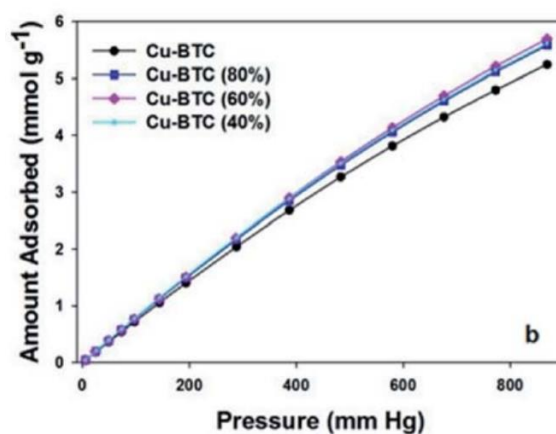


Figure 2.18 CO₂ gas adsorption by copper-based metal organic framework at 25°C (Liu et al., 2018)

2.4.2.2 Effect of temperature

The adjustment of operating temperature also has a significant impact when synthesising MOFs. The hydrothermal method, for instance, has several benefits in contrast to other methods. Sud and Kaur (2021) conducted the

study to investigate the effect of temperature on the structure of synthesised MOFs. Cobalt based metal organic framework, Co-MOFs are composed of a mixture of cobalt salt $[\text{Co}(\text{NO}_3)_2 \cdot 6\text{H}_2\text{O}]$, 2,6-naphthalenedicarboxylic acid (NDCA), and trans-1,2-bis(4-pyridyl)ethylene (bipyen) were synthesised via microwave-assisted method at different operating temperatures. Nanorod crystals were formed at the temperature of 120°C , whereas microrod crystals formed at the operating temperature of 160°C as exhibited in the morphology image (Figure 2.19(a) and (b)). Sarawade, Tan, and Polshettiwar (2013) suggested that temperature variation influences the size and the shape distribution of crystals formed.

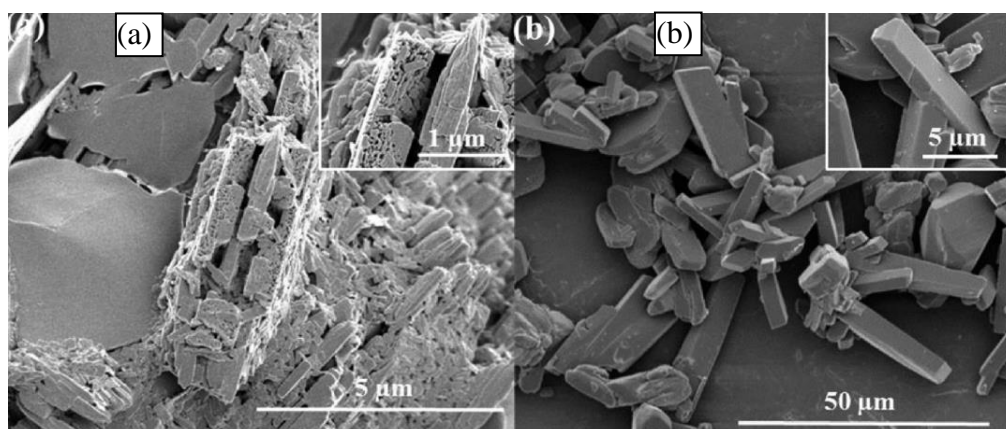


Figure 2.19 Morphology image of Co-MOF fabricated at temperature (a) 120°C , and (b) 160°C (Sarawade, Tan, and Polshettiwar, 2013)

At the meantime, de Oliveira and co-worker study the effect of the temperature on the formation of thulium-based MOF. The thulium succinate mixtures were prepared until two different temperature condition, i.e. 100°C and 180°C to understand the effect of temperature on the fabricated MOF. It is interestingly found that the structure of thulium-based MOF was affected by the temperature in term of the morphology, nano rod was form with the

temperature of 100°C whereas micro flake structure was obtained under 180°C (Figure 2.20). This study suggested that the shape of the fabricated MOF will be varies, depending on the fabrication temperature and other operating parameter during the fabrication (Obeidli et al., 2022).

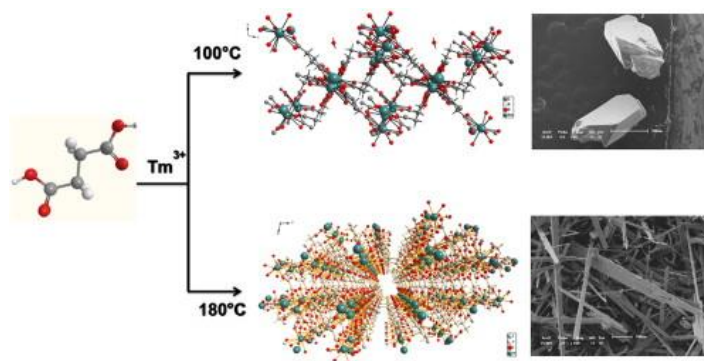


Figure 2.20 SEM morphology of thulium-based MOF fabrication at 100 and 180°C (Obeidli et al., 2022)

2.4.2.3 Effect of materials composition

In a general context, MOF composed of various metal constituents, exhibit distinctive physical and chemical attributes. However, MOFs with similar structures can be categorized into specific series. For example, the MIL (Matériel Institut Lavoisier) series of MOFs, initially discovered by Férey and colleagues in 2005 for gas adsorption applications (Férey et al., 2005), is a notable instance. Notably, MIL-101, a member of the MIL series, showcases exceptional CO₂ gas adsorption performance. The formation of MIL-101 involves the combination of metal ions (represented by M⁺ ions, which can encompass elements like chromium, iron, and aluminum) with organic ligands (Shin et al., 2020). Researchers have been captivated by the exceptional stability and well-defined three-dimensional structure inherent in MILs.

The impact of distinct metal precursors on CO₂ gas adsorption performance has been explored in the relevant literature. For instance, Sedighi and colleagues investigated the influence of various metal precursors on amine-functionalized MIL-101 for CO₂ gas adsorption (Sedighi et al., 2022). The specific surface areas, determined using BET analysis, were consistent among all the MIL-101 MOFs, with NH₂-MIL-101(Cr)-F, NH₂-MIL-101(Al)-F, and NH₂-MIL-101(Fe)-F exhibiting surface areas of 3363.65, 3775.61, and 3357.28 m²/g, respectively. Additionally, their study also revealed that NH₂-MIL-101(Cr)-F possessed the highest free volume at 1.716 cm³/g, compared to NH₂-MIL-101(Al)-F and NH₂-MIL-101(Fe)-F, measured at 1.603 and 1.456 cm³/g, respectively. In terms of CO₂ gas adsorption performance, NH₂-MIL-101(Cr)-F outperformed the other two MOFs, as depicted in Figure 2.21. These findings confirmed the pivotal role played by the metal precursors in determining gas adsorption performance, even when other fabrication parameters such as ligand type and temperature remained constant.

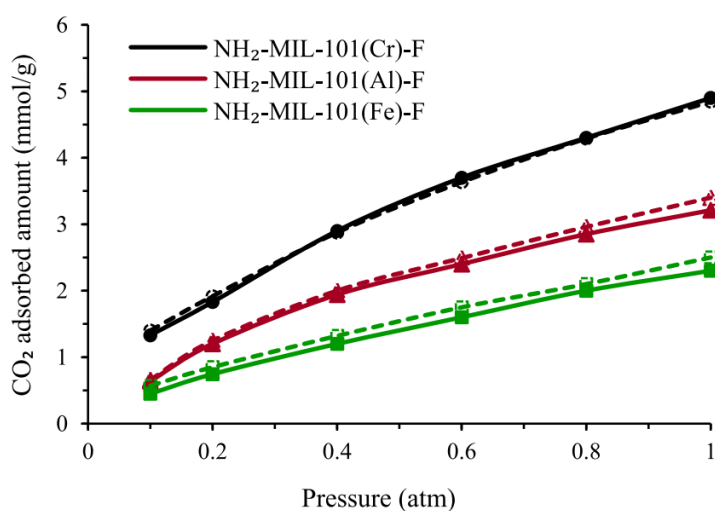


Figure 2.21 CO₂ adsorption of MOFs fabricated from different metal (Sedighi et al., 2022)

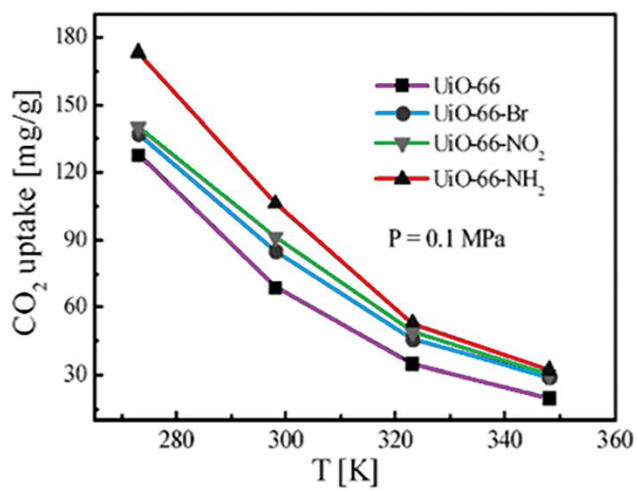
The primary function of an organic ligand is to bind the metal centres

together to form a structural framework. Similarly, the choice of organic linkers also influences CO₂ adsorption performance as a result of the differences in physical and chemical properties that each ligand possesses. Enlarging the surface area of MOF is the essential resolution for high CO₂ adsorption. Organic linkers are responsible for forming a framework allowing the establishment of pores. So, it is crucial to select organic linkers' size, which determines the pore size, surface area, and total pore volume of MOFs. Subsequently, large pores permit better CO₂ capture.

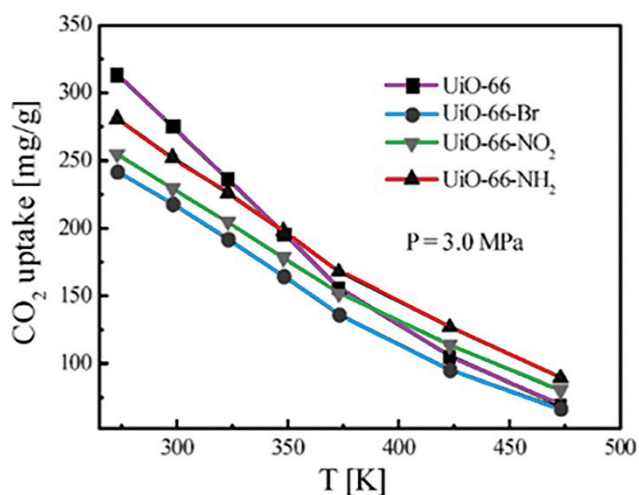
The organic ligand employed in MOF preparation can also serve as a solvent within the reaction mixture, actively participating in the MOF formation process. In the context of a solvothermal reaction, the organic ligand assumes a pivotal role as it is introduced alongside the metal precursors to establish the reaction mixture. This organic ligand can consist of a singular type or a combination of various ligands, all integrated to compose the reaction mixture. Consequently, the coordination dynamics between metal ions and these organic ligands during the liquid-phase synthesis significantly hinge on several factors, including the quantity of organic ligand added, the specific types of organic ligand employed, and the proportional ratios of each organic ligand within the mixture. These elements collectively shape the process of MOF creation in a liquid-phase synthesis environment.

The modification of ligands by introducing functional groups has two prospects where interaction between CO₂ molecules and MOF directly affects adsorption performance (Jiang et al., 2019). The incorporation of functional

groups will possibly increase the affinity of MOF for CO₂, subsequently improve CO₂ adsorption, termed as enthalpy factor. Another possible form is that a functional group may occupy the pores, which reduces the free volume of the framework and worsens CO₂ adsorption, termed as entropy factor. Jiang et al., (2019) studied the influence of ligand functionality on low-pressure CO₂ adsorption of MOF. Zirconium-based MOFs (UiO-66) was altered via the introduction of three different functional groups, bromine (Br), nitrite (NO₂) and amine (NH₂) groups. The results showed that incorporating polar groups produced a highly porous structure that enhances CO₂ adsorption at low pressure (0.1 MPa), as shown in Figure 2.22(a). The performance of the MOF incorporated functional groups are more prominent at a lower temperature due to loosely-packed CO₂ molecules in the pores. Also, the uptake of CO₂ is reflected in the polarity of the functional groups. On the downside, the CO₂ uptake capacity drop at high temperature where the perks of functionalised MOF become less prominent. The functionalised MOFs exhibit lower CO₂ uptake capacity compared to unfunctionalised MOF at higher pressure (3 MPa) from the reduction of free volume in MOF (Figure 2.22 (b)). The CO₂ uptake of functionalised MOFs eventually shows minor improvements at a higher temperature.



(a)



(b)

Figure 2.22 CO₂ uptake at different temperature for UiO-66, UiO-66-Br, UiO-66-NH₂ and UiO-66-NO₂ at (a) 0.1 MPa and (b) 3.0 MPa (Jiang et al., 2019)

2.4.3 Copper and chromium based metal organic framework

Copper-based MOF is characterized by its three-dimensional structure, where Cu²⁺ ions serve as the pivotal joints, and 1,3,5 benzene tricarboxylic acid (BTC) acts as the organic linker (Yulia, Nasruddin and Ruliandini, 2021). This MOF exhibits a distinctive paddle wheel structure, with each copper atom

forming coordinated bonds with four oxygen atoms derived from the BTC organic linker, along with an oxygen atom originating from a water molecule. Thanks to its remarkable attributes, including a notably high surface area, typically ranging from 600 to 1,600 m²/g, with the majority falling within the range of 700 to 1,000 m²/g, copper-based MOF has gained recognition as an effective porous sorbent for gas adsorption (Zhang et al., 2021). Meanwhile, chromium-based MOF, featuring a three-dimensional configuration, consists of trimeric chromium (III) octahedra connected to 1,4 benzene dicarboxylates (BDC) molecules. Each chromium atom is intricately coordinated to four oxygen atoms from the BDC ligand, with an additional oxygen atom sourced either from a fluorine group or a water molecule (Zhao et al., 2018). Following activation, it yields two mild Lewis acidic coordinatively unsaturated sites (CUS) per trimeric chromium (III) cluster. Notably, chromium-based MOF has exhibited substantial CO₂ adsorption capabilities in previous studies, owing to its promising attributes and abundant open metal sites (CUS) that serve as active sites for CO₂ adsorption (Wang and Astruc, 2020).

Table 2.4 summarizes various MOFs made from copper and chromium along with their respective metal precursors, organic ligands, and their CO₂ adsorption capacities. These MOFs have been studied for their potential in capturing CO₂ from gas mixtures. The notable findings include MOF-505 and Cu₃(BTC)₂ with high CO₂ adsorption capacities of 2.30 mmol/g and 2.42 mmol/g, respectively. Additionally, MIL-101 (Cr) exhibits a substantial CO₂ adsorption capacity of 2.24 mmol/g. On the other hand, HKUST-1, another

widely studied MOF, demonstrates good adsorption performance with a capacity of 1.19 mmol/g. This summary provides valuable insights into the CO₂ adsorption capabilities of different MOFs, which is crucial information for potential applications in carbon capture and gas separation processes.

Table 2.4 CO₂ gas adsorption by copper and chromium based MOF

MOF	Metal precursor	Organic ligand	CO ₂ adsorption (mmol/g)	Reference
Cu(I)Zn@MIL-100(Fe)-10	Cu, Zn	BTC	0.40	Le et al., 2021
HKUST-1	Cu	BTC	1.19	Xue et al., 2020
CuBDC	Cu	BDC	1.16	Tari et al., 2016
MOF-505	Cu	EBTC	2.30	Ghanbari, Abnisa and Daud, 2020
Cu ₃ (BTC) ₂	Cu	BTC	2.42	Ghanbari, Abnisa and Daud, 2020
TEPA-MIL-101	Cr	BDC, TEPA	0.65	Lawson et al., 2019
MIL-101 (Cr, Mg)	Cr, Mg	BDC	1.72	Gaikwad, Kim and Han, 2019
MIL-101 (Cr)	Cr	BDC	2.24	Mutyala et al., 2019
MIL-100 (Cr)	Cr	BTC	1.41	Teerachawanwong et al., 2023

CHAPTER 3

METHODOLOGY

3.1 Process Flow Chart

Figure 3.1 illustrates the overall process flow chart for the research activities.

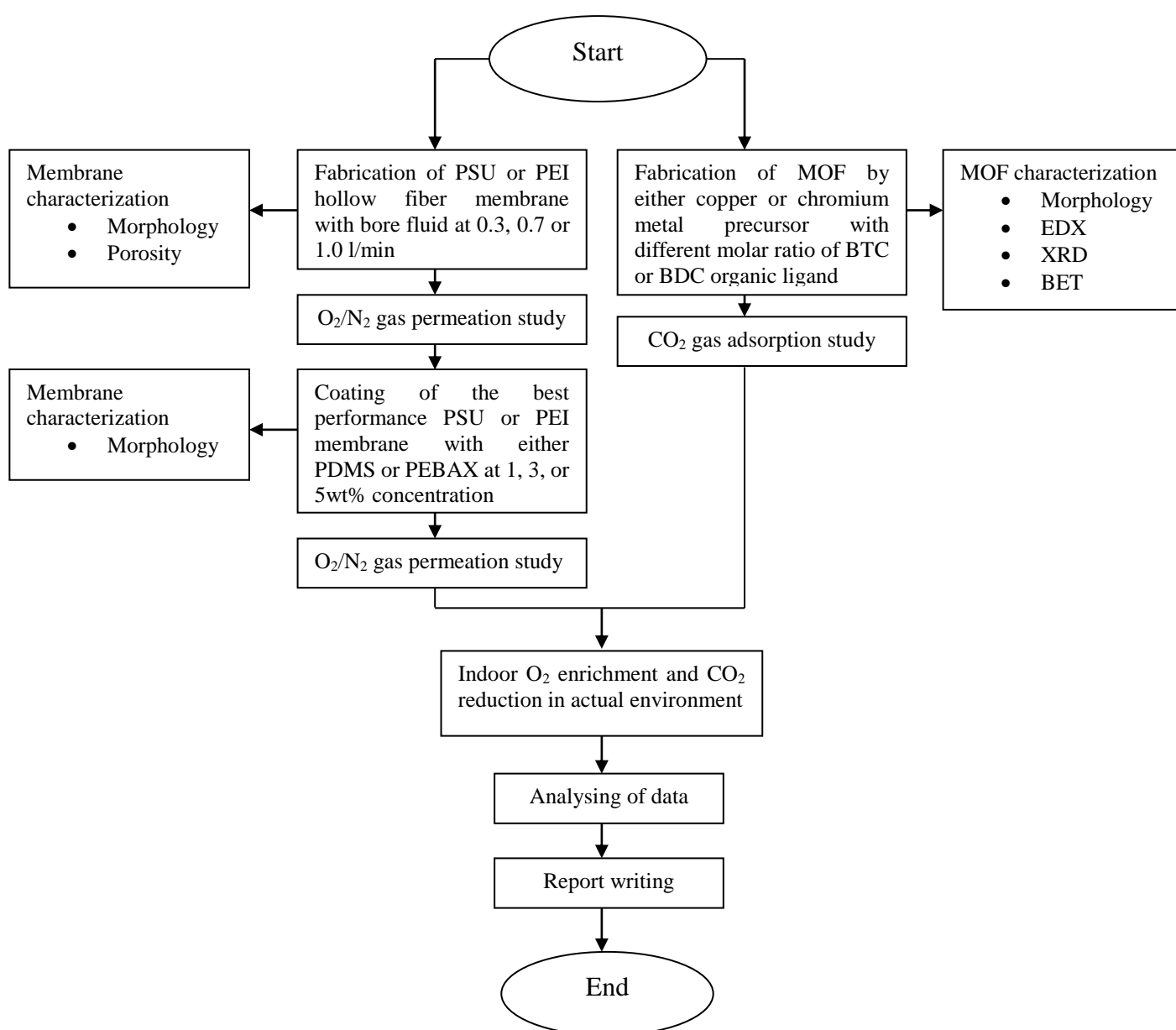


Figure 3.1 Overall process flow chart

3.2 Preparation of hollow fiber membrane and O₂/N₂ gas separation

3.2.1 Materials

Two primary polymeric materials, polysulfone (PSU) and polyetherimide (PEI), which are commonly used in O₂/N₂ gas separation, were obtained in pellet form from Amoco Chemicals and Merck, respectively. The primary solvents used in preparing the dope solutions were N,N-dimethylacetamide (DMAc) and ethanol (EtOH). Both solvents were purchased from Sigma Aldrich. The additive used in this study was Tetrahydrofuran (THF) obtained from QRec. THF was used in the dope solution to delay the demixing phase of the dope solution during the fabrication to produce a dense membrane that favours gas separation. The membrane coating materials were polydimethylsiloxane (PDMS) and polyether block amide (PEBAX) obtained from Sigma Aldrich and Arkema, respectively. n-hexane obtained from Merck was used as the solvent in the membrane coating solution preparation.

3.2.2 Fabrication method

A diagram representing the wet-dry phase inversion process for the fabrication of hollow fiber membranes is presented in Figure 3.2, along with the relevant fabrication parameters listed in Table 3.1. The process involves pouring a uniform dope solution containing either PSU or PEI polymer and solvent into a stainless-steel dope vessel. The gear pump provides pressure to

purge the dope solution out from the centre of the spinneret. The spinneret structure is composed of an extruder orifice consisting of an inner and outer needle to form a cylindrical structure of a hollow fiber membrane. The inner diameter of the needle was 0.3 mm, whereas the outer diameter of the needle was 0.6 mm. After the extrusion of the dope solution from the spinneret, the internal coagulant with the bore fluid flow rate at either 0.3, 0.7 or 1.0 mL/min were flow out from the inner part of the spinneret by a pump. The dope solution was travel through a predetermined air gap distance before it fell into the coagulation bath. In this study, tap water was used as a coagulation bath for the coagulation of nascent membrane. The nascent membrane internal surface was created by immersing it in a coagulation bath. In contrast, the outer surface of the hollow fiber member experienced gelation due to exposure to the air gap and contact with the external coagulation bath. The hollow fiber membrane was then winded up into a coil by the winding-up drum before the collection.

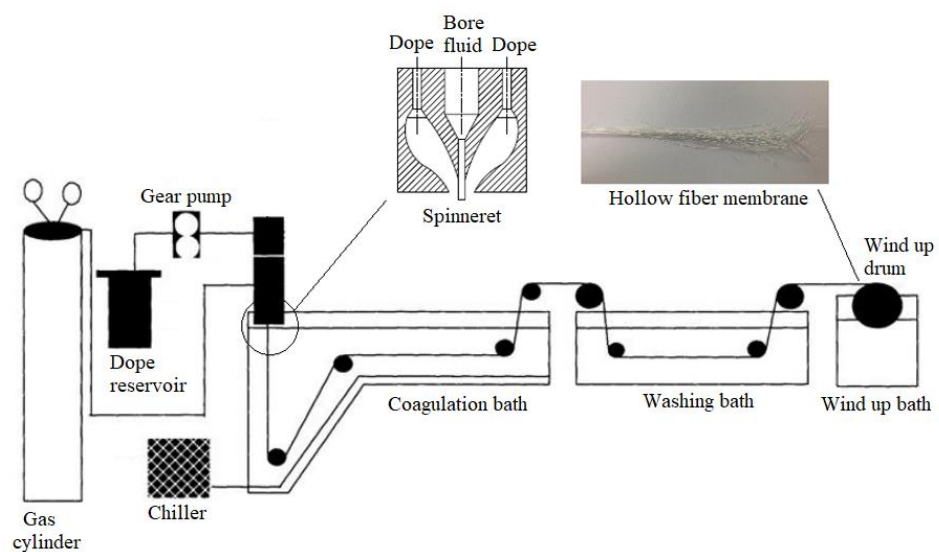


Figure 3.2 Schematic diagram on the setup used for the fabrication of hollow fiber membranes

Table 3.1 Membrane fabrication parameters

Spinning parameter	Value
Materials	PSU/PEI
Spinneret OD/ID (mm/mm)	0.6/0.3
Bore liquid	Distilled water
Bore liquid temperature (°C)	25
Bore liquid flowrate (mL/min)	0.3/0.7/1.0
External coagulant	Tap water
External coagulant temperature	25
Air gap (cm)	30
Room relative humidity (%)	55 ± 5

3.2.3 Hollow fiber membrane coating technique

Both PDMS and PEBAX coating solutions were prepared by mixing PDMS and PEBAX pellets with a predetermined amount of n-hexane to reach the desired concentration of PDMS or PEBAX solution as 1%, 3%, and 5% by weight ratio, respectively. The solution was then stirred on a magnetic stirrer for 2 hours to obtain the homogenous solution. The hollow fiber membrane was immersed into the coating solution for 3 minutes, then the membrane was withdrawn from the solution and dried at room temperature. Later, the pristine membrane was coated with PDMS or PEBAX using the dip-coating method (Figure 3.3). The coating process was repeated five times to ensure a uniform coating of the membrane with the solution. Table 3.2 presents a summary of the coating materials and concentrations used to coat the membrane.

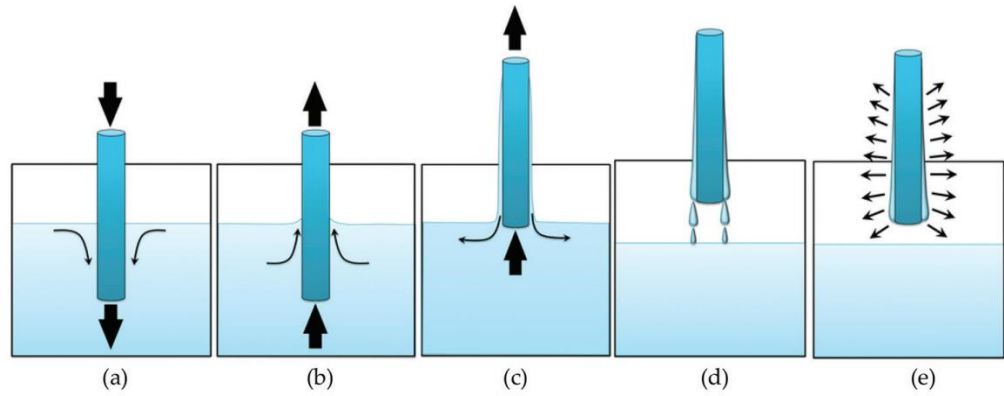


Figure 3.3 Dip coating technic of hollow membrane (Ji and Zhao, 2016)

Table 3.2 Coating condition for the PSU and PEI hollow fiber membranes

Membrane	PDMS (wt%)	PEBAX (wt%)
PSU	-	-
PSU-1PDMS	1	-
PSU-3PDMS	3	-
PSU-5PDMS	5	-
PSU-1PEBAX	-	1
PSU-3PEBAX	-	3
PSU-5PEBAX	-	5
PEI	-	-
PEI-1PDMS	1	-
PEI-3PDMS	3	-
PEI-5PDMS	5	-
PEI-1PEBAX	-	1
PEI-3PEBAX	-	3
PEI-5PEBAX	-	5

3.2.4 Characterisation method

The hollow fiber was characterised for its surface morphology using scanning electron microscopy with energy dispersive x-ray spectroscopy (SEM-EDX) (Hitachi S-3400N SEM). The process of coating the hollow fiber membrane involved affixing it onto a holder using carbon adhesive tape, and then using a sputter coater machine to apply a layer of palladium and gold (Emitech SC7620) to make the sample conductive. The membrane was then inserted into the sample chamber under the vacuum condition. High voltage electrons at 10 kV were bombarded at the sample to provides high resolution and magnification of the images produced. Before the morphology examination by SEM, EDX was used to determine the weight percentage of the elements contained in the membrane by exposing the membrane with a high X-ray in knocking out the electrons from the electrons shell for identification of the elements.

3.2.5 O₂/N₂ gas separation setup

Pure N₂ or O₂ gases with up to 99.99% of purity were used for the gas permeation of the fabricated membrane. The length of the membrane was 25 cm, and five hollow fiber membranes were bundled and inserted into a module through the application of epoxy resin. During the preparation, the ratio of resin to hardener was 1:1. One end of the module was sealed firmly to ensure the gas flowing only in one direction towards another module end that was linked to a soap-bubble flow meter. The flow meter consisted of two separate

inlets, with one connected to the membrane module and the other to the soap container (Figure 3.4).

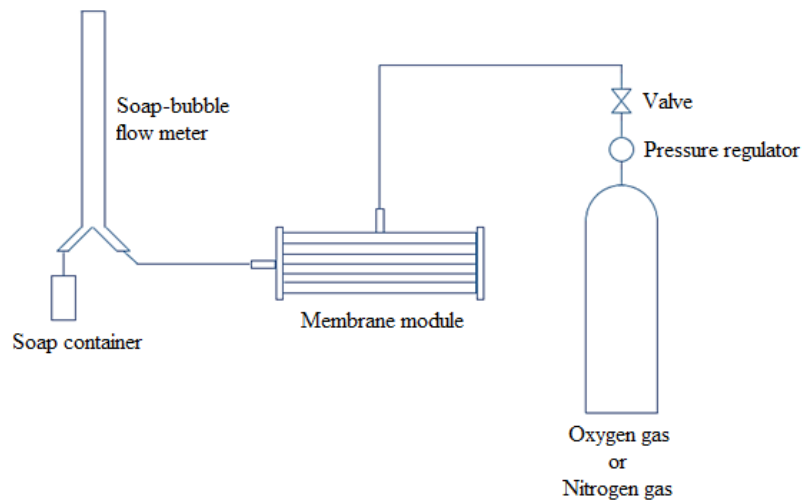


Figure 3.4 Schematic setup for pure gas permeation study

Pure N_2 or O_2 gas with the pressure of either 1, 3 or 5 bar was delivered to the membrane module and the gas was transported based on the shell side in the configuration, transport across the shell of the membrane into the lumen of the membrane. Then, it pushed the soap bubble to flow upwards the flow meter. The flow rate of the feed gas transport over the hollow fiber membrane (Q) at standard temperature and pressure (STP) was evaluated by the time taken (t) for the bubble to travel 10 mL distance in the soap bubble burette. The process was repeated five times for each sample to ensure the precision and reproducibility of the outcomes.

Experimental calculation of membrane permeance in GPU can be achieved using Equation 3.1, which is the ratio of the permeability (P_{O_2}) to the unit length (l) of the hollow fiber membrane.

$$\frac{P_{O_2}}{l} = \frac{273.15 \times 10^6 \times Q}{AT\Delta P} \quad \text{Equation 3.1}$$

where A is the area of the hollow fiber membrane area (cm^2), T is the operating temperature at 300 K, and ΔP is the pressure difference across the membrane (cm Hg). A unit of GPU is equal to $10^{-6} \text{ cm}^3(\text{STP})/\text{cm}^2 \text{ cm Hg}$. Additionally, the selectivity was calculated using Equation 3.2, where P_{O_2} and P_{N_2} are the permeability of gases A and B, respectively.

$$\alpha_{O_2/N_2} = \frac{P_{O_2}}{P_{N_2}} \quad \text{Equation 3.2}$$

3.3 Preparation of metal organic framework and CO₂ gas adsorption

3.3.1 Materials

In this study, two primary metals, namely chromium, and copper, were used as the core material and precursor to investigate CO₂ gas adsorption using MOF. The type of chromium and copper are chromium (VI) oxide (Cr) and copper (II) nitrate trihydrate (Cu), respectively which all are obtained from Sigma Aldrich. Terephthalic (BDC) and trimesic (BTC) acid used as organic ligands were obtained from Sigma Aldrich, while ethanol used as solvent used was purchased from Sigma Aldrich. All the materials used in this study were used without further purification.

3.3.2 Fabrication method

The solvothermal method described by Leng et al. (2016) was employed to prepare the MOFs in this study. Firstly, a predetermined mass of

metal precursor was mixed with distilled water with the assistance of a mechanical stirrer. Meanwhile, the predetermined mass of the organic ligand was mixed with ethanol to obtain the organic ligand solution. Both metal precursor and organic ligand solutions were mixed and stirred into homogenous solutions at room temperature by a mechanical stirrer. Later, the homogenous mixture was transferred to the Teflon line autoclave and heated to 80°C in a vacuum oven for 72 hours to allow the formation of crystallisation. Additionally, the crystal powder was allowed to cool to room temperature and then washed with ethanol at 60°C to remove any residual reactants. Lastly, the wetted crystal powder was cooled to ambient temperature and kept vacuum cabinet for further application. The composition of the MOF sample is tabulated in Table 3.3.

Table 3.3 Composition of MOFs sample

Metal Organic Framework	Chromium (mmol)	Copper (mmol)	BDC (mmol)	BTC (mmol)
Cr-BDC-1:1	1	-	1	-
Cr-BDC-1:2	1	-	2	-
Cr-BDC-1:3	1	-	3	-
Cr-BDC-1:4	1	-	4	-
Cr-BDC-1:5	1	-	5	-
Cr-BTC-1:1	1	-	-	1
Cr-BTC-1:2	1	-	-	2
Cr-BTC-1:3	1	-	-	3
Cr-BTC-1:4	1	-	-	4
Cr-BTC-1:5	1	-	-	5

Cu-BDC-1:1	-	1	1	-
Cu-BDC-1:2	-	1	2	-
Cu-BDC-1:3	-	1	3	-
Cu-BDC-1:4	-	1	4	-
Cu-BDC-1:5	-	1	5	-
Cu-BTC-1:1	-	1	-	1
Cu-BTC-1:2	-	1	-	2
Cu-BTC-1:3	-	1	-	3
Cu-BTC-1:4	-	1	-	4
Cu-BTC-1:5	-	1	-	5

Cr - Chromium (VI) oxide Cu - Copper (II) nitrate trihydrate

BDC - Terephthalic acid BTC - Trimesic acid

3.3.3 Characterisation methods

In this study, the MOFs were characterised for their physicochemical properties, including surface morphology using scanning electron microscopy with energy dispersive x-ray spectroscopy (Hitachi S-3400N), crystallographic structure using x-ray diffraction (Shimadzu XRD-6000), surface characteristics (surface area, pore size, and pore size distribution) using sorptometric surface analyzer (N₂ BET method) (Thermo Scientific SorptometricSO1990).

3.3.3.1 Scanning electron microscopy with energy dispersive X-ray (SEM-EDX)

The MOF was placed on a holder with carbon adhesive tape and coated with palladium and gold using sputter coater machine (Emitech SC7620) to make the sample conductive. The MOF was then inserted into the sample chamber under the vacuum condition. High voltage electrons at 10 kV were bombarded at the sample to provide high resolution and magnification of the images produced. Before the morphology examination by SEM, EDX was used to determine the weight percentage of the elements contained in the MOF by exposing the sample with a high X-ray in knocking out the electrons from the electrons shell for identification of the elements.

3.3.3.2 Powder X-Ray diffraction (XRD)

X-Ray Diffraction (Shimadzu XRD-6000) was used to examine crystallographic structure of the MOFs. The synthesised MOFs were placed on the sample holder. The diffractometer was operated at 20 kV and 20 mA with Cu K α of $\lambda = 1.54\text{\AA}$. The deflection angle, 2θ , was then set to scan from 5° to 40° with a speed of $1.2^\circ/\text{min}$.

3.3.3.3 Brunauer-Emmett-Teller (BET)

The BET surface area analysis involves the nitrogen adsorption at 77.35K was adopted to determine the surface area of MOFs. This analysis determined the porosity and surface area of the MOFs by performing the

adsorption of gas particles on the surface of the MOFs. The MOFs were heated with the flow of N₂ gas to remove moisture content on the surface and eliminate impurities trapped on the surface before the adsorption. The MOFs were then inserted into a vacuum chamber and a constant temperature of N₂ gas under different pressure streams was purge into the chamber to create either adsorption or desorption isotherms of the samples.

3.3.4 CO₂ gas adsorption setup

An experimental setup as shown in Figure 3.5 was used to measure the CO₂ adsorption by MOF. Before the gas adsorption experiment, the empty teabag mass and MOF starting mass were weighed and recorded. Subsequently, the hollow stainless-steel cylinder tube was utilized to house the teabag containing MOF, with both ends of the tube securely sealed to prevent any CO₂ gas leakage. CO₂ gas was then introduced into the cylinder tube via a pipe and allowed to remain for around two hours to enable the MOF to adsorb the supplied CO₂ within a closed system. The difference between the inlet and outlet concentrations of CO₂ was measured every five minutes to compute the CO₂ adsorption capacity of the MOF.

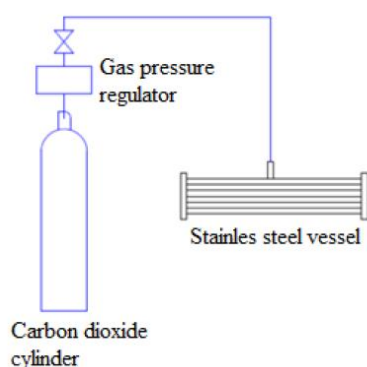


Figure 3.5. Schematic setup for CO₂ gas adsorption study

3.4 Indoor O₂ enrichment and CO₂ reduction setup

The gas permeation system as shown in Figure 3.6 is the apparatus setup used for a gas permeation study to indicate an increment of the oxygen concentration before and after the sampling time. The experimental study was conducted in an enclosed room with a volume of 21 m³ (room area and height were approximately 7.8 m² and 2.7 m, respectively). The membranes were tested at room temperature at 22 ± 1°C, relative humidity of 55 ± 5%, and the occupancy rate of one person was calculated based on the ASHRAE standard 62.1-2013 at the occupant density of 5 persons per 100 m².

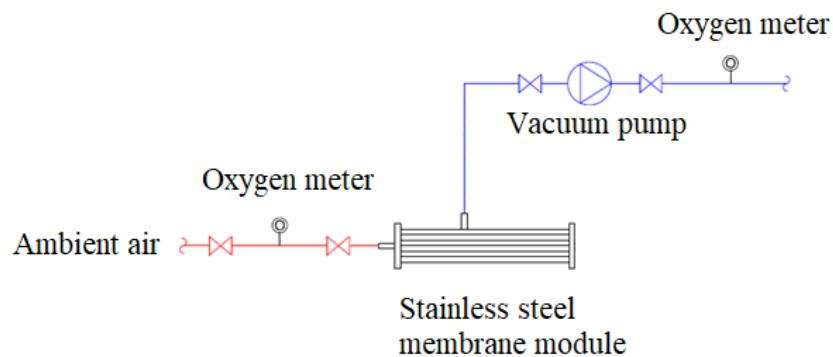


Figure 3.6 Schematic setup for indoor O₂ gas enrichment study

Following the CO₂ adsorption study, the most effective MOF was selected to assess CO₂ reduction in an enclosed indoor volume of approximately 21 m³. Initially, the CO₂ concentration was measured with a CO₂ meter (CO₂ meter, AZ-0002), and the indoor air was subsequently drawn into a stainless-steel vessel containing the MOF. The CO₂ concentration at the outlet of the stainless-steel vessel was also monitored, and the difference between the initial and outlet CO₂ concentrations was utilized to determine the

quantity of CO₂ that was adsorbed (Figure 3.7).

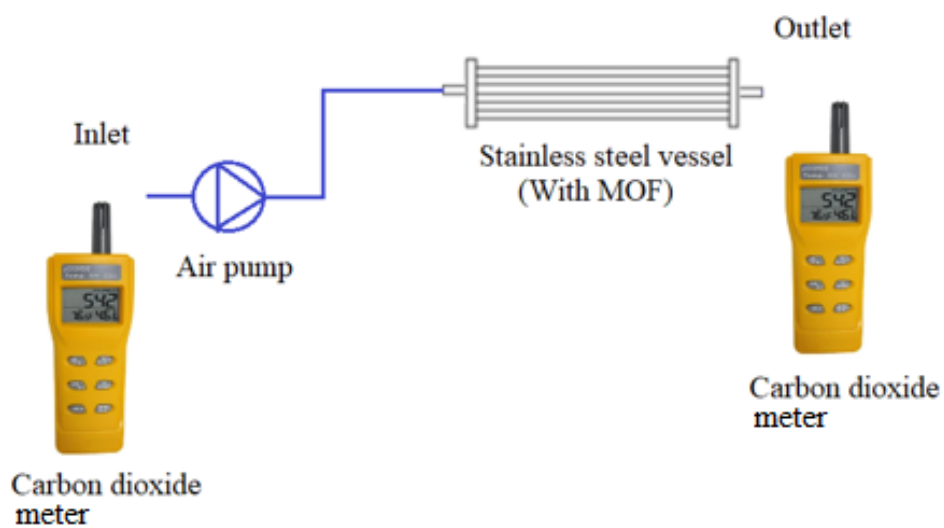


Figure 3.7 Schematic setup for indoor CO₂ gas adsorption study

CHAPTER 4

RESULTS AND DISCUSSION

4.1 Effect of polymeric materials and fabrication parameter on O₂/N₂ gas separation

4.1.1 Characterisation of physical properties

PSU hollow fiber membranes, labeled as PSU-1, PSU-2, and PSU-3, were prepared with bore fluid flow rates of 0.3, 0.7, and 1.0 mL/min, respectively, as shown in Figures 4.1(a) to (c). In the meantime, Figures 4.1(d) to (f) present the PEI hollow fiber membrane fabricated with the bore fluid flow rate of 0.3, 0.7 and 1.0 mL/min, which were labeled as PEI-1, PEI-2 and PEI-3, respectively.

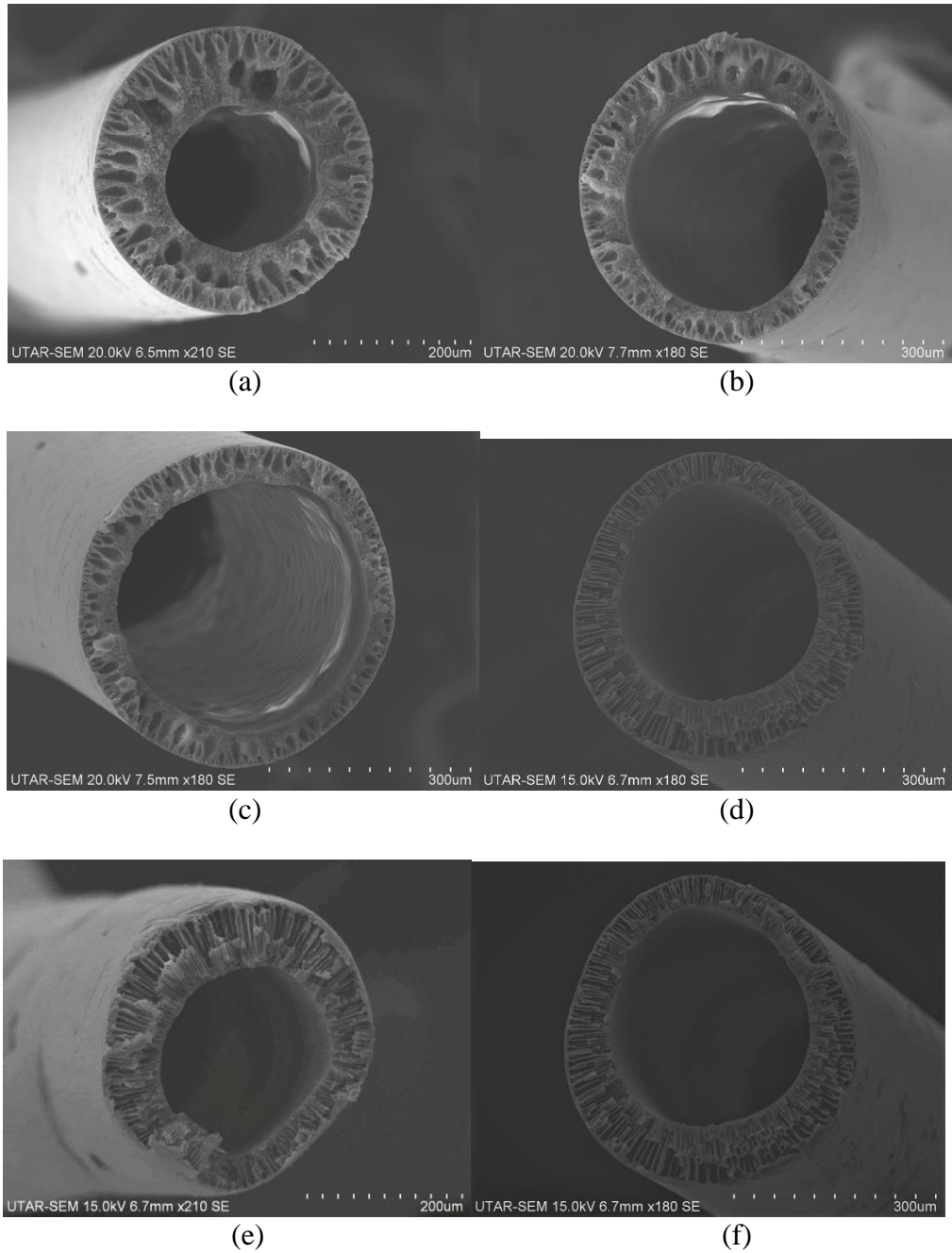


Figure 4.1 Cross sectional morphology of (a) PSU-1, (b) PSU-2, (c) PSU-3, (d) PEI-1, (e) PEI-2 and (f) PEI-3

The results showed that the cross-sectional membranes exhibited asymmetric structure. This structure arose from the interaction between the strong solvent used in this study and water, leading to an aggressive solvent/non-solvent exchange, and thus forming the finger-like layer. All the

PSU hollow fiber membranes demonstrated identical membrane structure in which the dense structure extended from the lumen, followed by teardrop microvoid structure at the shell side. In the meantime, the structure at the PEI hollow fiber membrane's lumen side also possessed a similar dense layer structure which extended to the finger-like structure developed at the shell side. The difference in the structure between the PSU and PEI hollow fiber membrane was a result of the lower density of the PSU polymer compared to that of the PEI polymer during the dope solution preparation which is similar to the previous studies reported by previous literature findings (Talukder et al., 2023). The lower viscosity of the dope solution led to lower resistance to the diffusion of the solvent during the phase inversion reaction, and thus, a less dense structure was formed (Matveev et al., 2022).

Table 4.1 Physical properties of the PSU and PEI hollow fiber membranes

Membrane	Internal diameter (μm)	Wall thickness (μm)	Porosity, ϵ (%)
PSU-1	210 ± 10	90 ± 5	18.37 ± 1.5
PSU-2	310 ± 12	60 ± 7	17.84 ± 2.4
PSU-3	370 ± 10	50 ± 4	18.18 ± 1.9
PEI-1	233 ± 21	68 ± 4	21.57 ± 2.5
PEI-2	311 ± 18	63 ± 3	21.24 ± 1.7
PEI-3	223 ± 24	57 ± 5	21.65 ± 1.8

In addition to the structure of the membrane as discussed earlier, Figures 4.1(a) to (e) showed an interesting phenomenon where the thickness of both PSU and PEI hollow fiber membranes decreased with respect to the

increase in the bore fluid flow rate as tabulated in Table 4.1. This observation was similar to the result reported by Alobaidy et al. (2017) where increasing the flow rate led to higher bore fluid pressure and shear stress, which caused the inner lumen of the membrane to stretch and its thickness to decrease. Despite this effect, the porosity of the resulting hollow fiber membranes remained relatively consistent, with a range of 17.84% to 21.65%, indicating that the bore fluid flow rate had no significant impact on membrane porosity (Table 4.1).

4.1.2 Performance of O₂/N₂ gas separation

The O₂/N₂ gas permeation and selectivity performance are presented in Figures 4.2. Generally, PSU hollow fiber membrane outperformed the PEI hollow fiber membrane in terms of the oxygen gas separation. The PSU-3 hollow fiber membrane recorded the highest permeance of oxygen gas at 62.15 GPU, whereas the PEI-1 hollow fiber membrane recorded the lowest oxygen gas permeance at 42.79 GPU. The PSU hollow fiber membranes recorded relatively consistent permeance on the nitrogen gas separation in the range between 13.49 and 15.14 GPU. The PEI-1 hollow fiber membrane exhibited the highest nitrogen gas permeance at 12.26 GPU compared to the other two PEI hollow fiber membranes. The selectivity of both PSU and PEI hollow fiber membranes fell within the range of 3.70 to 4.11.

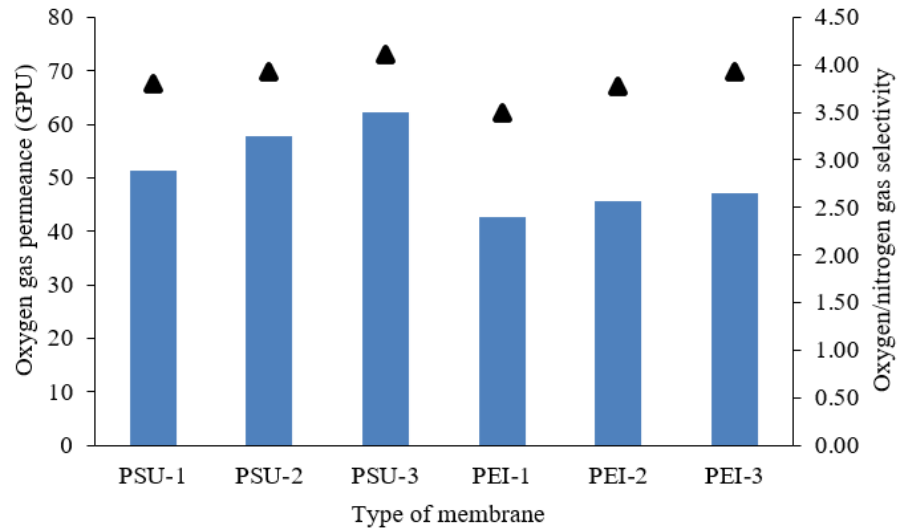


Figure 4.2 Oxygen gas permeance and oxygen/nitrogen gas selectivity of PSU and PEI hollow fiber membranes with different bore fluid flow rates

The PSU-3 and PEI-3 hollow fiber membranes showed better permeance performance compared with those of other same materials (PSU-1, PSU-2, and PEI-1, PEI-2) at different bore fluid flow rates. It could be observed that the gas permeances of both O₂ and N₂ were in the descending order of PSU-3 > PSU-2 > PSU-1 and PEI-3 > PEI-2 > PEI-1, respectively. A similar trend was also observed in the gas selectivity. Both PSU and PEI hollow fiber membranes experienced the same phenomenon where bore fluid flow rate had directly proportional relationship gas permeation and selectivity. The phenomenon of decreased membrane thickness at higher bore fluid flow rates was attributed to the nature of the hollow fiber membranes themselves (Matveev et al., 2022). Both the PSU and PEI membranes experienced a reduction in thickness as the bore fluid flow rate increased (Alobaidy et al., 2017). As the membrane thickness decreases, the structural packing density of the membrane is enhanced owing to the lower shear stress exerted by the higher bore fluid flow rate. Additionally, the reduction of membrane thickness

also leads to the decrease in the mass transfer resistance, allowing more gas particle to transport across the membrane (Alobaidy et al., 2017). The lower mass transfer resistance on the thin membrane thickness can result in a greater interstitial space, ultimately improving selectivity and permeability (Zulhairun et al., 2014; Liang, Chung and Lai, 2019). As such, using a lower bore fluid flow rate may lead to hollow fiber membranes with a more tightly-packed structure, ultimately resulting in higher permeance and selectivity (Talukder, 2023).

On the other hand, the material comparison between the PSU and PEI hollow fiber membranes determined that the PSU hollow fiber membrane recorded better performance in terms of permeance and selectivity due to the higher structure packing density as discussed earlier (the thickness of the PSU hollow fiber membrane was greater than that of the PEI hollow fiber membrane under similar fabricating parameters). As observed from Table 4.1, the porosity of the PSU hollow fiber membrane was approximately 18%, whereas the porosity of the PEI hollow fiber membrane was approximately 21%. The greater porosity of the membrane resulted in a reduction of the mass transfer resistance, which allowed more significant amount of gas to diffuse across the membrane (Liang, Chung and Lai., 2019).

4.1.3 Summary

The aim of this section was to investigate the influence of bore fluid flow rate and polymeric materials on the gas permeance performance in the

separation of O₂ and N₂. It was observed that both PSU-3 and PEI-3 (bore fluid flowrate of 1.0 mL/min) exhibited better performance compared to other bore fluid flowrate. At the meantime, the materials comparison between PSU and PEI hollow fiber membranes suggested that PSU recorded a better overall performance in terms of permeance and selectivity in O₂ and N₂ gas separation relative to PEI.

4.2 Performance of dual-layer membrane on O₂/N₂ gas separation

4.2.1 Characterisation of physical and chemical properties

The surface morphology results of the dual-layer membranes (coated with PDMS or PEBAX) are depicted in Figure 4.3. It was suggested that PDMS or PEBAX was successfully coated on the outer membrane surface as an additional layer formed on the shell side of the membrane. Based on the morphology results presented, it was noteworthy to mention that the thickness of the coating layer on the membrane increased with the increment of the coating concentration for both PDMS and PEBAX dual-layer hollow fiber membranes. The coating thickness of PDMS and PEBAX on the PSU hollow fiber membrane was increased from 0.7 to 1.7 μm and 0.3 to 1.2 μm, respectively, with the coating concentration increasing from 1 to 5% (Table 4.2). The increase in coating thickness of PDMS and PEBAX on the PEI hollow fiber membrane followed a similar pattern, where the thickness increased from 1.1 to 3.5 μm and 1.3 to 3.9 μm, respectively. This observation was consistent with the findings reported by Zulhairun et al. (2014), which showed that the concentration of coating materials had a positive impact on

the membrane thickness. It was also noted that the thicknesses of the PEBAX-coated PSU and PEI dual-layer hollow fiber membranes (red inserted arrow in Figure 4.3c) were generally lower than those of the PDMS-coated PSU and PEI dual-layer hollow fiber membranes (red inserted arrow in Figure 4.3b) at the same coating concentration. PEBAX solution with a nature of rapid gelation during the curing process and greater ease in penetrating the membrane pore compared to the PDMS coating (Hu et al., 2022).

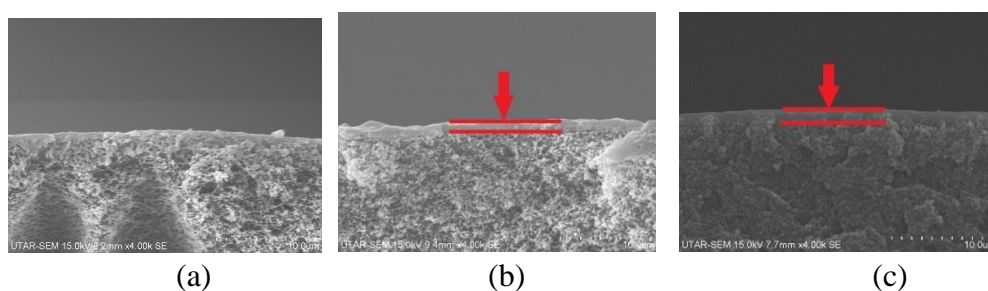


Figure 4.3 Cross sectional morphology of (a) pristine membrane, (b) PDMS dual-layer hollow fiber membrane and (c) PEBAX dual-layer hollow fiber membrane

Table 4.2 Coating thickness of PSU and PEI dual-layer hollow fiber membranes

Membrane	Thickness (μm)
PSU-3	-
PSU-1PDMS	0.7 ± 0.07
PSU-3PDMS	1.1 ± 0.05
PSU-5PDMS	1.7 ± 0.06
PSU-1PEBAX	0.3 ± 0.10
PSU-3PEBAX	0.8 ± 0.09
PSU-5PEBAX	1.2 ± 0.14
PEI-3	-
PEI-1PDMS	1.1 ± 0.12
PEI-3PDMS	2.1 ± 0.19
PEI-5PDMS	3.5 ± 0.22
PEI-1PEBAX	1.3 ± 0.17
PEI-3PEBAX	2.5 ± 0.28
PEI-5PEBAX	3.9 ± 0.33

Tables 4.3 and 4.4 tabulate the EDX elementary analysis of both PSU and PEI dual-layer hollow fiber membranes under different coating conditions. Carbon, oxygen and sulphur elements were detected on the surface of the uncoated pristine PSU membrane as the composition of the PSU polymer consists of the subunit of aryl-SO₂-aryl. On the other hand, carbon and oxygen elements were detected in the PEI dual-layer hollow fiber membranes arisen from the chemical structure of PEI. New trace elements were detected on the surface of both PSU and PEI dual-layer hollow fiber membranes corresponding to the type of coating materials with different concentrations. The presence of silicon element on both PSU and PEI dual-layer hollow fiber membranes indicated the successful coating of PDMS. Moreover, the concentration of silicon element increased proportionally with the increase in PDMS coating concentration. A similar trend was observed on the PSU and PEI dual-layer hollow fiber membranes with PEBAX coating. The nitrogen element that was not present in the PSU membrane was discovered in the PSU membrane with PEBAX coating. In contrast, the concentration of the nitrogen element increased for the PEI membrane with PEBAX coating. Similarly, the nitrogen element increased with the increasing coating concentration of PEBAX on both PSU and PEI dual-layer hollow fiber membranes.

Table 4.3 Elemental analysis of PSU dual-layer hollow fiber membranes

Membrane	Element (at%)				
	Carbon (C)	Oxygen (O)	Sulphur (S)	Silicon (Si)	Nitrogen (N)
PSU-3	79.84 ± 3.51	17.88 ± 1.89	2.28 ± 0.16	ND	ND
PSU-1PDMS	79.67 ± 3.19	15.41 ± 1.21	3.32 ± 0.23	1.60 ± 0.12	ND
PSU-3PDMS	78.60 ± 4.02	15.71 ± 0.93	2.97 ± 0.19	2.72 ± 0.22	ND
PSU-5PDMS	70.57 ± 3.85	23.14 ± 1.92	1.55 ± 0.12	4.74 ± 0.34	ND
PSU-1PEBAX	79.66 ± 4.13	15.34 ± 1.02	3.44 ± 0.31	ND	1.56 ± 0.17
PSU-3PEBAX	78.83 ± 4.26	15.60 ± 1.17	2.98 ± 0.26	ND	2.59 ± 0.21
PSU-5PEBAX	71.95 ± 3.92	21.27 ± 2.39	1.80 ± 0.16	ND	4.98 ± 0.36

ND = Not detected

Table 4.4 Elemental analysis of PEI dual-layer hollow fiber membranes

Membrane	Element (at%)				
	Carbon (C)	Oxygen (O)	Sulphur (S)	Silicon (Si)	Nitrogen (N)
PEI-3	83.58 ± 4.78	16.42 ± 0.94	ND	ND	ND
PEI-1PDMS	82.31 ± 4.59	15.26 ± 0.74	ND	2.43 ± 0.13	ND
PEI-3PDMS	80.94 ± 4.92	15.34 ± 0.69	ND	3.72 ± 0.19	ND
PEI-5PDMS	79.65 ± 4.07	15.42 ± 0.71	ND	4.93 ± 0.22	ND
PEI-1PEBAX	81.42 ± 4.52	15.46 ± 0.65	ND	ND	3.12 ± 0.16
PEI-3PEBAX	80.17 ± 4.13	14.92 ± 0.57	ND	ND	4.91 ± 0.24
PEI-5PEBAX	78.84 ± 3.41	14.80 ± 0.61	ND	ND	6.36 ± 0.52

ND = Not detected

4.2.2 Effect of coating material on O₂/N₂ gas separation

4.2.2.1 Gas permeance and selectivity of PSU dual-layer hollow fiber membranes

Figure 4.4 shows that the PSU dual-layer hollow fiber membranes coated with PDMS generated better gas permeance compared with that of the pristine PSU membrane (PSU-3). In contrast, the PEBAX-coated PSU dual-layer hollow fiber membranes recorded lower gas permeance. The permeances of oxygen and nitrogen gas for pristine PSU membrane (PSU-3) were recorded at 62.15 and 15.14 GPU, respectively. In contrast, PSU-3PDMS performed the best in the gas separation with oxygen and nitrogen gas permeances at 73.25 and 16.05 GPU, respectively. The increase of gas permeance was equal to 17.9% and 6.0% for oxygen and nitrogen gas, respectively. In the meantime, the O₂/N₂ selectivity of the PDMS-coated PSU dual-layer hollow fiber membranes ranged from 4.17 to 4.56. In the meantime, the PSU dual-layer hollow fiber membranes with PEBAX coating recorded a generally lower gas permeance and selectivity than its pristine membrane. The oxygen and nitrogen gas permeance ranges were 37.84 to 48.91 GPU and 10.50 to 12.42 GPU, respectively.

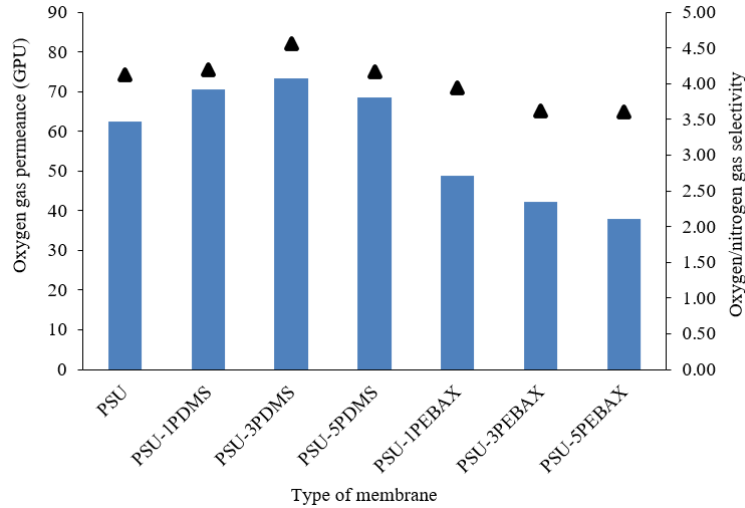


Figure 4.4 Oxygen gas permeance and oxygen/nitrogen gas selectivity of PSU dual-layer hollow fiber membrane with PDMS or PEBAX coating

4.2.2.2 Gas permeance and selectivity of PEI dual-layer hollow fiber membranes

Figures 4.5 depicts that PEI dual-layer hollow fiber membranes coated with PDMS possessed better gas permeance compared with the pristine hollow fiber PEI membrane (PEI-3). In contrast, the PEBAX coated PEI dual-layer hollow fiber membranes recorded lower gas permeance. This finding is similar to the PSU dual-layer hollow fiber membranes, as discussed in the section 4.2.3.1. The oxygen and nitrogen gas permeance for pristine PEI membrane (PEI-3) was recorded at 47.15 and 12.03 GPU, respectively, whereas the PEI-3PDMS dual-layer hollow fiber membranes yielded the highest oxygen and nitrogen gas permeances at 57.51 and 13.73 GPU, respectively. In the meantime, the O_2/N_2 selectivity of the PEI dual-layer hollow fiber membranes with PDMS coating ranged from 4.01 to 4.19.

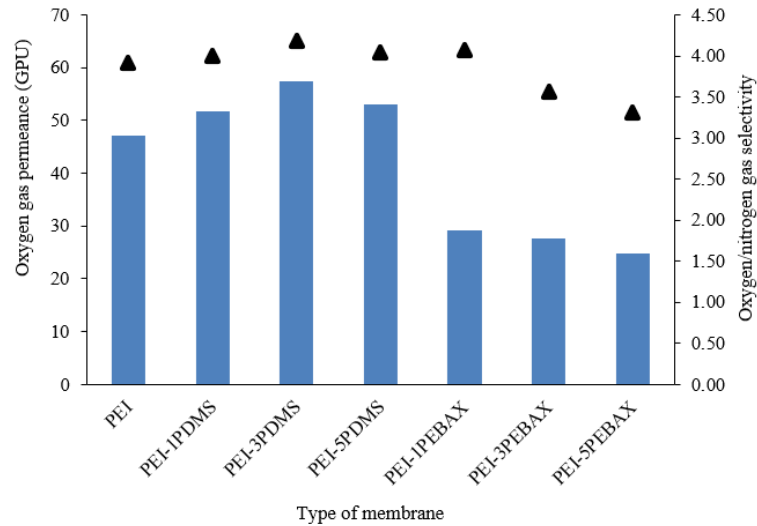


Figure 4.5 Oxygen gas permeance and oxygen/nitrogen gas selectivity of PEI dual-layer hollow fiber membrane with PDMS or PEBAX coating

The coating layer had successfully improved the membrane performance in terms of permeance and selectivity. Both PSU and PEI pristine membranes recorded an improvement in the range of 9.8 to 22.0% for O₂/N₂ gas permeance. The PDMS coating layer in the dual-layer membrane indicated the coating could improve surface defects on the membrane. Moreover, it had a more superior affinity with O₂ and N₂ gases that enabled better diffusion of these gases across the membrane as stated in the literature (Suleman, Lau and Yong, 2017). Additionally, PDMS coating possessed a low surface energy, which reduced the resistance for gas permeation. This low surface energy encouraged gases to diffuse more easily across the membrane surface (Roslan et al., 2020). PDMS was also a material that could undergo swelling when exposed to gases. This swelling opened up pathways for gas molecules to pass through, increasing the permeance (Haider et al., 2020). Similar to both PDMS and PEBAX dual-layer hollow fiber membranes, the separation performance

decreased when the coating concentration increased. This phenomenon was arisen due to the increase in the coating thickness on the membrane surface (Li et al., 2020), resulting in the increase in the mass transfer resistance, and therefore reducing the gas permeance across the membrane. These findings were in coherence with the literature where a high coating layer concentration reduced gas permeance and selectivity due to an increase in the coating thickness (Prajapati, Kansara and Singh, 2016; Dong et al., 2020). In the meantime, it was observed that PEBAX dual-layer hollow fiber membranes in both PSU and PEI experienced a lower gas permeation and selectivity compared with those for both pristine and PDMS dual-layer hollow fiber membranes. PEBAX coating solution experienced rapid gelation during the preparation and coating processes (Han et al, 2019). On the other hand, the previous findings in the literature reported the oxygen gas permeance ranging from 0.6 to 38.8 GPU, the nitrogen gas permeance ranging from 0.05 to 24.94 GPU and the O₂/N₂ selectivity ranging from 5.29 to 8.8 for the dual-layer hollow fiber membranes coated with either PDMS or PEBAX (Roslan et al., 2017; Chen et al., 2019). The gas permeance results for both oxygen and nitrogen gases in this study were found to be almost two folds higher compared with those reported by Roslan et al. (2017) and Chen et al. (2019) on dual-layer membrane. However, the oxygen and nitrogen gas selectivity found in this work was similar to that reported in the literature.

Based on the results, it was suggested that the best coating material and optimum coating concentration for dual-layer hollow fiber membranes for O₂/N₂ separation were PSU and 3%, respectively, and thus the PSU-3PDMS

dual-layer hollow fiber membranes yielded the highest permeance and selectivity in the oxygen and nitrogen gas separation compared with those of other dual-layer hollow fiber membranes studied in this research.

4.2.3 Summary

This section investigated the effect of PDMS or PEBAX coating layer in the dual-layer membrane on O₂/N₂ gas separation. The result suggested PDMS coating yielded better permeance performance relative to PEBAX coating for both PSU and PEI dual-layer membrane. These findings were coherent with the previous literature studies where the PDMS possessed better gas affinity with O₂ and N₂, allowing greater permeance performance. The optimum PDMS coating concentration in the dual-layer membrane was 3%, whereas the PSU dual-layer membrane possessed greater permeance and separation performance relative to PEI dual-layer membrane.

4.3 Effect of MOF materials and composition in CO₂ adsorption

4.3.1 Characterisation of physical and chemical properties

4.3.1.1 Surface morphology studies by scanning electron microscopy (SEM)

SEM analysis was performed to examine the surface morphology of Cr-MOFs fabricated from BTC or BDC, as shown in Figures 4.6 and 4.7. Both Cr-BTC and Cr-BDC MOFs displayed a similar surface morphology characterized by randomly dispersed, irregular diagonal particle shapes. This

surface morphology obtained was similar to that for a group of chromium-based MOFs fabricated by other researchers (Lu et al., 2022). A noticeable more regular shape was observed for both Cr-BDC and Cr-BTC MOFs as the molar ratio of metal oxide to organic acid decreased from 1:1 to 1:4. The size of crystal structures obtained was relatively wide, from about the size range of several micrometres to a few hundred micrometres. Moreover, the surface morphology results also indicated that a rough surface and porous structure favoured the adsorption of CO₂. Comparing the surface morphology of Cr-MOFs derived from BTC or BDC, it was observed that Cr-BTC had a more uniform structure than Cr-BDC, indicating a higher surface area to volume ratio and potentially better gas adsorption capacity.

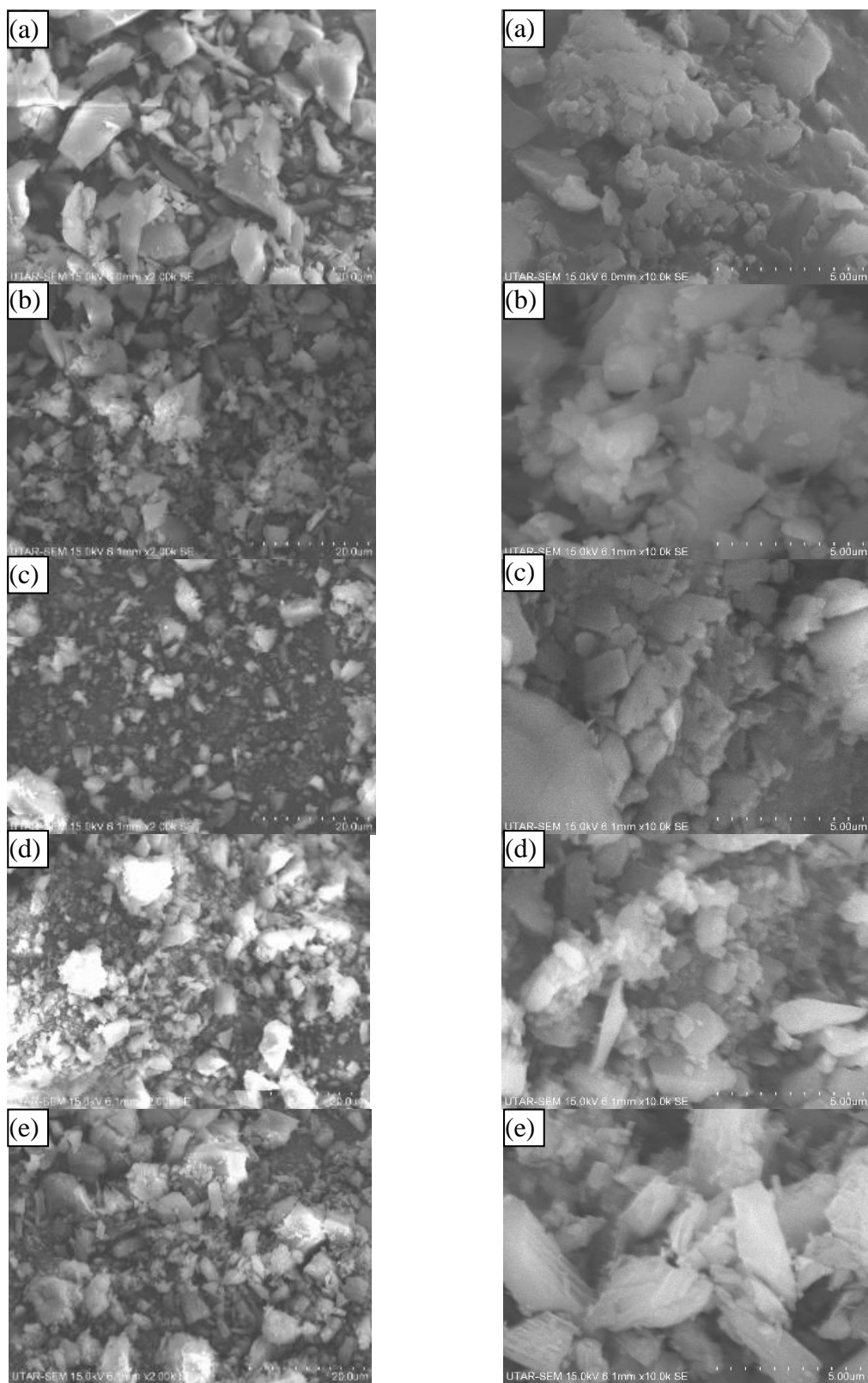


Figure 4.6. SEM morphologies at 2,000x and 10,000x magnification, respectively for (a) Cr-BDC-1:1, (b) Cr-BDC-1:2, (c) Cr-BDC-1:3, (d) Cr-BDC-1:4 and (e) Cr-BDC-1:5

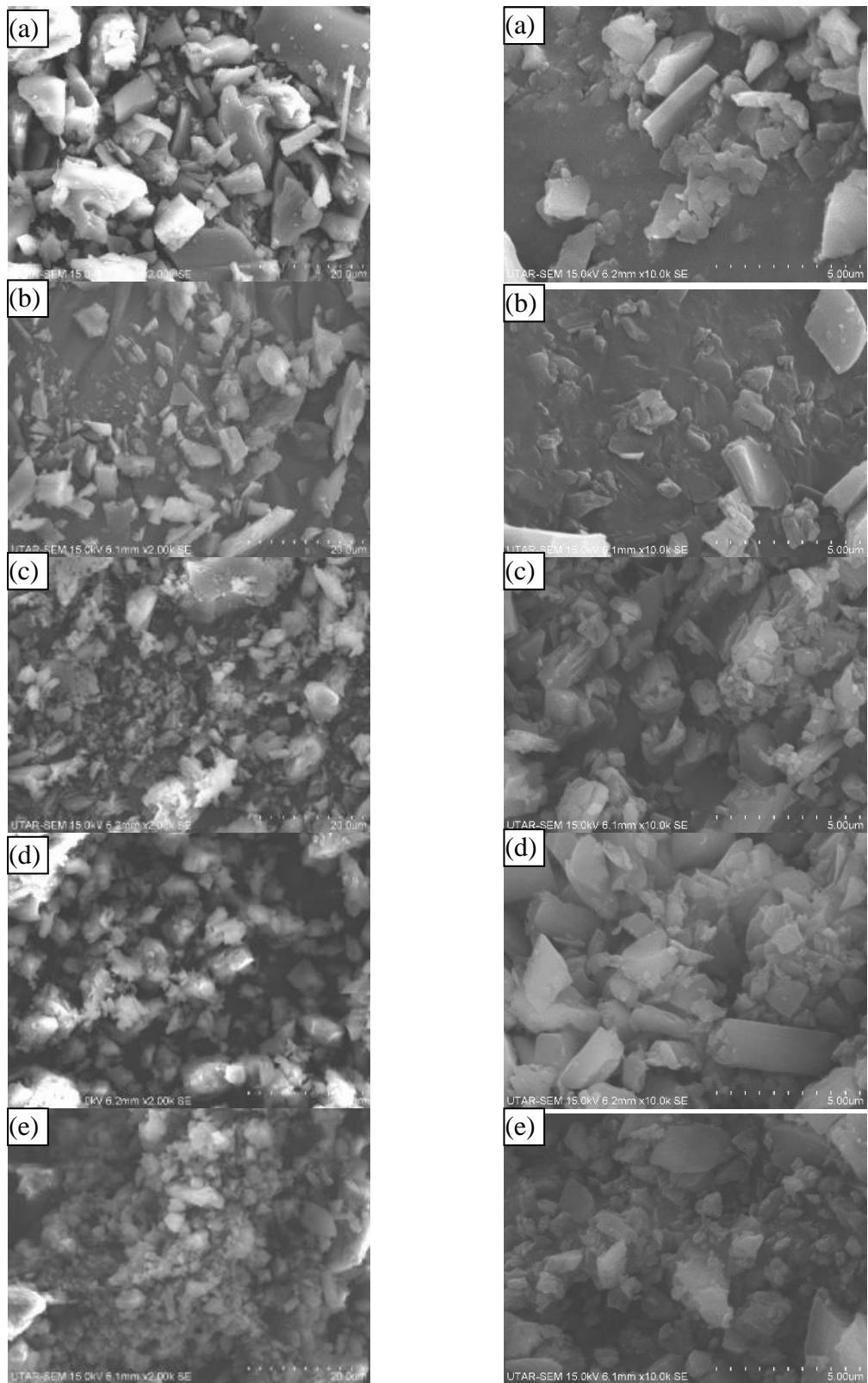


Figure 4.7. SEM surface morphology at 2,000x and 10,000x magnification, respectively for (a) Cr-BTC-1:1, (b) Cr-BTC-1:2, (c) Cr-BTC-1:3, (d) Cr-BTC-1:4 and (e) Cr-BTC-1:5

Figure 4.8 presents the SEM images for the Cu-BDC-1:1 to 1:5 MOFs. The fabricated Cu-BDC MOF showed a regular crystal with a square lattice structure. It was noted that the size of the crystals increased as the ratio of copper precursor to BDC increased from 1:2 to 1:5. Theoretically, the smaller size of the crystals tends to have a higher surface area to volume ratio and thus resulting in better performance in CO₂ gas adsorption (Qiu et al., 2020). Furthermore, no well-defined shape pattern was found in the SEM images of the Cu-BDC-1:3, 1:4 and 1:5 MOFs. This finding could be explained by reaction time and temperature (Lee, Kim and Ahn, 2013). In addition, a series of consecutive steps consisting of an intermediate solid phase was expected to follow during the formation of HKUST (Xu et al., 2020). Thus, the generation of the MOF that appeared as intermediate solid phase in this study were due to the insufficient reaction time to allow the crystal to be formed. Meanwhile, the Cu-BTC MOFs generally exhibited a slight spherical nanocrystal with hexagonal facets (Figure 4.9), similar to the HKUST crystal structure reported in the literature (Xue et al., 2019; Yulia, Nasruddin and Ruliandini, 2021). The size of the dense nanocrystal structure found in the Cu-BTC 1:1 MOF was approximately 1.5 to 3.5 μm. This dense structure suggested that the Cu-BTC MOF had a higher surface area to volume ratio, which could lead to a better gas adsorption capacity (Zhang et al., 2021; Ma et al., 2022).

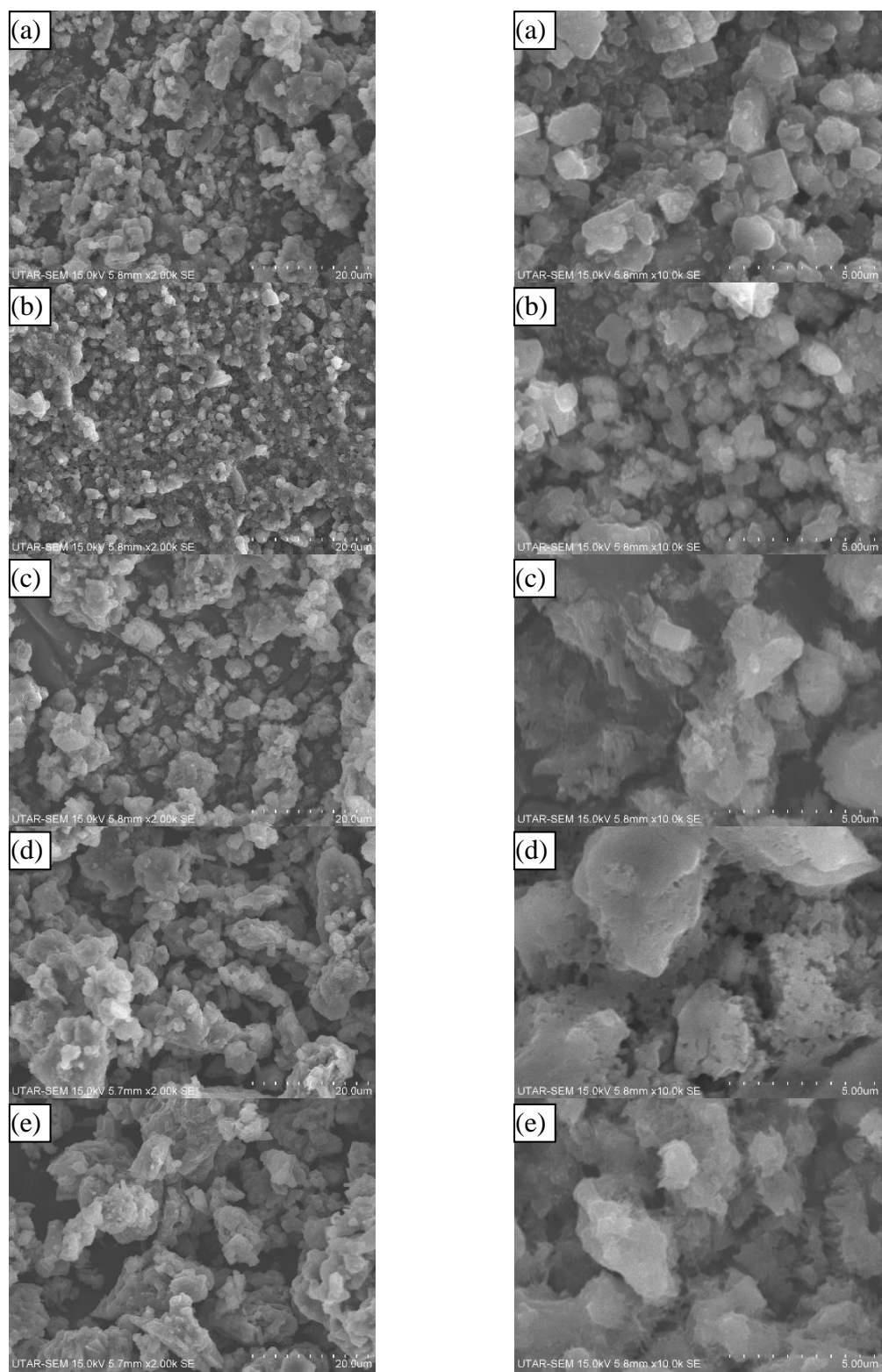


Figure 4.8. SEM surface morphology at 2,000x and 10,000x magnification, respectively for (a) Cu-BDC-1:1, (b) Cu-BDC-1:2, (c) Cu-BDC-1:3, (d) Cu-BDC-1:4 and (e) Cu-BDC-1:5

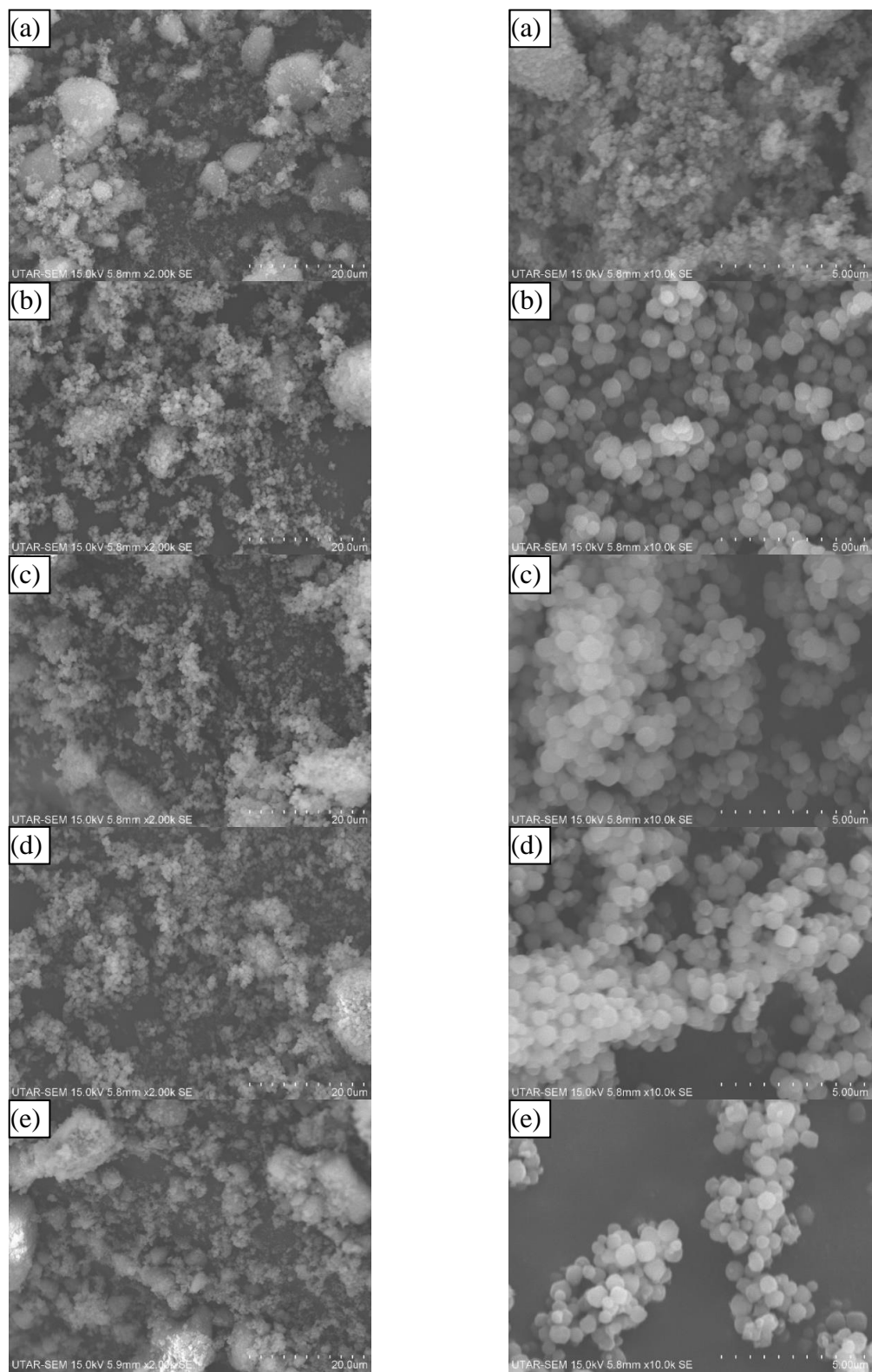


Figure 4.9. SEM morphologies at 2,000x and 10,000x magnification, respective for (a) Cu-BTC-1:1, (b) Cu- BTC-1:2, (c) Cu- BTC-1:3, (d) Cu- BTC-1:4 and (e) Cu- BTC -1:5

4.3.1.2 Elemental analysis by energy dispersion X-ray (EDX)

EDX analysis was employed to determine the elemental composition for both chromium and copper-based MOFs (Tables 4.5 and 4.6).

Table 4.5 Elemental analysis of chromium-based MOFs

Metal Organic Framework	Carbon, C (at%)	Oxygen, O (at%)	Chromium, Cr (at%)
Cr-BDC-1:1	44.84	42.87	12.29
Cr-BDC-1:2	42.21	47.60	10.19
Cr-BDC-1:3	43.10	46.60	10.30
Cr-BDC-1:4	42.26	46.13	11.61
Cr-BDC-1:5	45.00	48.18	6.82
Cr-BTC-1:1	39.59	48.92	11.49
Cr-BTC-1:2	48.45	41.08	10.47
Cr-BTC-1:3	47.89	41.84	10.27
Cr-BTC-1:4	45.06	44.95	9.99
Cr-BTC-1:5	48.94	44.94	6.12

Table 4.6 Elemental analysis of copper-based MOFs

Metal Organic Framework	Carbon, C (at%)	Oxygen, O (at%)	Copper, Co (at%)
Cu-BDC-1:1	39.87	42.65	17.48
Cu-BDC-1:2	42.23	41.42	16.35
Cu-BDC-1:3	43.06	42.12	14.82
Cu-BDC-1:4	44.35	42.02	13.63
Cu-BDC-1:5	46.35	42.99	10.66
Cu-BTC-1:1	40.28	38.88	20.84
Cu-BTC-1:2	45.92	34.32	19.76
Cu-BTC-1:3	43.39	39.95	16.66
Cu-BTC-1:4	44.01	45.01	10.98
Cu-BTC-1:5	45.20	49.55	5.25

The EDX results revealed that chromium and copper precursors were successfully incorporated into all the fabricated chromium and copper-based MOFs, respectively (Table 4.5 and 4.6). Additionally, carbon (C) and oxygen (O) atoms found in the carboxylic organic linkers (BDC and BTC) were discovered in all the chromium and copper-based MOFs. Both Cr-BDC and Cr-BTC MOFs experienced a decline in the weight percent of chromium during a surge in the total weight percent of C and O as a result of an increment in organic ligand molar ratio. It was also noteworthy that a similar phenomenon was observed in copper-based MOFs, showing a good agreement of the findings.

4.3.1.3 Crystallographic structure studies by X-ray diffraction analysis (XRD)

Figure 4.10 shows the XRD pattern for the chromium-based and copper-based MOFs. The XRD diffractogram of the chromium-based MOFs fabricated with either BDC or BTC ligand depicted a similar pattern with the peak at 2θ value at 10° , which was similar to the findings of the MIL-101 MOF in the literature (Montazerolghaem et al., 2017). Nevertheless, several minor peaks discovered at the Cr-BTC-1:3, 1:4 and 1:5 suggested that the MOFs might contain impurities. In the meantime, the XRD diffractogram of the copper-based MOFs fabricated with either BDC and BTC ligand demonstrated a comparable pattern to the HKUST MOF where at 2θ value at 6.3° , 9.2° , 10.7° and 12.6° , respectively which were well agreed with the results reported by Montazerolghaem et al. (2017) and Ma et al. (2022).

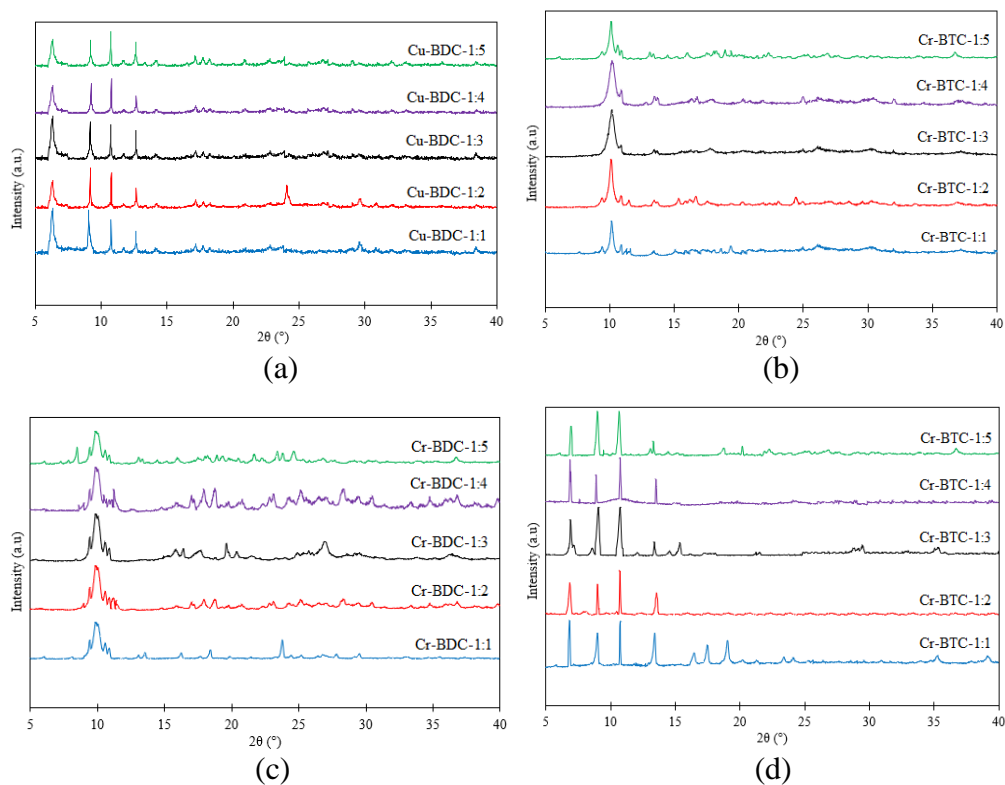


Figure 4.10. XRD analysis for (a) Cr-BDC, (b) Cr-BTC, (c) Cu-BDC and (d)

Cu-BTC

4.3.1.4 Surface area analysis by BET

The BET analysis was employed to determine the surface area for both chromium and copper-based MOFs (Table 4.7). The chromium and copper-based MOFs' success in the literature studies were attributed to the superior BET surface area and its effectiveness in carbon dioxide adsorption (Seetharaj et al., 2019). The literature reported BET surface area of the chromium-based (MIL-101) and copper-based MOF (HKUST) recorded at the range of 1,326 to 2,549 m²/g. Nevertheless, the range of the BET surface area of the MOFs was wide, depending on the fabrication methods, parameters and ratio of raw materials. In this study, the BET surface area of chromium-based MOFs was

measured in the range from 380.21 to 963.10 m²/g, whereas the BET surface area range of the copper-based MOF was from 312.92 to 1,039.28 m²/g (Table 4.7). Therefore, the results in this study were generally lower than those reported in literature despite sharing a similar XRD pattern to the renowned MOFs such as MIL-101 and HKUST. This phenomenon might be attributed to the fabrication method at lower heating temperature and time compared with the conventional solvothermal method, leading to the formation of lower surface area due to the agglomeration of the metal precursor with the organic ligand (Seetharaj et al., 2019).

Table 4.7 BET surface area analysis of MOFs

Metal Organic Framework	BET surface area (m²/g)	Metal Organic Framework	BET surface area (m²/g)
Cr-BDC-1:1	380.21	Cu-BDC-1:1	683.63
Cr-BDC-1:2	420.13	Cu-BDC-1:2	620.35
Cr-BDC-1:3	396.93	Cu-BDC-1:3	426.04
Cr-BDC-1:4	417.02	Cu-BDC-1:4	385.62
Cr-BDC-1:5	487.57	Cu-BDC-1:5	312.92
Cr-BTC-1:1	531.23	Cu-BTC-1:1	1,039.28
Cr-BTC-1:2	575.72	Cu-BTC-1:2	903.57
Cr-BTC-1:3	796.14	Cu-BTC-1:3	774.82
Cr-BTC-1:4	909.64	Cu-BTC-1:4	549.72
Cr-BTC-1:5	963.10	Cu-BTC-1:5	516.28

4.3.2 Performance of CO₂ adsorption

The chromium and copper-based MOFs fabricated in this study were tested for its performance in the CO₂ gas adsorption test. The CO₂ adsorption performance of the fabricated MOFs is summarized in Table 4.8.

Table 4.8 CO₂ gas adsorption of MOFs

Metal Organic Framework	Adsorption (mmol/g)	Metal Organic Framework	Adsorption (mmol/g)
Cr-BDC-1:1	0.07 ± 0.004	Cu-BDC-1:1	0.23 ± 0.014
Cr-BDC-1:2	0.10 ± 0.007	Cu-BDC-1:2	0.17 ± 0.009
Cr-BDC-1:3	0.13 ± 0.005	Cu-BDC-1:3	0.11 ± 0.006
Cr-BDC-1:4	0.18 ± 0.003	Cu-BDC-1:4	0.10 ± 0.007
Cr-BDC-1:5	0.21 ± 0.006	Cu-BDC-1:5	0.08 ± 0.008
Cr-BTC-1:1	0.25 ± 0.012	Cu-BTC-1:1	1.31 ± 0.042
Cr-BTC-1:2	0.37 ± 0.035	Cu-BTC-1:2	0.93 ± 0.034
Cr-BTC-1:3	0.51 ± 0.027	Cu-BTC-1:3	0.84 ± 0.038
Cr-BTC-1:4	0.89 ± 0.039	Cu-BTC-1:4	0.75 ± 0.041
Cr-BTC-1:5	0.95 ± 0.032	Cu-BTC-1:5	0.61 ± 0.037

In general, the CO₂ gas adsorption performance for the Cr-BDC and Cr-BTC MOFs increased with the molar ratio. This phenomenon might be caused by the increase in the BET surface area for the Cr-BDC MOF with the increasing molar ratio (Zhao et al., 2018). Nevertheless, it was observed that the CO₂ adsorption exhibited by the Cr-BTC MOF appeared to be greater than

the Cr-BDC MOF due to the higher superior surface area and degree of crystallization structure of the MOF. It is worth highlighted that the intriguing observation that Cu and Cr-based MOFs, especially BTC as the organic ligand, consistently demonstrated superior adsorption capabilities in contrast to BDC organic ligand (Yulia, Nasruddin and Ruliandini, 2021). On the other hand, the copper-based MOF presented an opposite phenomenon, where the increment of the molar ratio reduced CO₂ adsorption. The BET surface area where the increment of the molar ratio led to the more inferior crystal structure of the MOFs as the size of the crystals obtained increased and the BET surface area decreased. In general, it was concluded that the copper-based MOFs could produce a better CO₂ adsorption result, i.e., best performance of the chromium and copper-based MOFs were recorded at 0.95 mmol/g (Cr-BTC-1:5) and 1.31 mmol/g (Cu-BTC-1:1), respectively. This phenomenon could be attributed to the enhanced electrostatic interaction between the BTC ligand and Cu, leading to the formation of coordinatively unsaturated metal centers that facilitated greater adsorption of CO₂ (Chowdhury et al., 2012).

4.3.3 Summary

In a nutshell, this section investigated the use of the MOFs in the evaluation of the CO₂ gas adsorption performance. Two types of MOF were investigated, namely chromium and copper-based MOFs with either BDC or BTC as organic ligand. Solvothermal method was used to successfully fabricate the MOFs, which were characterised for their physiochemical properties. In general, the chromium-based MOF exhibited a crystal structure

of non-uniform dispersed irregular multifaceted diagonal shape of particles. In contrast, the copper-based MOF illustrated a regular crystal structure with a square lattice structure. The XRD analysis confirmed the successful fabrication of the MOFs, whereby all the peaks from necessary elements derived from the raw materials were identified, suggesting that the organic ligand was well linked the metal precursors. Additionally, the XRD peaks of the chromium-based and copper-based MOFs in this study were similar to those reported for the MIL-101 and HKUST MOFs in the literature, respectively. The BET surface analysis suggested that the Cu-BTC MOFs generally showed a greater surface area amongst all the MOF samples. Based on the previously reported CO₂ adsorption performance using chromium and copper based MOF such as MIL-101 and HKUST with the range from 0.15 to 2.5 mmol/g, respectively (Mu et al., 2018), there is still room for improvement for the best MOF (Cu BTC-1:1) fabricated in this study with the measured CO₂ adsorption performance of 1.31 mmol/g in the future. The physiochemical findings were coherent with the CO₂ gas adsorption results, whereby the Cu-BTC MOFs typically recorded a better CO₂ adsorption performance, and among them Cu-BTC-1:1 recorded the highest CO₂ adsorption at 1.31 mmol/g. This noteworthy finding aligns with previous literature studies. Specifically, Cu-BTC MOFs consistently exhibit higher CO₂ adsorption capacities than Cr-BTC MOFs (Zhao et al., 2018). This phenomenon can be attributed to the enhanced electrostatic interaction between the BTC ligand and Cu, leading to the formation of coordinatively unsaturated metal centers that facilitate greater adsorption of CO₂.

4.4 O₂ enrichment and CO₂ reduction in the actual environment

4.4.1 Indoor O₂ enrichment

The indoor O₂ enrichment experiment was carried out to study the O₂ separation performance by the PSU-3PDMS hollow fiber membrane from the air with respect to the sampling time. The test was carried at the humidity of $55 \pm 5\%$, room temperature of 24°C , and atmospheric pressure.

As observed from Figure 4.11, the inlet oxygen concentration was recorded at $20.74 \pm 1\%$, which was similar to the ambient air oxygen concentration. The outlet oxygen concentration was measured in the range of 20.87 to 20.94%, with an enrichment of maximum at 0.2% or an overall enrichment of 1.00% with respect to the inlet oxygen concentration of 20.74%. The performance of the O₂ enrichment decreased with respect to time and it was found that humidity from the air exerted a negative impact on membranes. This influence would reduce membrane selectivity, and in more severe instances, it might induce membrane swelling (Ansaloni et al., 2014). The enrichment of 0.2% was appeared to be a significant result based on the lab-scale experimental study. Zhang et al. (2021) reported the similar studies in introducing oxygen enriched air into the air-conditioned space using PSA method to improve the symptom of micro-hypoxia experienced by indoor occupants. Their study revealed that the PSA method was able to improve the indoor oxygen concentration from ambient oxygen concentration up to 22%, but with an annual operation cost of RMB 2,500 (RM 1,600) for a room with the dimension of 6.8 m length, 4 m width and 2.9 m height. A comparison was conducted between the literature and this study, and the result showed that the

membrane technology involves a lower annual operation cost (annual energy cost of RM 290) with comparable oxygen concentration. Moreover, the plateau of indoor oxygen concentration for the good health effect was at 20.95%, indicating the current oxygen concentration measured in this study was optimum for the human health (Ha, Metia and Phung, 2020). It was noteworthy to mention that the separation performance was observed to be in the decreasing trend throughout the 12 hours of sampling time, from the beginning oxygen concentration of 20.94% to 20.87% at the 12th hour. These findings suggested that the dual-layer membrane possesses the potential to enrich the O₂ concentration in the actual environment.

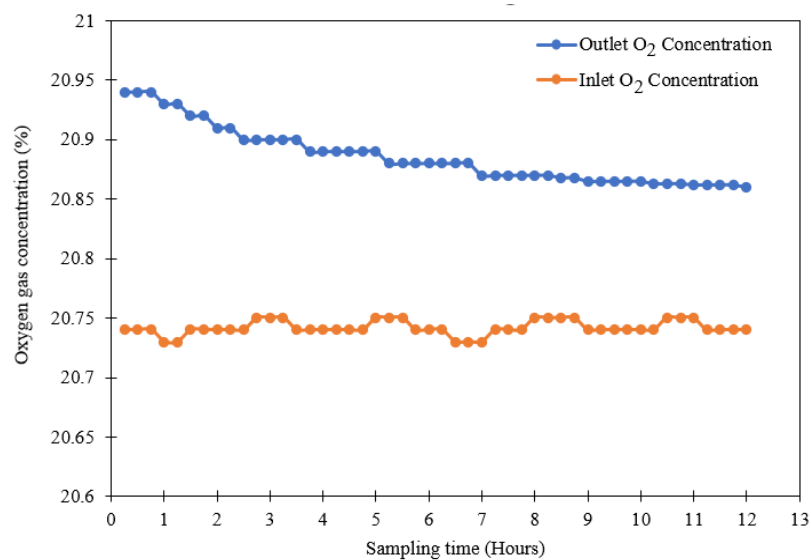


Figure 4.11 Temporal changes of the oxygen gas concentration with respect to the sampling time

4.4.2 Indoor CO₂ reduction

The indoor CO₂ reduction study was carried out to investigate the CO₂ adsorption performance by the Cu-BTC-1:1 MOF from the air with respect to

the sampling time. The study was carried at the humidity of $55 \pm 5\%$, room temperature of 24°C , and atmospheric pressure.

Figure 4.12 shows that the inlet CO_2 concentration was measured at 881 ± 6 ppm. The CO_2 level with one occupancy in the enclosed volume indicated that it was still found to be within the threshold of 1,000 ppm as regulated by the Department of Occupational Safety and Health, Malaysia. The outlet CO_2 concentration was measured at 865 ± 8 ppm, with an average reduction of 16 ppm or 1.81%. As observed in Figure 4.13, the adsorption performance of the Cu-BTC-1:1 MOF experienced a slight decrease as a similar pattern was found in the literature, suggesting the pore volume of the MOF was experiencing a negative trend in the capture of the CO_2 gas (Liu et al., 2018). The findings suggested that the copper-based MOF possesses the potential to enhance CO_2 reduction in the actual environment. With further improvement of the MOF, a more superior CO_2 reduction can be anticipated.

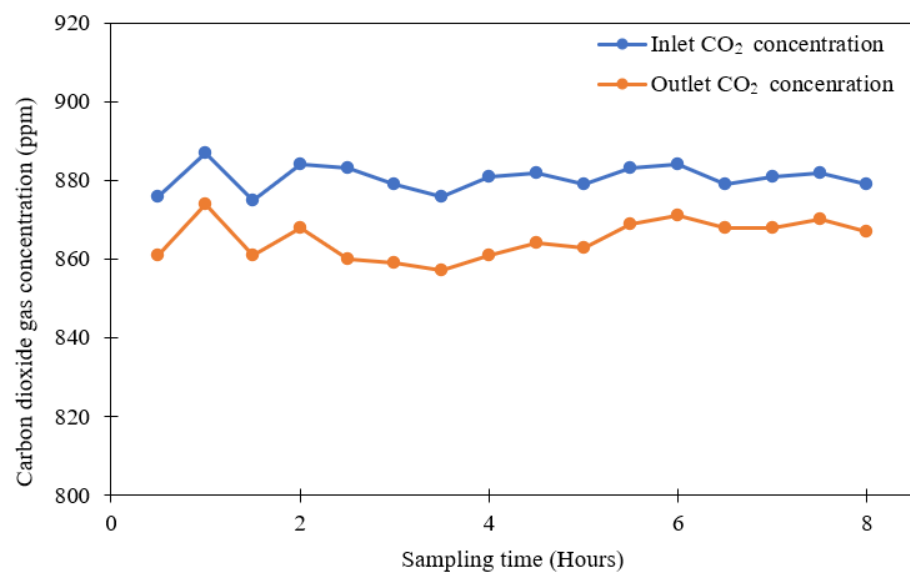


Figure 4.12 Temporal changes of the carbon dioxide gas concentration with respect to the sampling time

4.4.3 Summary

In summary, this section attempted to resolve indoor air pollution by proposing a novel method in enhancing the O₂ gas concentration and reducing CO₂ gas concentration. The proposed solution was to use the dual-layer membrane to separate the O₂ gas from the ambient air and transfer it into the indoor environment to increase the freshness of the air breathed in by humans. Additionally, the reduction of the CO₂ concentration is able to assist in lowering the sick building syndrome, which may lead to a reduction in productivity in the workplace and attendance rate in an educational institution. The PSU-3PDMS hollow fiber membrane was found to be able to increase the O₂ concentration up to 0.2%, and the Cu-BTC-1:1 MOF showed the best performance of CO₂ reduction up to 16 ppm. The results from this study suggested the possibility of integrating the dual-layer membrane and MOF to improve indoor air quality for the betterment of human life.

CHAPTER 5

CONCLUSIONS AND RECOMMENDATIONS

5.1 Conclusions

In this research, the performance results of O₂/N₂ gas separation via membrane technology and CO₂ gas adsorption using MOF were determined. PSU-3 and PEI-3 showed a better permeance performance relative to the same materials (PSU-1, PSU-2, and PEI-1, PEI-2) at different bore fluid flow rates. Both PSU and PEI membranes experienced the same phenomenon, where bore fluid flow rate had a positive effect on both the oxygen and nitrogen gas permeation and selectivity. On the other hand, the material comparison between the PSU and PEI hollow fiber membrane suggested that the PSU hollow fiber membrane achieved better performance in terms of permeance and selectivity. The better performance recorded by the PSU hollow fiber membrane was attributed to the membrane thickness of PSU was greater than PEI hollow fiber membrane under similar fabricating parameters and the effect of porosity.

The PDMS coating layer in the dual-layer membrane indicated that the coating improved surface defects on the membrane. Moreover, it had a more superior affinity with O₂ and N₂ gases that enable better diffusion of these gases across the membrane as depicted in the literature studies (Haider et al.,

2020). In the meantime, it was observed that the PEBAX dual-layer membrane in both PSU and PEI experienced a lower gas permeation and selectivity relative to both pristine and PDMS dual-layer membranes. The optimum coating and concentration for dual-layer membrane for O₂/N₂ separation were PSU and 3%, respectively. This membrane (PSU-3PDMS) could yield the highest permeance and selectivity in the separation compared to other dual-layer membranes.

Two types of MOFs were investigated, namely chromium and copper-based MOFs with either BDC or BTC as organic ligand. The BET surface analysis suggested that Cu-BTC MOFs generally showed a greater surface area amongst all the MOF samples. The physiochemical findings were coherent with the CO₂ gas adsorption results whereby the Cu-BTC MOFs typically recorded a better CO₂ adsorption performance, and Cu-BTC-1:1 recorded the highest CO₂ adsorption at 1.31 mmol/g.

In summary, PSU-3PDMS was found to best increase the O₂ concentration up to 0.2%, and the Cu-BTC-1:1 possessed the best performance of CO₂ reduction up to 16 ppm. The results from this study implied the possibility of integrating the dual-layer membrane and MOF to improve indoor air quality for the betterment of human life.

5.2 Recommendations

Aside from the tasks accomplished in this study, there are numerous

compelling topics that could be explored in future investigations, including:

- To further improve the dual-layer membrane beyond the current study by achieving even higher permeance and selectivity, as well as exceptional long-term membrane characteristics during operation.
- To explore in future studies the synthesis of MOFs with higher CO₂ gas adsorption by further investigating the combination of metal precursors and organic ligands, while also ensuring excellent characteristics during long-term operating conditions.
- To assess the feasibility of a large-scale investigation on the O₂ enrichment by dual-layer membrane coupled with dehumidifier and CO₂ reduction by MOF in the actual environment for it to be a commercially viable as commercial product.

REFERENCES

Abdul, A.A., Naji, S.Z., Hashim, A.S., and Othman, M.R., 2020. Carbon dioxide removal through physical adsorption using carbonaceous and non-carbonaceous adsorbents: A review. *Journal of Environmental Chemical Engineering*, 8(5), pp. 104142–104162.

Adhikari, B., Orme, C.J., Klaehn, J.R., and Stewart, F.F., 2021. Technoeconomic analysis of oxygen-nitrogen separation for oxygen enrichment using membranes, *Separation and Purification Technology*, 268, pp. 118703–118715.

Afshoun, H.R., Chenar, M.P., Moradi, M.R., Ismail, A.F., and Matsuura, T., 2019. Effects of halloysite nanotubes on the morphology and CO₂/CH₄ separation performance of Pebax/polyetherimide thin-film composite membranes. *Journal of Applied Polymer Science*, 137(28), pp.48860–48860.

Al Obeidli, A., Salah, B.H., Al Murisi, M., and Sabouni, R., 2022. Recent advancements in MOFs synthesis and their green applications. *International Journal of Hydrogen Energy*, 47(4), pp.2561–2593.

Alobaidy, A.A., Sherhan, B.Y., Barood, A.D., and Alsahy, Q.F., 2017. Effect of bore fluid flow rate on formation and properties of hollow fibers. *Applied Water Science*, 7, pp. 4387–4398.

Alqaheem, Y., and Alomair, A., 2019. Recent developments in polyetherimide membrane for gas separation, *Journal of the Chinese Chemical Society*, 6(12), pp. 1738– 1744.

Al-Rowaili, F.N., Zahid, U., Onaizi, S., Khaled, M., Jamal, A., and AL-Mutairi, E.M., 2021, A review for metal-organic Frameworks (MOFs) utilization in capture and conversion of carbon dioxide into valuable products, *Journal of CO₂ Utilization*, 53, pp. 101715.

Ansaloni, L., Minelli, M., Giacinti Baschetti, M. and Sarti, G.C., 2014. Effect of relative humidity and temperature on gas transport in Matrimid®: Experimental study and modeling. *Journal of Membrane Science*, 471, pp. 392–401.

Babu, V.P., Kraftschik, B.E., and Koros, W.J., 2018. Crosslinkable TEGMC asymmetric hollow fiber membranes for aggressive sour gas separations. *Journal of Membrane Science*, 558, pp. 94–105.

Baker, R. W. 2002. Future directions of membrane gas separation technology. *Industrial & Engineering Chemistry Research*, 41(6), pp. 1393–1411.

Chen, F., and Chen, Z., 2020. Cost of economic growth: Air pollution and health expenditure, *Science of the Total Environment*, 755(1), pp. 142543–142594.

Chen, S.J., and Yu, B.Y., 2021. Rigorous simulation and techno-economic evaluation on the hybrid membrane/cryogenic distillation processes for air separation. *Journal of the Taiwan Institute of Chemical Engineers*, 127, pp. 56–68.

Chen, X., Gao, H., Tang, Z., and Wang, G., 2020. Metal-organic framework-based phase change materials for thermal energy storage. *Cell Reports Physical Sciences*, 1(10), pp. 100218–100246.

Chen, X.Y., Kaliaguine, S., and Rodrigue, D., 2019. Polymer hollow fiber membranes for gas separation: A comparison between three commercial resins. *AIP Conference Proceedings*, 2139 (070003), pp. 1–5.

Chin, C., Kamin, Z., Bahrin, M.H.V., and Bono, A., 2023. The production of industrial-Grade oxygen from air by pressure swing adsorption. *International Journal of Chemical Engineering*, 2023, pp. 2308227.

Choi, S.H., Sultan, M.M.B., Alsuwailem, A.A., and Zuabi, S.M., 2019. Preparation and characterization of multilayer thin-film composite hollow fiber membranes for helium extraction from its mixtures. *Separation and Purification Technology*, 222, pp. 152–161.

Chong, K.C. Lai, S.O., Lau, W.J., Thiam, H.S., Ismail, and A.F., Zulhairun, A.K., 2017. Fabrication and characterization of polysulfone membranes coated with polydimethylsiloxane for oxygen enrichment, *Aerosol and Air Quality Research*, 17(11), pp. 2735–2742.

Chong, K.C., Lai, S.O., Lau, W.J., Thiam, H.S., Ismail, A.F., and Roslan, R., 2018. Preparation, characterization, and performance evaluation of polysulfone hollow fiber membrane with PEBA_X or PDMS coating for oxygen enhancement process. *Polymers*, 10(2), pp. 126–136.

Chong, K.C., Lai, S.O., Thiam, H.S., Teoh, H.C., and Heng, S.L., 2016. Recent progress of oxygen/nitrogen separation using membrane technology, *Journal of Engineering and Science Technology*, 11(7), pp. 1016–1030.

Chuhadiya, S., Himanshu, Suthar, D., Patel, S.L., and Dhaka, M.S., 2021, Metal organic frameworks as hybrid porous materials for energy storage and conversion devices: A review, *Coordination Chemistry Reviews*, 446, pp. 214115–214140.

Deng, J., Huang, Z., Sundell, B.J., Harrigan, D.J., Sharber, S.A., Zhang, K., Guo, R., and Galizia, M., 2021. State of the art and prospects of chemically and thermally aggressive membrane gas separations: Insights from polymer science. *Polymer*, 229, pp. 123988–124027.

Dey, S., Bugel, S., Sorribas, S., Nuhenen, A., Bhunia, A., Coronas, J., and Janiak, C., 2019. Synthesis and characterization of covalent triazine framework CTF-1@Polysulfone mixed matrix membranes and their gas separation studies. *Frontiers in Chemistry*, 7(693), pp. 1–8.

Ding, X., Tan, F., Zhao, H., Hua, M., Wang, M., Xin, Q., and Zhang, Y., 2019. Enhancing gas permeation and separation performance of polymeric membrane by incorporating hollow polyamide nanoparticles with dense shell. *Journal of Membrane Science*, 570-571, pp. 53–60.

Dong, Z., Zhu, H., Hang, Y., Liu, G., and Jin, W., 2020. Polydimethylsiloxane (PDMS) composite membrane fabricated on the inner surface of a ceramic hollow fiber: From single-channel to multi-channel, *Engineering*, 6(1), pp. 89–99.

Edens, S.J., McGrath, M.S., Guo, S., Du, Z., Zhou, H., Zhong, L., Shi, Z., Wan, J., Bennett, T.D., Qiao, A., Tao, H., Li, N., and Cowan, M.G., 2023. An upper bound visualization of design trade-offs in adsorbent materials for gas separations: CO₂, N₂, CH₄, H₂, O₂, Xe, Kr, and Ar Adsorbents, *Advanced Science*, 10(8), pp. 1–30.

Feng, W., Liu, Y., Bi, Y., Su, X., Lu, C., Han, X., Ma, Y., Feng, C., and Ma, M., 2023. Recent advancement of magnetic MOF composites in microwave absorption. *Synthetic Metals*, 294, pp.117307–117307.

Férey G., Mellot-Draznieks, C., Serre, C., Millange, F., Dutour, J., Surblé, S, and Margiolaki, I., 2005. A chromium terephthalate-based solid with unusually large pore volumes and surface area. *Science*, 309(5743), pp. 2040–2042.

Fu, X., Norback, D., Yuan, Q., Li, Y., Zhu, X., Hashim, J.H., Hashim, Z., Ali, F., Hu, Q., Deng, Y., and Sun, Y., 2021, Association between indoor microbiome exposure and sick building syndrome (SBS) in junior high schools of Johor Bahru, Malaysia, *Science of The Total Environment*, 754, pp. 141904–141914.

Fuoco, A., Khdhayyer, M. R., Attfield, M. P., Esposito, E., Jansen, J. C., and Budd, P.M. 2017. Synthesis and Transport Properties of Novel MOF/PIM-1/MOF Sandwich Membranes for Gas Separation. *Membranes*, 7(1), pp. 7–24.

Gaikwad, S., Kim, S.J., and Han, S., 2019. CO₂ capture using amine-functionalized bimetallic MIL-101 MOFs and their stability on exposure to humid air and acid gases, *Microporous Mesoporous Materials*, 277, pp. 253–260.

Gao, X., Jali, Z.M., Aziz, A.R., Hizaddin, H.F., Buthiyappan, A., Jewaratnam, J., and Bello, M.M., 2021, Inherent health oriented design for preventing sick building syndrome during planning stage, *Journal of Building Engineering*, 44, pp. 103285.

Ghanbari, T., Abnisa, F., and Daud, W.M.A.W., 2020. A review on production of metal organic frameworks (MOF) for CO₂ adsorption, *Science of the Total Environment*, 707, pp. 13509 –135118.

Ha, Q.P., Metia, S., and Phung, M.D., 2020. Sensing data fusion for enhanced indoor air quality monitoring. *IEEE Sensors Journal*, 20(8), pp. 4430–4441.

Haider, B, Dilshad, M.R., Rehman, M.A., Akram, M.S., and Kaspereit, M. 2020. ‘Highly permeable innovative PDMS coated polyethersulfone membranes embedded with activated carbon for gas separation’, *Journal of Natural Gas Science and Engineering*, 81, pp. 103406

Han, J., Bai, L., Yang, B., Bai, Y., Luo, S., Zeng, S., Gao, H., Nie, Y. Ji, X., Zhang, S., and Zhang, X., 2019. Highly selective oxygen/nitrogen separation membrane engineered using a porphyrin-based oxygen carrier, *Membranes*, 9(115), pp. 1–14.

Hu, C.C., Yeh, H.H., Hu, C.P., Lecaros, L.G., Cheng, C.C., Hung, W.S., Tsai, H.A., Lee, K.R., and Lai, J.Y., 2022. The influence of intermediate layer and graphene oxide modification on the CO₂ capture efficiency of Pebax-GO/PDMS/PSf mixed matrix composite membranes. *Journal of The Taiwan Institute of Chemical Engineers*, 135, pp.104379–104379.

Jamil, A., Oh, P.C., and Shariff, A.M., 2018. Polyetherimide-montmorillonite mixed matrix hollow fiber membranes: effect of inorganic/organic montmorillonite on CO₂/CH₄ separation. *Separation and Purification Technology*, 206, pp. 256–267.

Jiang, H., Gao, Q., Wang, S., Chen, Y., and Zhang, M., 2019. The synergistic effect of Pd NPs and UiO-66 for enhanced activity of carbon dioxide

methanation. *Journal of CO₂ Utilization*, 31, pp. 167–172.

Ji, G. and Zhao, M., 2017. Membrane separation technology in carbon capture. *Recent Advances in Carbon Capture and Storage*.

Kamble, A.R., Patel, C.M. and and Murthy, Z.V.P., 2021. A review on the recent advances in mixed matrix membranes for gas separation processes. *Renewable and Sustainable Energy Reviews*, 145, p.111062.

Kamin, Z., Bahrin, M.H.V., and Bono, A., 2022. A short review on pressure swing adsorption (PSA) technology for nitrogen generation from air. *International Scientific Forum on Computer and Energy Sciences (WFCES-II 2021)*.

Kari, N., Bustam, M. and Ismail, M., 2021. Metal-organic frameworks: Screening M-MOF-74 (M = Co, Cr, Cu, Fe, Mg, Mn, Ni, Ti, and Zn) based for carbon dioxide adsorption, *E3S Web of Conferences*, 287 (02011), pp. 1–5.

Karim, S.S., Farrukh, S., Hussain, A., Noor, T., and Younas, M., 2021. A comprehensive overview of dual-layer composite membrane for air (O₂/N₂) separation. *Polymers & Polymer Composites*, 29(9), pp. S1630–S1640.

Khamal, R., Isa, Z., Sutan, R., Razif, N., and Ghazi, N. H., 2019. Indoor particulate matters, microbial count assessments, and wheezing symptoms among toddlers in urban day care centers in the district of Seremban, Malaysia,

Annals of Global Health, 85, pp. 1–12.

Kumar, A., Kuang, Y., Liang, Z., and Sun, X., 2020. Microwave chemistry, recent advancements, and eco-friendly microwave-assisted synthesis of nanoarchitectures and their applications: a review. *Materials Today Nano*, 11, pp. 100076–100096.

Lai, S.O., Chong, K.C., and Lau, W.J., 2019. ‘Prospects of nanocomposite membranes for nitrogen and oxygen enrichment’ in Sadrzadeh M. and Mohammadi T. (First edition) *Nanocomposite membranes for water and gas separation*. Amsterdam: Elsevier, pp. 379–396.

Lawson, S., Griffin, C., Rapp, K., Rownaghi, A.A., and Rezaei, F., 2019. Amine-functionalized MIL-101 monoliths for CO₂ removal from enclosed environments, *Energy Fuels*, 33, pp. 2399–2407.

Le, V.N., Vo, T.K., Lee, J.H., Kim, J.C., Kim, T.H., Oh, K.H., Bae, Y.S., Kwak, S.K., and Kim, J., 2021. A novel approach to prepare Cu(i)Zn@MIL-100(Fe) adsorbent with high CO adsorption capacity, CO/CO₂ selectivity and stability via controlled host-guest redox reaction, *Chemical Engineering Journal*, 404, pp. 126492–116503.

Lee, Y.R., Kim, J., and Ahn, W.S., 2013. Synthesis of metal-organic frameworks: A mini review. *Korean Journal of Chemical Engineering*, 30(9), pp. 1667–1680.

Li, G., Kujawski, W., Valek, R., and Koter, S., 2021. A review - The development of hollow fiber membranes for gas separation processes, *International Journal of Greenhouse Gas Control*, 104, pp. 103195–103125.

Li, Z., Gao, R., Feng, M., Deng, Y.-P., Xiao, D., Zheng, Y., Zhao, Z., Luo, D., Liu, Y., Zhang, Z., Wang, D., Li, Q., Li, H., Wang, X., and Chen, Z., 2021. Modulating metal–organic frameworks as advanced oxygen electrocatalysts, *Advanced Energy Materials*, 11(16), p. 2003291.

Liang, C.Z., Chung, T.S, and Lai, J.Y., 2019. A review of polymeric composite membranes for gas separation and energy production. *Progress in Polymer Science*, 97, pp. 101141–101159.

Liu, S., Zhou, G., Cheng, G., Wang, X., Liu, G., and Jin, W., 2022. Emerging membranes for separation of organic solvent mixtures by pervaporation or vapor permeation. *Separation and Purification Technology*, 299, pp. 121729–121747.

Liu, Y., Liu, S., Gonçalves, A.A.S., and Jaroniec, M., 2018. Effect of metal–ligand ratio on the CO₂ adsorption properties of Cu–BTC metal–organic frameworks. *RSC Advance*, 8, pp 35551–35556.

Lu, T., Fan, Y., Wang, X., Wang, Q., and Li, B., 2022. A microporous chromium-organic framework fabricated via solvent-assisted metal metathesis for C₂H₂/CO₂ separation. *Dalton Transactions*, 51(31), pp.11658–11664.

Lulianelli, A. and Drioli, E., 2020. Membrane engineering: Latest advancements in gas separation and pre-treatment processes, petrochemical industry and refinery, and future perspectives in emerging applications. *Fuel Processing Technology*, 206, pp. 106464–106482.

Luyben, W. L., 2018. Effect of feed composition on cryogenic distillation precooling configurations. *Computers & Chemical Engineering*, 118, pp. 261–267.

Ma, X., Wang, L., Wang, H., Deng, J., Song, Y., Li, Q., Li, X., and Dietrich, A.M., 2022. Insights into metal-organic frameworks HKUST-1 adsorption performance for natural organic matter removal from aqueous solution, *Journal of Hazardous Materials*, 424(C), pp. 126918.

Ma, Y., Liu, M., Wang, J., Zhu, B., and Li, Y., 2020. Enhanced gas separation performance by embedding submicron poly(ethylene glycol) capsules into polyetherimide membrane. *Chinese Journal of Polymer Science*, 39(3), pp.355–364.

Matveev, D., Borisov, I., Vasilevsky, V., Karpacheva, G., and Volkow, V., 2022. Spinning of polysulfone hollow fiber membranes using constant dope solution composition: Viscosity control via temperature, *Membranes*, 12(12), pp. 1257.

Ministry of Human Resources, Malaysia, 2010. Industry Code of Practice on Indoor Air Quality 2010. Kuala Lumpur: Department of Occupational Safety

and Health.

Montazerolghaem, M., Aghamiri, S., Khozani, M.R.T., and Tangestaninejad, S., 2017. A comparative investigation of CO₂ adsorption on powder and pellet forms of MIL-101. *Journal of the Taiwan Institute of Chemical Engineers*, 72, pp. 45–52.

Mu Q., Zhu W., Yan G., Lian Y., Yao Y., Li Q., Tian, Y., Zhang, P., Deng, Z., and Peng, Y., 2018. Activity and selectivity regulation through varying the size of cobalt active sites in photocatalytic CO₂ reduction. *Journal of Materials Chemistry A*, 6, pp. 21110–21119.

Mutyala, S., Jonnalagadda, M., Mitta, H., and Gundeboyina, R., 2019. CO₂ capture and adsorption kinetic study of amine-modified MIL-101 (Cr). *Chemical Engineering Research and Design*, 143, pp. 241–248.

Park, H.J., Bhatti, U.H., Nam, S.C., Park, S.Y., Lee, K.B., and Baek, I.H., 2019. Nafion/TiO₂ nanoparticle decorated thin film composite hollow fiber membrane for efficient removal of SO₂ gas. *Separation and Purification Technology*, 211, pp.377–390.

Prajapati, P.K., Kansara A.M., and Singh, P.S., 2016. Preparation and characterization of an oxygen permselective polydimethylsiloxane hollow fibre membrane, *RSC Advances*, 6, pp. 88943–88953.

Qian, Q., Asinger, P.A., Lee, M.J., Han, G., Rodriguez, K.M., Lin, S., Benedetti, F.M., Wu, A.X., Chi, W.S., and Smith, Z.P., 2020. MOF-based membranes for gas separations, *Chemical Reviews*, 120, pp. 8161–8266.

Robeson, L. M. 2008. The upper bound revisited. *Journal of Membrane Science*, 320(1-2), pp. 390–400.

Qiu, Y., Lin, Y., Yang, H., Wang, L., Wang, M., and Wen, B., 2020. Hollow Ni/C microspheres derived from Ni-metal organic framework for electromagnetic wave absorption. *Chemical Engineering Journal*, 383, pp.123207–123207.

Roslan, R.A., Lau, W.J., Lai, G.S., Zulhairun, A.K., Yeong, Y.F., Ismail, A.F., and Matsuura, T. 2020. Impacts of multilayer hybrid coating on PSF hollow fiber membrane for enhanced gas separation, *Membranes*, 10(11), p. 335–353.

Roslan, R.A., Lau, W.J., Sakthivel, D.B., Khademi, S., Zulhairun, A.K., Goh, P.S., Ismail, A.F., Chong, K.C., and Lai, S.O., 2018. Separation of CO₂/CH₄ and O₂/N₂ by polysulfone hollow fiber membranes: effects of membrane support properties and surface coating material, *Journal of Polymer Engineering*, 38(9), pp. 1–10.

Rumbo, J.Y., Torres, G.O., García, R.V., Alberto, C., Rodríguez, M.C., Bustos, E.S., Contreras, E.O., Hernández, A.A.F., César, J., Molina Y.A., and García, M.M., 2022. Review of the pressure swing adsorption process for the

production of biofuels and medical oxygen: Separation and purification technology. *Adsorption Science & Technology*, 2022, pp.1–50.

Salleh, N.M., Kamaruzzaman, S.N., Riley, M., Marinie, E., and Sulaiman A.Z.R., 2015. A quantitative evaluation of indoor environmental quality in refurbished kindergarten buildings: A Malaysian case study, *Building and Environment*, 94, pp. 723–733.

Sanaeepur, H., Ebadi Amooghin, A., Bandehali, S., Moghadassi, A., Matsuura, T., and Van der Bruggen, B., 2019. Polyimides in membrane gas separation: Monomer's molecular design and structural engineering. *Progress in Polymer Science*, 91, pp. 80–125.

Sarawade, P., Tan, H., and Polshettiwar, V., 2013. Shape and morphology controlled sustainable synthesis of Cu, Co, and In metal organic frameworks with high CO₂ capture capacity. *ACS Sustainable Chemistry & Engineering*, 1, pp. 66–74.

Sari, P., Gunawan, T., Salleh, W., Ismail, A. and Widiastuti, N., 2019. Simple method to enhance O₂/N₂ separation on P84 copolyimide hollow fiber membrane. In: 9th Annual Basic Science International Conference 2019 (BaSIC 2019).

Sarkar, S., and Chakraborty, S., 2021. Nanocomposite polymeric membrane a new trend of water and wastewater treatment: A short review, *Groundwater for*

Sustainable Development, 12, pp. 100533–100550.

Sasikumar, B., Arthanareeswaran, G., and Ismail, A., 2018. Recent progress in ionic liquid membranes for gas separation. *Journal of Molecular Liquids*, 266, pp. 330–341.

Sedighi, M., Talaie, M.R., Sabzyan, H., Aghamiri, S., and Chen, P., 2022. Evaluating equilibrium and kinetics of CO₂ and N₂ adsorption into amine-functionalized metal-substituted MIL-101 frameworks using molecular simulation. *Fuel*, 308, pp.121965–121981.

Serbanescu, O.S., Voicu, S.I., and Thakur, V.K., 2020. Polysulfone functionalized membranes: Properties and challenges. *Materials Today Chemistry*, 17, pp. 100302–100326.

Shen, Y., Shi, W., Zhang, D., Na, P., and Fu, B., 2018. The removal and capture of CO₂ from biogas by vacuum pressure swing process using silica gel. *Journal of CO₂ Utilization*, 27, pp. 259–271.

Shi, X., Shan, Y., Du, M., and Pang, H., 2021, Synthesis and application of metal-organic framework films, *Coordination Chemistry Reviews*, 44, pp. 214060–214080.

Shin, S., Dong Kyu Yoo, Bae, Y.S., and Jung, S.H., 2020. Polyvinylamine-loaded metal–organic framework MIL-101 for effective and selective CO₂

adsorption under atmospheric or lower pressure, *Chemical Engineering Journal*, 389, pp.123429–123429.

Sivarethinamohan, R., Sujatha, S., Priya, S., Sankaran, Gafoor, A., and Rahman, Z., 2021. Impact of air pollution in health and socio-economic aspects: Review on future approach. *Materials Today: Proceedings*, 37(2), pp. 2725–2729.

Sud, D., and Kaur, G., 2021. A comprehensive review on synthetic approaches for metal-organic frameworks: From traditional solvothermal to greener protocols. *Polyhedron*, 193, pp. 114897–114924.

Suleman, M. S., Lau, K., and Yeong, Y., 2016. Characterization and performance evaluation of PDMS/PSF membrane for CO₂/CH₄ separation under the effect of swelling. *Procedia Engineering*, 148, pp. 176–183.

Suzuki, N., Nakayama, Y., Nakaoka, H., Takaguchi, K., Tsumura, K., Hanazato, M., Hayashi, T., and Mori, C., 2021, Risk factors for the onset of sick building syndrome: A cross-sectional survey of housing and health in Japan, *Building and Environment*, 202, pp. 107976–108011.

Talukder, M.E., Alam, F., Talikder, M.R., Mishu, M.M.R., Perveez, M.N., Song, H., Russo, F., Galiaono, F., Lan, J., Stylios, G.K., Figoli, A., and Naddeo, V. 2023. Fabrication of a polyethersulfone/polyethyleneimine porous membrane for sustainable separation of proteins in water media,

Environmental Science: Water Research & Technology, Preprint.

Tang, Y., Lin, Y., Ford, D.M., Qian, X., Cervellere, M.R., Millett, P.C., and Wang, X., 2021. A review on models and simulations of membrane formation via phase inversion processes. *Journal of Membrane Science*, 640, pp. 119810–119834.

Tari, N.E., Tadjarodi, A., Tamnanloo, J., and Fatemi, S., 2016, Synthesis and property modification of MCM-41 composited with Cu (BDC) MOF for improvement of CO₂ adsorption selectivity, *Journal of CO₂ Utilization*, 14, pp. 125–134.

Teerachawanwong, P., Dilokekunakul, W., Phadungbut, R., Klomkliang, N., Supasitmongkol, S., Chaemchuen S., and Verpoort, F., 2023. Insights into the heat contributions and mechanism of CO₂ adsorption on metal–organic framework MIL-100 (Cr, Fe): Experiments And molecular Simulations, *Fuel*, 331, pp.125863–125863.

The American Society of Heating, Refrigerating and Air-Conditioning Engineers (ASHRAE), 2019. Standard 62.1-2019 Ventilation for Acceptable Indoor Air Quality provides standards for ventilation based on surface area and occupancy. Atlanta: The American Society of Heating, Refrigerating and Air-Conditioning Engineers (ASHRAE).

Vaitsis, C., Kanellou, E., Pandis, P.K., Papamichael, I., Sourkouni, G., Zorpas,

A.A., and Argiris, C., 2022. Sonochemical synthesis of zinc adipate Metal-Organic Framework (MOF) for the electrochemical reduction of CO₂: MOF and circular economy potential. *Sustainable Chemistry and Pharmacy*, 29, pp.100786–100786.

Valappil, S.K.R., Ghasem, N., and Al-Marzouqi, M., 2021. Current and future trends in polymer membrane-based gas separation technology: A comprehensive review. *Journal of Industrial and Engineering Chemistry*, 98, pp.103–129.

Wahab, M.S.A, and Rahman, S.A., 2018. The effect number of Pebax® 1657 coating layer on thin film composite (TFC) membrane for CO₂/N₂ separation. *Chiang Mai Journal of Science*, 45(1), pp. 484–491.

Wang, H, 2020. Global age-sex-specific fertility, mortality, healthy life expectancy (HALE), and population estimates in 204 countries and territories, 1950–2019: a comprehensive demographic analysis for the Global Burden of Disease Study 2019. *The Lancet*, 396(10258), pp.1160-1203.

Wang, Q., and Astruc, D., 2020. State of the art and prospects in metal–organic framework (MOF)-based and MOF-derived nanocatalysis, *Chemical Reviews*, 120(2), pp. 1438–1511.

Xia, W., 2018. Fabrication of metal–organic framework derived nanomaterials and their electrochemical applications, pp.1-43.

Xu, Z., Croft, Z.L., Guo, D., Cao, K., and Liu, G., 2021. Recent development of polyimides: Synthesis, processing, and application in gas separation. *Journal of Polymer Science*, 59(11), pp.943–962.

Xue, C., Zhang, Q., Wang, E., Huang, R., Wang, J., Hao, Y., and Hao, X., 2020, Encapsulated HKUST-1 nanocrystal with enhanced vapor stability and its CO₂ adsorption at low partial pressure in unitary and binary systems, *Journal of CO₂ Utilisation*, 36, pp. 1–8.

Xue, C., Zhang, Q., Wang, E., Huang, R., Wang, J., Hao, Y., and Hao, X., 2020. Encapsulated HKUST-1 nanocrystal with enhanced vapor stability and its CO₂ adsorption at low partial pressure in unitary and binary systems. *Journal of CO₂ Utilization*, 36, pp. 1–8.

Ye, S., Jiang, X., Ruan, L., Liu, B., Wang, Y., Zhu, J., and Li., Q., 2013. Post-combustion CO₂ capture with the HKUST-1 and MIL-101(Cr) metal–organic frameworks: Adsorption, separation and regeneration investigations, *Microporous and Mesoporous Materials*, 179, pp. 191–197.

Yin, P.X., Zhang, J., Qin, Y.Y., Cheng, J.K., Li, Z.J., and Yao, Y.G., 2011. Role of molar-ratio, temperature and solvent on the Zn/Cd 1,2,4-triazolate system with novel topological architectures. *CrystEngComm*, 13, pp. 3536–3545.

Yong, W.F., and Zhang, H., 2021. Recent advances in polymer blend membranes for gas separation and pervaporation. *Progress in Materials*

Science, 116, pp.100713–100746.

Yuan, H., Liu, J., Zhang, X., Chen, L., Zhang, Q., and Ma, L., 2023. Recent advances in membrane-based materials for desalination and gas separation. *Journal of Cleaner Production*, 387, pp.135845–135845.

Yulia, F., Nasruddin, Z.A., and Ruliandini, R., 2021. Metal-organic framework based chromium terephthalate (MIL-101 Cr) growth for carbon dioxide capture: A review. *Journal of Advanced Research in Fluid Mechanics and Thermal Sciences*, 57(2), pp. 158–174.

Zhang, C., Yang, X., Li, Z., Liu, Y., Zhao, Y., Wang, H., Ma, X., Li, C., and Zhang, Y., 2021. Experimental and numerical model investigations of oxygen-enriched characteristics in air-conditioned rooms. *Applied Sciences*, 11(11), pp. 4733–4748.

Zhang, X., Wan, K., Subramanian, P., Xu, M., Luo, J., and Fransaer, J., 2020. Electrochemical deposition of metal–organic framework films and their applications. *Journal of Materials Chemistry A*, 8(16), pp.7569–7587.

Zhang, Y., Gao, Z., Liu, W., Liu, G., Zhu, M., Wu, S., Yao, W., and Gao, E., 2021. Synthesis of copper-based metal-organic framework for sensing nitroaromatic compounds, *Inorganic Chemistry Communications*, 134, pp. 109017.

Zhao, M., Yang, Y., and Gu, X.S., 2023. MOF based CO₂ capture: Adsorption and membrane separation. *Inorganic Chemistry Communications*, 152, pp. 110722–110732.

Zhao, T., Li, S.H., Shen, L., Wang, Y., and Yang, X.Y., 2018. The sized controlled synthesis of MIL-101(Cr) with enhanced CO₂ adsorption property. *Inorganic Chemistry Communications*, 96, pp. 47–51.

Zulhairun, A.K., Fachrurrazi, Z.G., Nur Izwanne, M., and Ismail, A.F., 2015. Asymmetric hollow fiber membrane coated with polydimethylsiloxane–metal organic framework hybrid layer for gas separation. *Separation and Purification Technology*, 146, pp. 85–93.

Appendix A

List of Publication

1.0 Journal Publications

1. **Chong, K.C.**, Ho, P.S., Lai, S.O., Lee, S.S., Lau, W.J. Lu, S.Y., Ooi, B.S., 2022. Solvent-free synthesis of MIL-101 (Cr) for CO₂ gas adsorption: The effect of metal precursor and molar ratio. *Sustainability*, 14(3), pp. 1152–1162. (Indexed by Web of Science, IF 3.889 in 2021, Q2)
2. **Chong, K.C.**, Lai, S.O., Thiam, H.S., Mah, S.K., Lau, W.J., Ismail, A.F., 2021. Performance evaluation of PDMS or PEBAX-coated polyetherimide membrane for oxygen/nitrogen separation, *Sains Malaysiana*, 50 (11), pp. 3395 – 3404. (Indexed by Web of Science, IF 1.009 in 2021, Q4)
3. **Chong, K.C.**, Lai, S.O., Lau, W.J., Thiam, H.S., Ismail, A.F., Roslan, R., 2018. Preparation, characterization, and performance evaluation of polysulfone hollow fiber membrane with PEBAX or PDMS coating for oxygen enhancement process. *Polymers*,10(2), pp. 126–136. (Indexed by Web of Science, IF 4.967 in 2021, Q1)
4. Roslan, R.A., Lau, W.J., Sakthivel, D.B., Khademi, S., Zulhairun, A.K., Goh, P.S., Ismail, A.F., **Chong, K.C.**, Lai, S.O., 2018. Separation of CO₂/CH₄ and O₂/N₂ by polysulfone hollow fiber membranes: effects of membrane support properties and surface coating material, *Journal of*

Polymer Engineering, 38(9), pp. 1–10. (Indexed by Web of Science, IF 1.624 in 2021, Q3)

5. **Chong, K.C.**, Lai, S.O., Lau, W.J., Thiam, H.S., Ismail, A.F., Zulhairun, A.K., 2017. Fabrication and Characterization of Polysulfone Membranes Coated with Polydimethylsiloxane for Oxygen Enrichment, *Aerosol and Air Quality Research*, 17(11), pp. 2735–2742. (Indexed by Web of Science, IF 4.530 in 2021, Q1)
6. **Chong, K.C.**, Lai, S.O., Thiam, H.S., Teoh, H.C., Heng, S.L., 2016. Recent progress of oxygen/nitrogen separation using membrane technology, *Journal of Engineering and Science Technology*, 11(7), pp. 1016 – 1030. (Indexed by Scopus, CiteScore 1.5 in 2021)

2.0 Book Chapter

1. Lai, S.O., **Chong, K.C.**, Lau, W.J., 2019. Prospects of nanocomposite membranes for nitrogen and oxygen enrichment in Nanocomposite membranes for water and gas separation. Amsterdam: Elsevier, pp. 379-396.

3.0 Conference Proceedings

1. **Chong, K.C.**, Lau, W.J., Lai, S.O., Thiam, H.S., Ismail, A.F., 2019. Preparation and characterization of chromium metal organic framework for carbon dioxide adsorption, *IOP Conference Series: Earth and Environmental Science*, 268(1), pp. 012010–012015.

Appendix B

Annual cost calculation of membrane technology in indoor oxygen air enrichment

Vacuum pump rated energy = 230W

Total office hour per day = 8 hours

Electricity tariff = RM 0.435 per kWh

(TNB Tariff B – Low voltage commercial tariff)

Monthly energy cost = 230W x 8 hours x 30 days x RM 0.435 /kWh
= RM 24.01

Annual energy cost = RM 24.01 per month x 12 months
= RM 288.14 \approx RM 290.00